MAGNETIC NANOPARTICLES FOR REMOVAL OF FREE FATTY ACID FROM VEGETABLE AND BIODIESEL OILS

BY

RITWAN MASAE

A THESIS SUBMITTED IN PARTIAL FULFILLMENT OF
THE REQUIREMENTS FOR THE DEGREE OF MASTER OF
ENGINEERING (ENGINEERING TECHNOLOGY)
SIRINDHORN INTERNATIONAL INSTITUTE OF TECHNOLOGY
THAMMASAT UNIVERSITY
ACADEMIC YEAR 2015

MAGNETIC NANOPARTICLES FOR REMOVAL OF FREE FATTY ACID FROM VEGETABLE AND BIODIESEL OILS

BY

RITWAN MASAE

A THESIS SUBMITTED IN PARTIAL FULFILLMENT OF
THE REQUIREMENTS FOR THE DEGREE OF MASTER OF
ENGINEERING (ENGINEERING TECHNOLOGY)
SIRINDHORN INTERNATIONAL INSTITUTE OF TECH.
THAMMASAT UNIVERSITY
ACADEMIC YEAR 2015

MAGNETIC NANOPARTICLES FOR REMOVAL OF FREE FATTY ACID
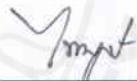FROM VEGETABLE AND BIODIESEL OILS

A Thesis Presented

By
RITWAN MASAE

Submitted to
Sirindhorn International Institute of Technology
Thammasat University
In partial fulfillment of the requirements for the degree of
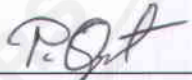MASTER OF ENGINEERING (ENGINEERING TECHNOLOGY)

Approved as to style and content by
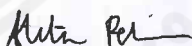
Advisor and Chairperson of Thesis Committee   _____

(Asst.Prof. Paiboon Sreearunothai, Ph.D.)

Co-Advisor   _____

(Assoc.Prof. Pakorn Opaprakasit, Ph.D.)

Committee Member and
Chairperson of Examination Committee   _____

(Atitsa Petchsuk, Ph.D.)

Committee Member   _____

(Duangporn Polpanich, Ph.D.)

NOVEMBER 2015

i

Abstract

MAGNETIC NANOPARTICLES FOR REMOVAL OF FREE FATTY ACID FROM VEGETABLE AND BIODIESEL OILS

by

RITWAN MASAE

Bachelor of Science in Petrochemical Technology, King Mongkut's Institute of Technology Ladkrabang, 2010

In conventional alkaline-based biodiesel production, free fatty acid (FFA) in oil feedstock can cause undesirable soap and high FFA content in biodiesel product also cause rancidity and corrosion. To develop a new technique for FFA removal in both biodiesel feedstock and biodiesel, iron oxide magnetic nanoparticles (MNP) synthesized by co-precipitation were introduced as an adsorbent, which can be easily separated from oil medium using simple external magnet. The synthesized MNP possesses superparamagnetic behavior with 83 emu/g of saturation magnetization. Transmission electron microscope images revealed the average particle size of about 10 – 14 nm in agreement with the result from X-ray diffraction. In oil, there are some cluster aggregations with the mean size of 442 ± 99 nm. The adsorption experiment could be well described by Langmuir isotherm with the maximum FFA adsorption capacity of 64 and 92 mg_{FFA}/g_{MNP} in the vegetable oil and biodiesel, respectively. The kinetics of adsorption of FFA onto MNP in biodiesel is about 6 times faster than that in vegetable oil due to the lower viscosity of biodiesel (6.78 mm^2/s) which is much smaller than that of vegetable oil (45.33 mm^2/s). The spent MNP could be regenerated with sodium hydroxide and reused for subsequent adsorption for at least 3 cycles with adsorption capacity of about 70%. Inductively coupled plasma revealed that the differences of iron content before and after adsorption are 2 and 5 ppm for vegetable and biodiesel oils, respectively. Percent weight loss of oleic acid on MNP is

equivalent to 65 and 66 mg$_{FFA}$/g$_{MNP}$. Thermogravimetric analysis showed the significant decomposition in the range of 200 - 450 °C, which can be assigned to the removal of FFA adsorbed on MNP surface. Fourier transform infrared spectroscopy shows that these FFA in oil media also adsorbed onto the iron oxide surface in the bridging and chelating bidentate configuration, which is similar to other works.

Keywords: Magnetic nanoparticles, Free fatty acid, Nano-adsorbent, Biodiesel

Acknowledgements

SIIT officials for their friendship, advice and being such a good companion throughout my study. They have made this experience fascinating and meaningful. Most importantly, I sincerely delicate a piece of work to my beloved family, including my father, my mother, my sisters and brother, for always pushing me, standing beside me and believing in me. I would like to say thank you to my beloved family who has been giving a support and love since the day I was born. Without their love and support, this research could not have been completed successfully.

Table of Contents

List of Tables

List of Figures

Chapter 1
Introduction

1.1 Concept and significance

Biodiesel has been an interesting candidate in the field of the alternative energies which can be used to substitute conventional diesel fuel. It can be generally produced via transesterification, the catalyzed chemical reaction involving triglycerides from vegetable oils or animal fats and simple monohydric alcohol, such as methanol, to eventually produce fatty acid alkyl esters known as biodiesel and its by-product (glycerol). Because of its primary feedstock, biodiesel is well-known as renewable and environmentally beneficial fuel. In addition, biodiesel operated in diesel engines has not only lower carbon monoxide emission, but also other unburned hydrocarbons than petroleum fuel [1]. Besides its environmental advantages, biodiesel can also relieve the pricing problem of conventional diesel fuel. For instance, Thailand imports crude oil more than 80% of total crude oil demand while the price of crude oil is drastically increased. The prices of high speed diesel in 2008 had risen more than those prices in 2003 about two times from 14.03 baht/liter in 2003 to 29.36 baht/liter in 2008 [2]. Consequently, biodiesel should be considered as a challengingly alternative energy which composes of not only environmental but pricing benefits too.

One of the critical factors affecting biodiesel production is free fatty acids (FFA), especially in the alkali-catalyzed transesterification [3]. Thus, the removal of FFA becomes important in biodiesel production as a pre-treatment process. There are several conventional methods for FFA removal, which depend on FFA contents. For instance, the alkali-catalyzed transesterification can still be performed with up to about 5% FFA. However, the additional alkali catalyst must be added to balance the lost catalyst. In this case, although alkali-catalyzed transesterification can reduce FFA to acceptable level by saponification, this process gives significant loss of oil, produces large amount of waste and also increases production processing cost during soap and glycerol separation [1]. Another means to remove FFA at lower percentage

is the use of commercial Magnesol 600R adsorbent [4]. This adsorbent appears to be inexpensive and workable for reducing FFA levels of 4% or below. At 2% FFA concentration, Magnesol 600R reduces the FFA level down to about 1.24% (2.45 mg_{KOH}/g) with 2% of Magnesol 600R loading. At this FFA level, the feedstock can be processed with the alkaline catalyst without undesirable problems associated with too high level of FFA.

In the case of high FFA feedstock (above 5% FFA), this feedstock is normally processed using two-step production [1], which is the pre-esterification of the FFA using acid catalyst, normally sulfuric acid, for esterifying the FFA to methyl esters, followed by alkali-catalyzed transesterification. Even though the acid catalyst can convert FFA to biodiesel effectively, there are some unpleasant problems about using acid catalyst, including the corrosion to the equipments and the acidic effluent from acid catalyst, which can be hazardous to the surroundings. In a previous study, the drop of free fatty acid level was investigated by using 20% palmitic acid spiked in soybean oil as a high FFA feedstock. The result revealed the free fatty acid content of the 20% palmitic acid spiked in soybean oil feedstock can be lowered to be less than 1% (2 mg_{KOH}/g) using the two-step acid catalyzed pre-treatment (10% sulfuric acid) followed by the alkali-catalyzed transesterification with 1 hr reaction time. In addition, other conventional methods to remove FFA, such as physical distillation, chemical neutralization and re-processing of the produced biodiesel, are all energy and chemical intensive [13]. Still, pre-treatment process for reducing FFA contents to the acceptable level is necessary for biodiesel production.

One of the most important characteristics of biodiesel produced is the acid value, which is mainly referred to the degree of oxidation and hydrolysis in biodiesel, and free fatty acid is the major cause of high acid value. According to ASTM D 6751, the number of acid values in biodiesel is maximized at 0.5 mg_{KOH}/g (0.25% FFA) [5]. With low acid value, biodiesel is harmless for storage and transportation, on the other hands biodiesel with acid value above the ASTM specification may cause rancidity and corrosion while storing. Consequently, FFA content, which contributes to the acid

value, should also be limited in biodiesel final product by introducing a post-treatment process to confirm the biodiesel specification and promote the use of safer biodiesel.

Interestingly, iron oxide magnetic nanoparticles (MNP) have high affinity towards the FFA, such as oleic acid, which are always used to stabilize MNP surface during synthesizing [6]. Considering the concepts of green chemistry, removal of FFA by adsorption on solid surface appears to be an environmentally friendly alternative method because of low temperature operation without organic solvents. The ease of separation process by using an external magnet can also be considered as the main advantage of using MNP and causes the convenient means to regenerate MNP adsorbent for several times. Additionally, the properties of MNP, including high surface area due to nano-size, biocompatibility, and well-documented synthesis method, are also beneficial. Therefore, MNP should be considered as an interesting adsorbent candidate for adsorbing FFA in biodiesel production for both pre-treatment of feedstock and post-treatment of biodiesel.

In this work, MNP in the form of magnetite (Fe_3O_4) is firstly synthesized by simple co-precipitation and further used as adsorbent to adsorb FFA in stimulated biodiesel feedstock, the spiked-oleic acid in commercial soybean oil with the %FFA ranges of 1-7%. This step is considered as pre-treatment process to provide acceptable and lower FFA concentration feedstock for processing in the alkali-catalyzed transesterification. Secondly, biodiesel final product is also tested with MNP in the post-treatment process in order that the acid value and FFA concentration can meet the biodiesel specification standard and reduce the undesirable problems of using biodiesel, like corrosion and rancidity. There are several factors investigated in this experiment, including MNP loading, equilibrium contact times, the order of kinetic reaction, and the maximum adsorption capacity using adsorption isotherm. Moreover, a variety of characterization techniques, including TEM, XRD, DLS, VSM, Zeta potential, ICP, TGA and FTIR, will be employed to study the physical, chemical and magnetic properties of MNP adsorbent. To get the most out of MNP, the used MNP will be easily separated from oil media using external magnetic field and regenerated

by desorbing FFA adsorbed on MNP surface for several uses before the removal efficiency starts to drop.

Therefore, the objective of this research is to develop a new technique in FFA removal from feedstock and biodiesel using MNP by adsorption as the pre-treatment and post-treatment processes. MNP can then be separated from the treated oil using magnetic field. The technique should provide a fast and inexpensive means compared to conventional treatment methods, such as acid-catalyzed FFA reduction which requires expensive acid-resistant equipment, high temperature and long reaction time.

1.2 Objectives of the study

1. To develop a new technique in removal of free fatty acid from biodiesel using iron oxide magnetic nanoparticles for FFA adsorption. The magnetic nanoparticles can then be separated from the treated oil using magnetic field. The technique should provide a fast and inexpensive means of FFA removal compared to conventional acid treatment (e.g. acid-catalyzed FFA reduction requires expensive acid-resistant equipment, high temperature and long reaction time).

2. To study and characterize the properties and performance of the synthesized magnetic nanoparticles use in oil-related applications, especially in simulated biodiesel feedstock and biodiesel.

1.3 Scope of the study

This research involves testing of iron oxide magnetic nanoparticles in the adsorption of free fatty acids from FFA-spiked commercial soybean oil, which was used as a model of biodiesel feedstock and this adsorption is considered as a pre-treatment process of biodiesel production. The adsorption capability will be evaluated as well as the reaction conditions, including the loading of adsorbent, contact time, the loading concentration, and the incubating temperature. The experiment also tests the FFA removal in the biodiesel produced as a post-treatment process in order to help reducing acid value further to meet the criteria. These magnetic nanoparticles can also

be reused and regenerated for repeated uses and these particles can be easily separated from oil media using a simple magnetic decantation with an external magnet. Additionally, both bare and used iron oxide magnetic nanoparticles will be characterized for physical and chemical properties with different characterization techniques.

Chapter 2
Literature Review

2.1 Biodiesel production

Biodiesel is referred to a fuel which normally composed of a mixture of long chain alkyl esters of fatty acids, such as methyl ester or ethyl ester, originated from either vegetable oils or animal fats. Biodiesel possesses both properties and characteristics that are similar or close to petroleum-based diesel. As a result, biodiesel can be applied either as a substitution for diesel fuel or as a fuel blends. Biodiesel needs to satisfy the requirements of ASTM D 6751 (Table 2.1) [5]. Biodiesel also provides many benefits compared to conventional diesel; for example, the presence of oxygen atom in the biodiesel molecule of about 10% by weight can improve the combustion and reduces the emission of carbon monoxide, hydrocarbons and incomplete combustion carbon particulates. Biodiesel has a higher cetane number, flash point and lubricity compared to petroleum-based diesel. In addition, the combination of biodiesel and diesel has a designated letter symbol B and followed by the content of biodiesel in volume percent of the blend. For instance, B20 means 20 vol% of biodiesel and 80 vol% of diesels. B5 and B20 are some of the popular blends, which can be used in unmodified diesel engines [2].

Table 2.1 The specification of biodiesel on ASTM D 6751 and EN 14214 [5].

Property	ASTM D 6751		EN 14214	
	Test method	Limits	Test method	Limits
Ester content	–	–	EN 14103	96.5% (mol mol^{-1}) min
Linolenic acid content	–	–	EN 14103	12.0% (mol mol^{-1}) max
Content of FAME[a] with $\geq$4 double bonds	–	–	–	1.0% (mol mol^{-1}) max
MAG[b] content	–	–	EN 14105	0.80% (mol mol^{-1}) max
DAG[c] content	–	–	EN 14105	0.20% (mol mol^{-1}) max
TAG[d] content	–	–	EN 14105	0.20% (mol mol^{-1}) max
Free glycerine	ASTM D 6584	0.020% (w/w) max	EN 14105	0.020% (mol mol^{-1}) max
Total glycerine	ASTM D 6584	0.240% (w/w) max	EN 14105	0.25% (mol mol^{-1}) max
Water and sediment or water content	ASTM D 2709	0.050% (v/v) max	EN ISO 12937	500 mg kg^{-1} max
Methanol content	–	–	EN 14110	0.20% (mol mol^{-1}) max
(Na + K) content	UOP 391	5.0 mg kg^{-1} max	EN 14108	5.0 mg kg^{-1} max
(Ca + Mg) content	–	–	prEN 14538	5.0 mg kg^{-1} max
P content	ASTM D 4951	0.001% (w/w) max	EN 14107	10.0 mg kg^{-1} max
Oxidative stability (110 °C)	–	–	EN 14112	6 h min
Density (15 °C)	–	–	EN ISO 3675	860–900 kg m^{-3}
Kinematic viscosity or viscosity (40 °C)	ASTM D 445	1.9–6.0 mm^2 s^{-1}	EN ISO 3104	3.5–5.0 mm^2 s^{-1}
Flash point	ASTM D 93	130 °C min	EN ISO 3679	120 °C min
Cloud point	ASTM D 2500	Not specified	–	–
Sulphur content	ASTM D 5453	0.05% (w/w) max	EN ISO 20864	10.0 mg kg^{-1} max
Carbon residue	ASTM D 4530	0.050% (w/w) max	EN ISO 10370	0.30% (mol mol^{-1}) max
Cetane number	ASTM D 613	47 min	EN ISO 5165	51 min
Sulphated ash	ASTM D 874	0.020% (w/w) max	ISO 3987	0.02% (mol mol^{-1}) max
Total contamination	–	–	EN 12662	24 mg kg^{-1} max
Copper strip corrosion (3 h, 50 °C)	ASTM D 130	No. 3 max	EN ISO 2160	1 (degree of corrosion)
Acid number or acid value	ASTM D 664	0.50 mg KOH g^{-1} max	EN 14104	0.50 mg KOH g^{-1} max
Iodine value	–	–	EN 14111	120 g I$_2$·100 g^{-1} max
Distillation temperature (90% recovered)	ASTM D 1160	360 °C max	–	–

2.1.1 Oil palm as biodiesel feedstock

Animal fat and vegetable oil are generally used as biodiesel feedstock. However, in Thailand, the plants, which are grown to yield oil, are oil palm, coconut, soybean, peanut, sesame and castor, and oil palm possessed 4 million tons of annual oil yield, followed by coconut and soybean as the information can be seen in Table 2.2. For world market, Thailand provides only 3.76% of the world's palm oil production and it is ranked in the third largest producer. Malaysia and Indonesia are ranked in the first and second palm oil producers, respectively.

Table 2.2 Oil yielding plants production in Thailand from 1996 to 2003 [2].

Unit: thousand tons

Year	Oil Palm	Coconut	Soybean	Peanut	Sesame	Castor
1996	2,255	1,413	386	147	34	6
1997	2,688	1,419	359	147	34	6
1998	2,681	1,386	338	126	35	6
1999	2,465	1,372	321	135	36	7
2000	3,514	1,381	319	138	37	7
2001	3,256	1,400	312	132	39	9
2002	4,089	1,396	261	107	39	9
2003	4,001	1,418	260	112	40	10

Oil palm is considered as the basic feedstock normally used in biodiesel production in many countries, including Thailand. CPO refers to crude palm oil which was cropped from oil palm trees and CPO will be transported and refined in palm oil refinery plant. After refining the refined palm oil (RPO), this oil will be then transformed into alkyl ester or biodiesel. This biodiesel shows low percent emissions with high oxidation stability. The pathway of biodiesel from palm oil is shown in Figure 2.1, where CPO is refined into refined palm oil and then transformed into biodiesel or blended petroleum fuel [8]. Table 2.3 shows the fatty acid compositions of crude palm oil determined by PORIM, abbreviated from Palm Oil Research Institute of Malaysia [7].
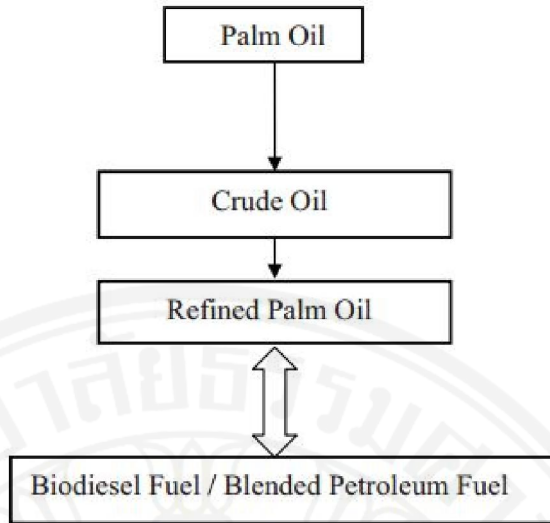
Figure 2.1 Palm oil to biodiesel process [8].

An important raw material used as biodiesel feedstock in Thailand is palm oil due to the high crop yield. By 2011, Thailand government has targeted biodiesel based on palm oil around 8.5 million liters a day. Four to five tons of CPO can be annually produced from a hectare of oil palm and these trees can yield CPO for more than 20 years. A number of palm oils, during 2003–2007, are 4,902,555 tons, 5,181,797 tons, 5,002,670 tons, 6,240,753 tons and 7,378,230 tons, respectively [9].

Table 2.3 Quality characteristics of palm oil as defined by PORIM [7].

Parameters	PORIM[a] specification
Moisture (% w/w)	ND
Acid value (mg KOH/g)	ND
Fatty acid composition	
Lauric	0–0.4
Myristic	0.6–1.6
Palmitic	41–47
Palmitoleic	0–0.6
Stearic	3.7–5.6
Oleic	38.2–43.5
Linoleic	6.6–11.9
Linolenic	0–0.5
Arachidic	0–0.8
Mean molecular weight (g)	
Unsaturated fatty acids (%)	44.8–57.3
Saturated fatty acids (%)	45.3–55.4

Edward *et al.* had optimized the parameters in transesterification of CPO to methyl ester [7]. The fuel properties obtained from this reaction had been studied. Table 2.3 indicates the free fatty acid characteristics of CPO determined and particularized by PORIM. The optimized parameters were reaction at 95°C for 9 h. These optimized parameters also suggest that using acid-catalyzed transesterification should be performed at rising temperature with 9 hr of reaction time which is quite long when it was compared to basic-catalyzed transesterification.

Song *et al.* synthesized biodiesel using palm oil as feedstock by supercritical methanol method without any catalysts [10]. In order to produce biodiesel from palm oil, a batch reactor system was applied in supercritical methanol by using no catalyst. The operation parameters, including temperature ranges from 200 to 400 °C, 3 - 80 mole ratio of methanol to palm oil and reaction time range from 0.5 to 20 min, were experimented. A gas chromatography was used to characterize fatty acid methyl esters (FAMEs) synthesized in this experiment. The results indicated that over the critical point temperature, there is a dramatic increase in the amount of FAMEs at around 30 mole ratio of methanol to palm oil. However, this FAME amount was limited by higher temperature or thermal decomposition above 300 °C. Moreover, this experiment requires both high investment cost and high energy cost because of very high temperature and pressure at supercritical point.

2.1.2 Waste cooking oil as biodiesel feedstock

In Thailand, waste cooking oil (WCO) should be considered as a candidate for using as biodiesel feedstock as it is produced more than 100 million liters per year. 0.9 Liter of biodiesel can be processed from a liter of residual waste cooking oil, so that tremendous quantities of waste cooking oil are assessable to provide as a biodiesel feedstock [11]. Biodiesel produced from WCO has the fuel properties which are comparable to conventional diesel according to ASTM D 6751 or EN 14214 [12], especially the kinematic viscosity, flash point and pour point. Biodiesel from WCO is generally synthesized by transesterification reaction which totally depends on many factors, including reaction time and temperature, types of alcohol, types and

concentration of catalyst, concentration of moisture and free fatty acid. For residual oil, it can be used in soap production and it can be used as an ingredient for animal feed. Otherwise, this residual oil can simply cause environmental crisis.

Meng *et al*. reported that biodiesel obtained from WCO and produced by transesterification reaction [12]. Its significant factors are illustrated in Table 2.4. These factors are related to EN14214 standards for kinematic viscosity, copper strip corrosion, density, acid number, cetane number, caloric value, and glycerol content. This experiment concentrated on experimental conditions, such as methanol to oil molar ratio, alkaline catalyst amount used, and reaction period and temperature. The optimal experimental conditions obtained are 9:1 methanol to oil molar ratio with 1.0 wt.% loading of NaOH catalyst at 50 °C for 90 min. With these optimal reaction conditions, WCO conversion efficiency to biodiesel is about 89.8%. Moreover, not only physical properties but also chemical characteristics of biodiesel derived from WCO met the requirement of international standards as shown in Table 2.4. Table 2.5 shows the comparison of free fatty acid content between different sources of biodiesel including waste cooking oil (WCO).

Table 2.4 The comparison between the properties of synthesized biodiesel and conventional diesel fuel [12].

Parameter	Samples	Diesel fuel	EN14214
Density (15 °C, kg/m^3)	890	NA	860–900
Flash point (°C)	171	>65	>101
Kinematic viscosity (40 °C, mm^2/s)	4.23	3.0–8.0	3.5–5.0
Sulfur content (wt.%)	0.007	<0.05	<0.01
10% Conradson carbon residue	0.2	0.3	0.3
Copper strip corrosion (3 h, 50 °C)	1a	class1	class1
Water content (mg/Kg)	150	NA	<500
Cold filter plugging point (°C)	1	≤4	NA
Free glycerol (%)	0.008	NA	0.02
Total glycerol (%)	0.21	NA	0.25
Acid value (mg KOH/g)	0.48	<0.1	≤0.5
Cetane number	54.5	>49	≥51
Caloric value (MJ/kg)	32.9	41.8	NA

NA stands for not available.

Table 2.5 Comparison of several kinds of free fatty acid content between different sources of biodiesel [12].

Property	WCO	Cottonseed oil l	Rapeseed oil	Soybean oil
Fatty acid composition (%)				
Palmitic acid C16:0	16	11.67	3.49	11.75
Stearic acid C18:0	5.21	0.89	0.85	3.15
Oleic acid C18:1	34.28	13.27	64.4	23.26
Linoleic acid C18:2	40.76	57.51	22.3	55.53
Linolenic acid C18:3	0	0	8.23	6.31
Specific gravity	0.925	0.912	0.914	0.92
Viscosity (mm^2/s) at 40 °C	66.6	50	39. 5	65
Acid value (mg KOH/g)	7.25	0.11	1.14	0.2

2.1.3 Transesterification

Among the biodiesel production methodologies, transesterification is considered as the best current process. Most of the commercial biodiesel production is synthesized by the alkali-catalyzed transesterification because this transesterification can be performed under   mild condition to simply yield efficient conversion. Besides, minimal side reactions and reaction time is low when it was compared to acid-catalyzed transesterification.

Transesterification is a reversible reaction used to convert an ester into another ester. Specifically, triglyceride (TG) molecule (primary compound in vegetable oils) reacts with a low molecular weight alcohol yielding a mono alkyl ester and by-product glycerol, which is used in pharmaceutical and cosmetic industries. The transesterification reaction for biodiesel synthesis is shown in Figure 2.2. Because of the reversibility of transesterification, alcohols are excessively put in the reaction to fasten the triglyceride conversion and to certify that the conversion was complete. Methanol and ethanol are commonly used because of their low cost especially methanol. Acid or basic catalysts can significantly improve the conversion rate in which alkali catalysts is more pleasing due to satisfactory conversion within shorter reaction time [13].

11

Nonetheless, the appearance of water and free fatty acids in feedstock can cause undesirable biodiesel production problems. Water can easily hydrolyze triglycerides and esters products (biodiesel) into FFA which is undesirable. Formation of unpleasing soap can also happen in presence of basic homogeneous catalysts, generating serious problems for biodiesel separation, and eventually limiting catalyst activity. As a result, highly refined vegetable oils are required for the process. Otherwise, the pretreatment steps are necessitated for the feedstock to reduce the acid value and water concentration.
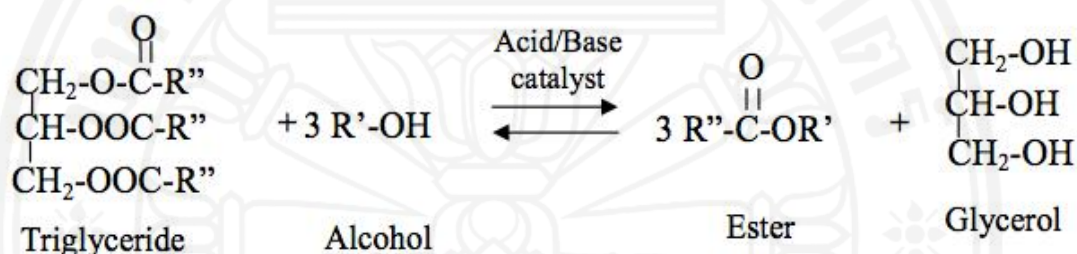
Figure 2.2 Transesterification which is normally used for producing biodiesel [13].

2.2 Free fatty acid

A fatty acid is a kind of carboxylic acid compounds consisting of the long chain aliphatic end. This end or tail can be either saturated or unsaturated. Normally, even number of carbon atom occurs naturally in fatty acids ranging from 4 to 28. Triglycerides and phospholipids are the source of fatty acids. They have been called as "free fatty acid or FFA" because of not contacting or attaching with other molecules. Unsaturated free fatty acids refer to fatty acid with carbon-carbon double bond. In other word, fatty acids with the absence of any double bond are classified as saturated fatty acid. Both types can be different in length of carbon chain. The examples of free fatty acids that mostly present in biodiesel feedstock are oleic acid and palmitic acid.

Oleic acid, one of free fatty acid, presents intrinsically in several sources, such as animal fat and vegetable oils. It seems to be odorless and colorless. Its appearance

looks like oil and commercial oleic acid seems to be yellowish. Oleic acid, shortened as lipid number of 18:1 cis-9, is chemically categorized as a mono-unsaturatedomega-9 fatty acid. The formula of oleic acid is $CH_3(CH_2)_7CH=CH(CH_2)_7COOH$. The word "oleic" is originated from olive. This means the oil mainly contain oleic acid as free fatty acid.

Palmitic acid $(CH_3(CH_2)_{14}CO_2H)$ known as hexadecanoic acid in IUPAC nomenclature can presents in many sources, like animals, plants and some kinds of microorganism. The word "palmitic" comes from the main component of the oil from palm trees, such as palm oil and palm kernel oil. Moreover, palmitic acid also presents in meats, and dairy goods. The salts and esters of palmitic acid is palmitate. At basic pH, anion of palmitate is observed. The chemical structure of both oleic and palmitic acids are shown in Figure 2.3.
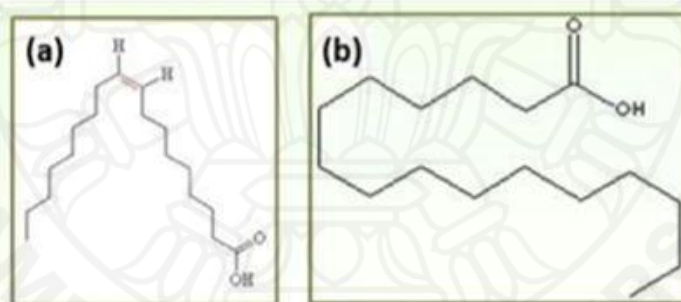
Figure 2.3 Examples of free fatty acids, including (a) oleic acid and (b) palmitic acid.

Because the raw material for biodiesel production can be obtained from many sources such as crude palm oil, jatropha oil, coconut oil, soybean oil, tallow or waste cooking oil. The oil from each source will have different amounts of impurities. The quality and quantity of biodiesel produced will depend on the amount of contaminant, especially free fatty acids content (FFA) showing in the oil. FFA is formed naturally as the result of hydrolysis reaction of triglyceride with trace amount of water or moisture in the oil. The process is accelerated at high temperature. Hence, the waste cooking oils, which have undergone high heat, will usually contain high level of FFA, possibly up to 10% v/v of FFA in oil [1].

2.2.1 Free fatty acid removal method

Since free fatty acids cause undesirable problem to alkali-transesterification, special processes are requested to lower the FFA percentage in biodiesel feedstock. Especially, if the animal fat or vegetable oil is composed of significant amounts of free fatty acids (FFA), this will need to pass biodiesel feedstock through special processes. Used waste cooking oil (WCO) essentially contains FFA around 2 - 7% FFA and animal fat regularly contains FFA ranging from 5% to 30% FFA. There is biodiesel feedstock that composes of a very low quality feedstock or high FFA percentage, such as trap grease, and FFA percentage can reach to 100%. Consequently, when the alkali catalysts are added to feedstock in transesterification reaction, the free fatty acid will spontaneously interact with those catalysts to produce both water and soap. This chemical mechanism to form soap (saponification) can be seen in Figure 2.4 [1].
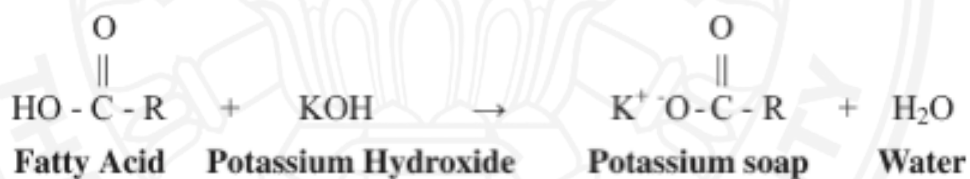
Figure 2.4 Saponification reactions between fatty acids and alkali catalyst (KOH) [1]

Up to about 5% FFA, the alkali catalysts can still be used to catalyze the reaction, which will convert triglyceride into ester, yet an increasing catalyst has to be added to recompense the loss of catalyst lost for soap formation. The saponification generated while the reaction is being processed can be got rid with glycerol or washed with water. If the FFA level exceeds 5%, this soap generated from saponification will hinder the separation of the glycerol and methyl esters. This will finally contribute towards the formation of emulsion in the water washing stage. In this case, the acid catalyst, including sulfuric acid, should be applied instead of basic catalyst to esterify free fatty acids to methyl esters as it is shown in Figure 2.5. Using an acid catalyst can be a process for pre-treating biodiesel feedstock and converting the free fatty acid in bad feedstock with high FFA content to methyl esters in order to eventually lower

FFA content. So, the low free fatty acid in pretreated oil will be transesterified with the basic catalyst to alternate triglyceride to methyl ester [1]. Moreover, water produced either from the oils and fats during the saponification reaction can hydrolyze the triglycerides to diglycerides and forms more free fatty acids. The typical hydrolysis reaction is illustrated in Figure 2.6.

$$HO-\overset{\overset{\displaystyle O}{\|}}{C}-R \quad + \quad CH_3OH \quad \overset{(H_2SO_4)}{\rightarrow} \quad CH_3-O-\overset{\overset{\displaystyle O}{\|}}{C}-R \quad + \quad H_2O$$

Fatty Acid   **Methanol**   **Methyl ester**   **Water**
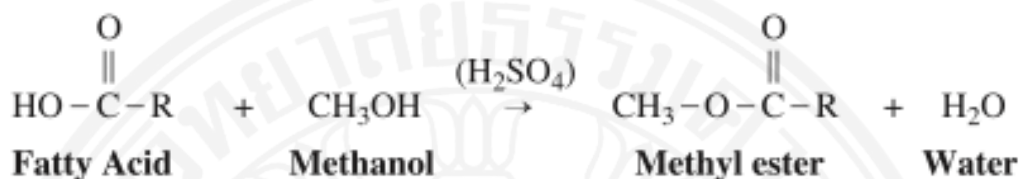
Figure 2.5 The esterification of FFA into methyl ester by using acid catalysts [13].

$$
\begin{array}{l}
CH_2\text{-}O\text{-}CO\text{-}R_1 \\
| \\
CH\text{-}O\text{-}CO\text{-}R_2 \quad + \quad H_2O \quad \longrightarrow \\
| \\
CH_2\text{-}O\text{-}CO\text{-}R_3
\end{array}
\qquad
\begin{array}{l}
CH_2\text{-}OH \\
| \\
CH\text{-}O\text{-}CO\text{-}R_2 \quad + \quad R_1\text{-}COOH \\
| \\
CH_2\text{-}O\text{-}CO\text{-}R_3
\end{array}
$$

(Triglyceride)   (Water)   (Diglyceride)   (FFA)

Figure 2.6 The hydrolysis of triglyceride to form more undesirable FFA [13].

Adeeb *et al.* revealed that in the pretreatment stage of sludge palm oil, sulfuric acid (H_2SO_4) can be initially considered as an acid catalyst for producing biodiesel by an esterification and the process is then catalyzed by an alkali-transesterification. Because acid catalysts can be used in esterification process to diminish FFA content in sample with very high FFA, like SPO, the treated SPO from esterification is then transesterification with base. This experiment had studied the effects of various parameters, including 6:1 - 14:1 molar ratio of methanol to SPO, temperature ranges from 40 to 80 °C, reaction time ranges from 30 to 120 min and 200 - 800 rpm stirring rate [5].

The outcome from the experiment indicated the optimal conditions are the decline in FFA content from around 23.2% to 2% with 0.75% wt/wt of acid catalysts (sulfuric acid). 8:1 was found to be suitable molar ration of methanol to oil. The reaction time and temperature are 60 min and 60 °C, respectively. The biodiesel yield was found to be 83.72% with the following optimal conditions, including 1% wt/wt of KOH, 10:1 molar ratio of methanol to SPO, 60 min of reaction time 60 min, 60 °C of reaction temperature and 400 rpm of stirring rate. In addition, the biodiesel processed from SPO was comparable to the EN 14214 standard as it was shown in Table 2.6 [5].

Table 2.6 Specified standard of biodiesel processed from SPO using two stages, including acid esterification and basic transesterification processes [5].

Properties	Biodiesel from Sludge palm oil	EN 14214	
		Test Method	Limits
Ester content	97% (mol mol^{-1})	EN 14103	96.5% (mol mol^{-1}) min
Monoglycerides content	0.48% (mol mol^{-1})	EN 14105	0.80% (mol mol^{-1}) max
Diglycerides content	<0.01% (mol mol^{-1})	EN 14105	0.20% (mol mol^{-1}) max
Triglycerides content	<0.01% (mol mol^{-1})	EN 14105	0.20% (mol mol^{-1}) max
Free glycerine content	<0.01% (mol mol^{-1})	EN 14105	0.02% (mol mol^{-1}) max
Total glycerine content	0.12% (mol mol^{-1})	EN 14105	0.25% (mol mol^{-1}) max
K content	3 mg kg^{-1} max	EN 14108	5.0 mg kg^{-1} max
P content	8 mg kg^{-1} max	EN 14107	10.0 mg kg^{-1} max
Density (15 °C)	878.5 kgm^{-3}	EN ISO 3675	860–900 kgm^{-3}
Kinematic viscosity (40 °C)	5.00 mm^2 s^{-1}	EN ISO 3104	3.5–5.0 mm^2 s^{-1}
Flash point	182.7 °C	EN ISO 3679	120 °C min
Cloud point	15.65 °C	-	-
Sulphated ash	<0.005% (w/w)	ISO 3987	0.02% (mol mol^{-1}) max
Total contamination	0.01 mg kg^{-1}	EN 12662	24 mg kg^{-1} max
Acid value	0.1533 mg KOH g^{-1}	EN 14104	0.50 mg KOH g^{-1} max
Iodine value	53.2 g I2·100 g^{-1}	EN 14111	120 g I2·100 g^{-1} max
Cetane Number	79	EN ISO 5165	51 min

In summary, often the triglyceride molecules react with trace water or moisture in the oil and form FFA instead. Due to the acidic nature of the FFA, it will react with the base catalyst used in the so-called saponification reaction to produce soap. Soap production is a severe problem in biodiesel production and should be avoided at all cost since it will emulsify the alkyl ester with glycerol hindering the separation and purification of the biodiesel produced resulting in low biodiesel yield. The usual rule of thumb is that if FFA content in starting oil is more than 5%, that oil cannot undergo the base-catalyst transesterification reaction, but has to either be treated

16

for FFA removal in the refinery process, or undergo the acid-catalyst esterification instead. Both routes demand significant amount of both energy and processing time. If the starting oils are not pre-treated to reduce FFA, the final yield of biodiesel produced in base-catalyst process can be reduced significantly due to the loss of biodiesel in the wash step with the soap produced from FFA reaction.

2.2.1 Determination of acid value and free fatty acid with Potentiometric titration

Standard reference method for determining acid number of both biodiesel and diesel based on petroleum is American Society for Testing and Materials abbreviated as ASTM D 664. It designates procedures to evaluate acidic components in biodiesel and conventional diesel in order to claim for a good repeatability during application. ASTM standard is used to limit the amount of minor components that are undesirable and can affect biodiesel quality.

ASTM D 664 is the recommendation method to evaluate the total acid number (TAN) of biodiesel. The TAN value mainly represents to the degree of oxidation and hydrolysis of oil, and TAN can be expressed as the milligrams of potassium hydroxide (KOH) that needs to neutralize TAN or acids presenting in oil in a gram of oil. In biodiesel, the maximum TAN value regulated by ASTM D 6751 is 0.50 mg_{KOH}/g. The free fatty acid contributes to a major cause of the high amount of total acid number in biodiesel. Lower TAN in biodiesel is normally evaluated as a safe fuel which is suitable for transportation and storage; on the other hand, biodiesel with TAN above the ASTM specification may cause rancidity and corrosion to the container during storage and transportation as well [14].

The acid value (or acid number) and FFA percentage can be calculated by these following equations as shown in Figure 2.7. The titration can be performed by preparing the solution of toluene and iso-propanol, and then titrating oil with potassium hydroxide and using phenolphthalein as indicator until the end point is shown as pale pink color [20].

$$AV = \frac{56.1 \, x \, N \, x \, V}{m}$$

Where;
AV = acid value (mg_{KOH}/g_{oil})
N = concentration of KOH (N)
V = volume of KOH used in titration (ml)
m = weight of oil
56.1 = molecular weight of KOH (g/mol)

$$\%FFA \text{ (as palmitic acid)} = \frac{AV}{2.19}$$

Where;
%FFA = percentage of free fatty acid (%)
AV = acid value (mg_{KOH}/g_{oil})
2.19 = molecular weight of KOH/ molecular weight of palmitic acid

Figure 2.7 Equations to determine acid value and percent FFA as ASTM D 664 [20].

2.3 Magnetic nanoparticles

Because separation of FFA from the majority triglyceride oil molecules is not easy and can be costly, waste cooking oil or other raw materials of biodiesel with excessive FFA usually has to undergo acid-catalyst esterification reaction before the base-catalyst transesterification can be used.   This causes the process to be complicated. Magnetic nanoparticle surface consists of Fe-O bond which has high affinity towards the charged group such as the carboxylic acid at the end of the FFA chain. The major component of waste cooking oil is the triglyceride molecules which have neutral charge and almost zero dipole moment. Therefore, upon dispersing the magnetic nanoparticles in oil feedstock, the FFA shall form very strong complex with the magnetic nanoparticles. These magnetic nanoparticle-FFA complexes can be easily removed from the oil using just magnetic force. Hence after treatment, the oil should have a much lower free fatty acid level and can therefore undergo base-catalyst transesterification process straightaway without the cumbersome acid-catalyst esterification.

Magnetic nanoparticle is a category of nanoparticles. These particles are easily operated by manipulating external magnetic field. These nanoparticles surely compose of magnetic element, like iron, cobalt, nickel and other chemical

compounds. To be called as nanoparticles, their sizes need to be in the range of 5 to 500 nanometers in diameter or less than 1 micrometer. Many research fields recently concern with many applications due to their striking properties, including catalysis, biomedicine and environmental remediation [16].

Because of the unique physical properties of magnetic nanoparticles including superparamagnetism and high saturation field, not only the applications and demand are expanding but also the synthesis methods become challenging to provide the stability of particles under various conditions. Moreover, most of successful applications perform well when the size of magnetic nanoparticles is around 10 - 20 nm, it can be considered as a size in critical value, where the shape or morphology of magnetic nanoparticles is controllable causing some better effects in many applications [16]. The critical size of magnetic nanoparticles plays an important role because each magnetic nanoparticles possesses a single magnetic domain causing superparamagnetism, in which each particles have a huge stable magnetic moment and remain very large paramagnetic with a very quick response to the external fields with insignificant residual magnetism and coercivity [16]. Besides, the relationship between size and its activity also needs to be considered. The decline of particle size causes a number the atoms being shared and staying on the surface. In other words, the ratio of high surface area and volume causes some effects of the material properties on particle surface. The example of these superparamagnetic applications is the fluorescence emission from semiconductor nanocrystals. Its properties are varied depending on the particle size. The decrease of size will limit the electron motion and then the electron bands of crystal get slowly quantized. Thus, the band gap energy would be increased.

Additionally, instability of magnetic nanoparticles over longer periods of time could be unavoidable problem. Firstly, unprotected magnetic nanoparticles normally tend to agglomerate to become a cluster in order that these particles can lower the energy related to ratio of the high surface area to volume. Secondly, the bare metal particles are chemically sensitive and easy to react with oxygen in air. Consequently, the instability of unprotected magnetic nanoparticles results the reduction of the activity,

magnetism and dispersibility. For instance, the magnetic saturation value is 81.9 emug^{-1} for magnetite (Fe_3O_4) obtained from solvothermal reduction method. After oxidation of Fe_3O_4 in HNO_3, the magnetic saturation value slightly reduces to 72 emug^{-1} in the form of maghemite (γ-Fe_2O_3). Nonetheless, if maghemite (γ-Fe_3O_4) is continually oxidized at 400 °C for 3 hours in air, hematite (α-Fe_2O_3) will be formed and the magnetic saturation value will be negligible causing the loss of magnetism [17]. It is essential to terminate the growth of nanoparticles and secure the surface stability in order to provide stable articles and maintain their high activity. The protection of magnetic nanoparticles becomes crucial strategy for many applications including a broad range of biomedical application, which needs to reduce the risk of particle forming at room temperature. In many circumstances, the metallic shells with protection will maintain the stability of the nanoparticles and can be applied for other functionalizations. Surfactants or polymers as organic compound can be used in these strategies by coating and grafting. Silica or carbon as inorganic compounds can also be coated on the shell, depending on desired application. For example, coating with surfactant that has long chain alkyl its polar head of surfactants can attach to the particles surface via covalent bonding or electrostatic interaction. The secure of stabilization could be described by steric effect from covalent bonding, electrostatic effect or the combination of both effects [18]. Figure 2.8 shows the stabilization of magnetic nanoparticles caused by electrostatic effect (a) and steric effect (b), which could be further functionalized in various applications.
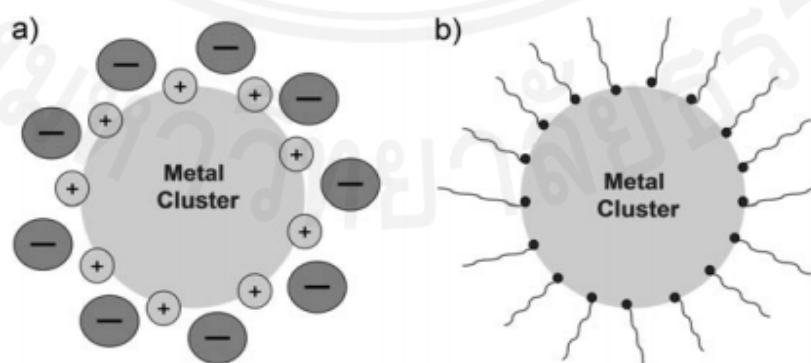
Figure 2.8 Stabilized MNP by a) electrostatic effect and b) steric effect [18].

2.3.1 Synthesis methods of iron oxide magnetic nanoparticles

Intensive studies of magnetic nanoparticle synthesis are currently focused on the experimental conditions including types of precursors and their ratio, solvents, surface capping agents, pH, reaction temperature and reaction period, which can lead to the development of various sizes and shapes of the particles. Additionally, magnetic colloids can be in the forms of many metals, like Co and Fe, metal oxides, like FeO, Fe_2O_3 and Fe_3O_4, ferrites, like $CoFe_2O_4$, and $MnFe_2O_4$ and alloys, like FePt and $FePt_3$. As a result, these forms of magnetic nanoparticles can possess superparamagnetic behavior [18].

To synthesize iron oxide nanoparticles, iron chloride and iron acetate are normally used as precursors while $Fe(CO)_5$ as a precursor is generally applied to synthesize iron based nanoparticles. Unfortunately, bare metal nanoparticle synthesis is quite laborious because iron is so promptly oxidized under normal conditions that various oxides will cover and attach the surface of the particles [18]. In case of spinel type of ferrites, their formula is MFe_2O_4 (M = Co, Mn or Ni), heterogeneous catalysis applications always apply by using these ferrites. The magnetism of both iron and its ferrite needs to be studied.

For instance, the insertion of Co^{2+} ion into the body of metal oxide and $CoFe_2O_4$ is yielded. This ferrite can enhance the magnetic magnitude compared to the bare Fe_3O_4 nanoparticles of the same size, yet the incorporate of Mn^{2+} ion as $MnFe_2O_4$ will decrease the magnetic magnitude of the particles [17]. Alternatively, developing into alloy particles can significantly alter the properties of mono-metal element chemically and magnetically. For instance, MPt alloy, where M is Fe or other metals, contains crystalline form with largest magnetic magnitude and this alloy is less responsive to oxidation reaction compared to bare iron and free platinum metals [18].

2.3.1.1 Co-precipitation method

In terms of simplicity, co-precipitation is the most favored route because of its facileness and convenience. Particularly, using aqueous Fe^{2+}/Fe^{3+} salt solution and adding basic solution, under unresponsive atmosphere either at ambient temperature or at accelerated temperature, can be easily performed to prepare iron oxides, like magnetite (Fe_3O_4) and maghemite γ-(Fe_2O_3). There are many factors affecting particle size and its morphology, including salt types, which are applied in the reaction such as chloride salt and sulfate salt, the ratio of Fe^{2+}/Fe^{3+} ratio, temperature used in the reaction and pH value. With this synthesis, magnetite (Fe_3O_4) has 30 - 50 emug^{-1} of the magnetic saturation values. This experimental value is less than 90 emug^{-1} of bulk value [16].

Current studies show that oleic acid (OA) is the most suitable choice to stabilize magnetite [7]. Two competing mechanisms from organic ion can cause the influence on the metal oxide formation. To protect nucleation, chelation of the metal ions is the key to avoid the formation of larger particles as the formed nuclei is smaller and particle growth governs the system. Moreover, the additive adsorption on the nuclei can hinder the particle growth, which they are favored to form from small units.

Figure 2.9 shows the Fe_3O_4 size and its distribution characterized by TEM of co-precipitation method by using different precursors. Synthesizing Fe_3O_4 nanoparticles using 1,6-hexanediamine as a basic solution in aqueous solution, which contains both ferrous salt and ferric salt with different ratio, shows that ratio of Fe^{2+} to Fe^{3+} directly affect to Fe_3O_4 reaction. This means that increase of ferrous to ferric ion ratio can promote OH$^-$ particle as a precursor of Fe_3O_4 and further results in the rise of particle size. Thus, the synthesized magnetite mean diameter swells from 9 to 37 nm [20].
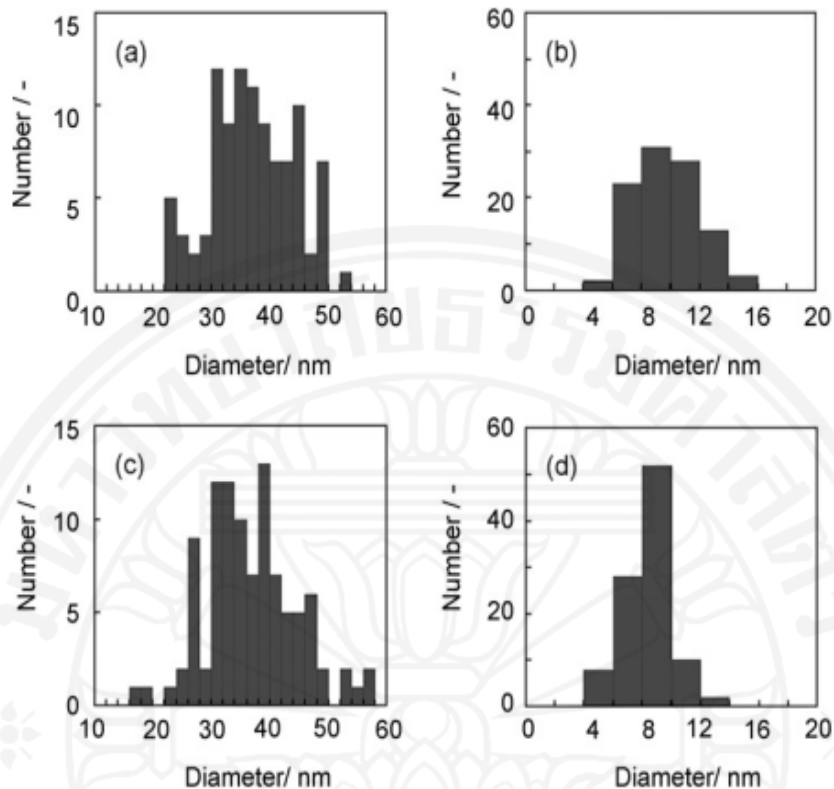
Figure 2.9 Size distributions by co-precipitation of magnetite nanoparticles with different precursors including (a) ferrous sulfate, (b) ferrous and ferric sulfate, (c) ferrous chloride and (d) ferrous and ferric chloride [20].

2.3.1.2 Hydrothermal method

Hydrothermal can be synthesized above 100 °C and 1 bar in aqueous media as a heterogeneous reaction. In other words, the substance crystallization at very high temperature and vapor pressures of aqueous solution is performed as hydrothermal. A single crystal can be obtained from this method. It is also dependent on the mineral solubility in very high temperature water under very high pressure.

A steel pressure vessel, known as autoclave, can be used as special equipment for crystal growth. Compared to other types of crystal growth, hydrothermal shows some benefits, including the capability to form crystalline phases, which are not constant at the melting point. Moreover, materials with high vapor pressure near their

23

melting point can also be propagated with hydrothermal method. The disadvantages of this method are the necessity of very expensive steel pressure vessel and the impossibility to observe the growth of crystals while the reaction was running.

In order to synthesize iron oxide nanoparticles with governable diameters, narrow size distribution and desirable properties of magnetism. A simple one step hydrothermal can be applied. The nanoparticles were carried out in base solution by oxidizing $FeCl_2 \cdot 4H_2O$ under very high temperature and pressure. The characterization techniques, including transmission electron microscopy (TEM) and X-ray diffraction (XRD), indicated that the synthesized iron oxide is well crystalline. 15 nm to 31 nm diameters are varied by altering the reaction conditions. The synthesized particles possess 53.3 - 97.4 emu/g which quite high saturation magnetization [21].

Figure 2.10 shows X-ray diffraction patterns of nanoparticle synthesized by hydrothermal at various temperatures and 30 MPa. These particles were obtained by continuous hydrothermal synthesis. The result reveals that the powder obtained at 200 °C was in amorphous phase. When the temperature is over 250 °C, the α-Fe_2O_3 (hematite) crystalline phase can be noticed. Interestingly, from 250 °C to 350 °C, the crystalline of particles increased with the increasing temperature. The crystalline started to decrease when the temperature was risen over 350 °C. At 200 °C, The amorphous powders were obtained with the size of less than 20 nm. Over 250 °C, particle size mounts with increasing temperature. In addition, at 420 °C, 40 nm of α-Fe_2O_3 particles can be obtained. At 350 °C, the particle size is around 60 nm. Scherrer equation was used to calculate these sizes and it shows that α -Fe_2O_3 particle is a single crystal [22].
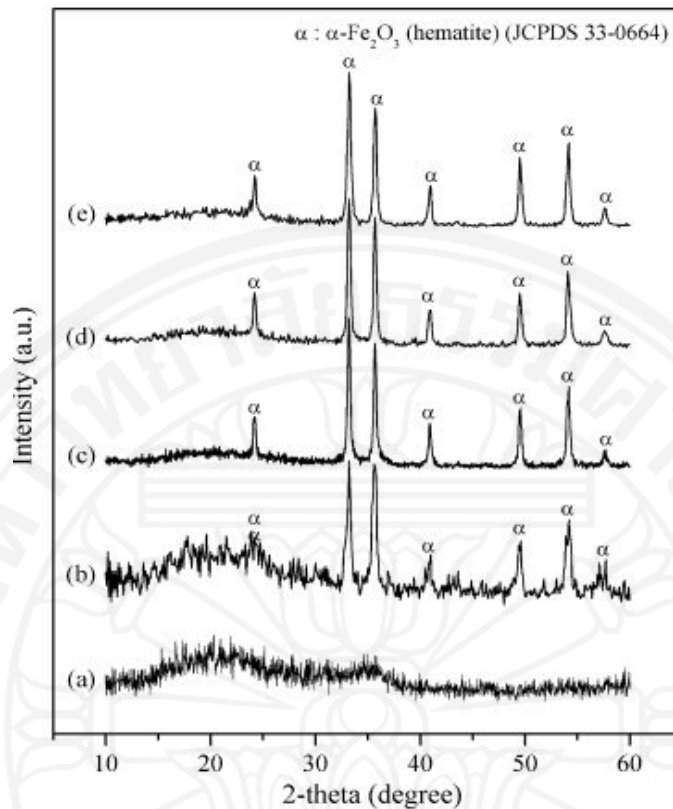
Figure 2.10 XRD patterns of different temperatures used to synthesized the particles with hydrothermal method at 30 MPa, including (a) 200 °C, (b) 250 °C, (c) 350 °C, (d) 380 °C, and (e) 420 °C, respectively [22].

2.3.1.3 Solvothermal reduction method

Multicomponent reaction mixtures in order to obtain the desired properties, including monodispersity, hydrophilic with microsphere structure and single-crystalline ferrite, can be used to modify this method. Multicomponent mixtures consist of ethylene glycol, sodium acetate, polyethylene glycol and $FeCl_3$ as iron source. These compounds are added with different purposes. For instance, a high-boiling point reducing agent is referred to ethylene glycol in this experiment so as to provide metal oxide nanoparticles with monodispersity. To prevent particle agglomeration, electrostatic stabilizer is referred to sodium acetate and to against the agglomeration of particles, surfactant had been used as polyethylene glycol. The mechanism of this

method is not clearly described while hydrothermal reduction method is powerfully used to prevent particle agglomeration and promote the applicable ability [16].

Solvothermal reduction method is one of the modified hydrothermal synthesis methods. Monodisperse magnetic single-crystal ferrite microsphere can be obtained by using multicomponent mixtures. This modified method can be used to yield larger size of particles for using in specific applications. The results indicate the tunable monodisperse diameters ranging from 200 to 800 nm as shown in Figure 2.11, which the larger particle size depends on higher time and concentration. The magnetic saturation values of ferrite (MFe_2O_4) microsphere are 81.9 emug^{-1} for magnetite (Fe_3O_4), 72.0 emug^{-1} for maghemite (γ-Fe_3O_4) and magnetic saturation value will be negligible because of the magnetism loss in case of hematite (α-Fe_3O_4). For other spinel ferrite values are 53.2, 60.0 and 61.6 emug^{-1} for $MnFe_2O_4$, $ZnFe_2O_4$ and $CoFe_2O_4$, respectively [17].

Additionally, the experimental procedure of solvothermal reduction method is illustrated with these following steps. To form a clear solution, 1.35 g of $FeCl_3 \cdot 6H_2O$ is liquefied in 40 mL of ethylene glycol, and 3.6 g of NaAc and 1.0 g of polyethylene glycol are added to this solution. The solution is elevated by stirring for 30 minutes and this solution is covered in an autoclave. This apparatus is heated to 200 ˚C for 8 - 72 hours and finally left to cool until it reaches room temperature. After the reaction, the obtained products with black color are washed many times with ethanol and dehydrated at 60 ˚C for 6 hours. The mentioned processes may also be applied to synthesize other particles including some microsphere ferrites (MFe_2O_4) by co-precipitating M^{II} and Fe^{III} chlorides (M^{2+}/Fe^{3+} = 0.5). For instance, 0.50 g of $MnCl_2 \cdot 4H_2O$ and 1.35 g of $FeCl_3 \cdot 6 H_2O$ are mixed to synthesize microspheres under the similar conditions and eventually produced microspheres of ferrite, called as $MnFe_2O_4$ [17].
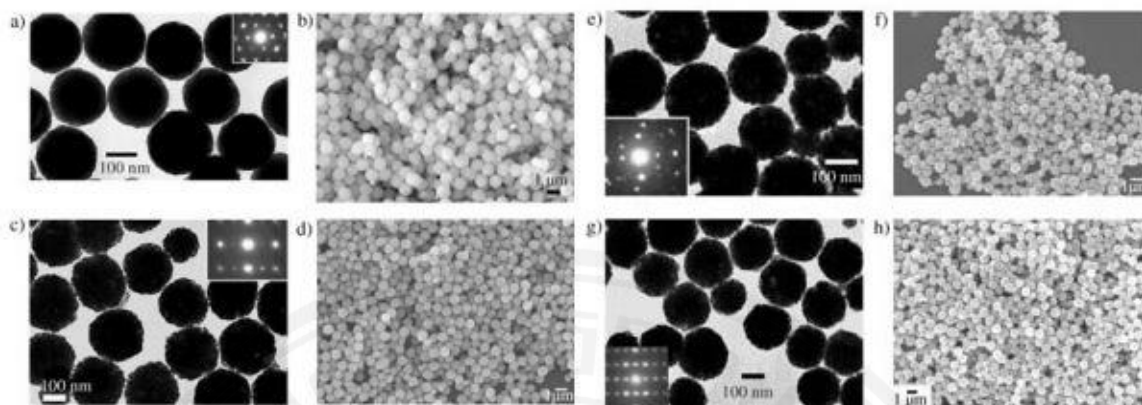
Figure 2.11 Different microspheres, including Fe_3O_4, (a and b), $MnFe_2O_4$, (c and d), $ZnFe_2O_4$, (e and f) and $CoFe_2O_4$, (g and h) obtained from TEM images (a, c, e, and g) and SEM images (are b, d, f, and h). The microsphere size from SEM is 800 nm and 200 nm from TEM [17].

2.4 Characterization techniques

A variety of physicochemical characterization techniques can be applied in order to find out not only the size but also morphology of particles, the crystalline of particles, the purity of particles, the magnetic behaviors and other magnetism properties.

2.4.1 X-ray diffraction

XRD is one of the most common characterization techniques basically used for proving the structure of crystal and the purity of synthesized nanoparticles. For example, comparing the experimental and reference diffractograms can determine the formation of magnetite (Fe_3O_4), like JCPDS# 19-629. The d value of (311) lattice space shown in Figure 2.12 was calculated to be 2.53 - 2.54 Å by inserting information into the Bragg equation (Equation 2.1) at 36° of 2θ as reflection peak. The experimental value is corresponding with 2.532 Å of standard value. Additionally, without using a delicate determination of d value, it would be difficult to distinguish Fe_3O_4 (magnetite) from γ-Fe_2O_3 (maghemite), because of the similarity of crystal structure and lattice spacing [20].

$$n\lambda = 2d\sin\theta \tag{2.1}$$

According to the Bragg equation, λ refers to the wavelength of waves, d represents the space between the planes, θ is the angle between the coming ray and the reflecting plane and n represents any integer. In addition, particle that moves in this nanoparticle, including electrons, protons and neutrons, has De Broglie wavelength reference. Furthermore, owing to the application of Scherrer equation, the particle size could be calculated from Equation 2.2 by using XRD information, such as the (311) reflection peak at 36° of 2θ (shown in Figure 2.12), which indicates 8 nm formation of Fe_3O_4 (magnetite) in diameter in case of the particles prepared by co-precipitation method with both ferrous salt and ferric salt.

$$\tau = \frac{K\lambda}{\beta\cos\theta} \tag{2.2}$$

Where λ refers to the x-ray wavelength, β is the line broadening at half the maximum intensity abbreviated as FWHM in radians, θ is the Bragg angle, K represents the shape factor, and τ is the mean size of the ordered crystalline domains. This value can be smaller or equal to the grain size. Moreover, a typical value of 0.9 is normally referred to the dimensionless shape factor although it is dependent on the real shape of the crystal. However, Scherrer formula is suitable for nanoparticles.
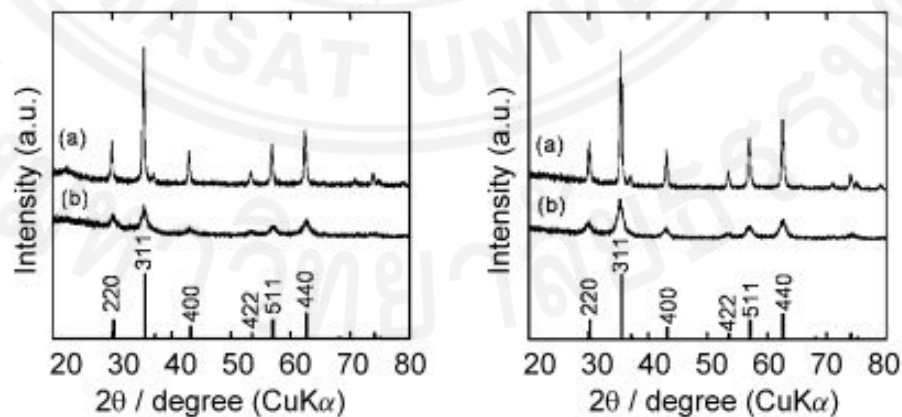
Figure 2.12 XRD patterns of MNP synthesized with iron sulfate (left) and iron chloride (right). Lines (a) in both figures were prepared with Fe^{2+} salt only; however, lines (b) were prepared with both Fe^{2+} and Fe^{3+}. Fe_3O_4 reference of JCPDS# 19-629 is illustrated as thick bars [20].

2.4.2 Transmission Electron microscopy

Transmission electron microscopy (TEM) integrated with EDX, standing for energy dispersive X-ray analysis, is a very popular technique applied to determine the size and shape uniformity of synthesized particles. This technique can also be used to evaluate the elemental composition of the core structures. For example, TEM image can clearly show the differences of morphologies whether the shape is well controlled or not (as shown in Figure 2.13). Alternatively, high-resolution TEM (HR-TEM) images (as shown in Figure 2.14) can be used to provide the pattern of electron diffraction of each particle. HR-TEM can also be applied to characterize the thickness of the shell and its core of particle. In contrast, normal TEM can be used to provide the chance to evaluate the electron diffraction from single particle that can identify the local particle phases. Nevertheless, synthesis of nanoparticle sample is a critical part in TEM method as it can directly affect the colloidal particle aggregation so that the result may not consequently show the real size and synthesized particle distribution. Figure 2.15 shows the combined information of Fe_3O_4 morphologies by using TEM and SEM.
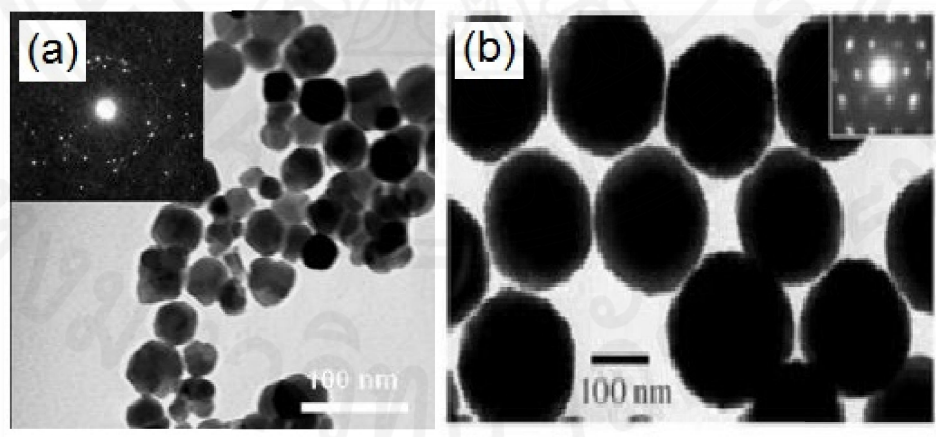
Figure 2.13 TEM images; (a) magnetite (Fe_3O_4) obtained from Co-precipitation and (b) magnetite (Fe_3O_4) obtained from Solvothermal reduction [17].
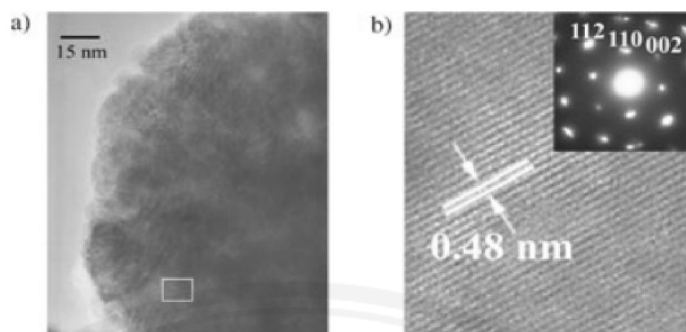
Figure 2.14 a) TEM image shows microsphere of Fe_3O_4 synthesized by solvothermal reduction method with diameter around 200 nm; b) HR-TEM image shows in the boxed part (a) and the pattern of electron diffraction of magnetite microsphere [17].
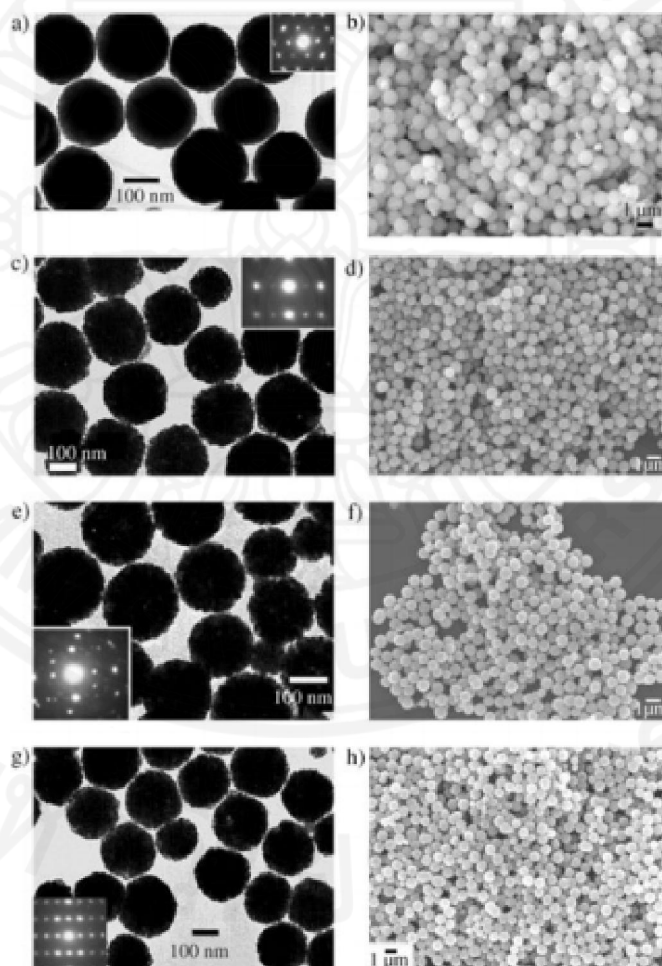
Figure 2.15 TEM results are at left and SEM results are at right. a and b are Fe_3O_4, c and d are $MnFe_2O_4$, e and f are $ZnFe_2O_4$, and g and h are Fe_2O_4. Their size is around 800 nm in SEM and 200 nm in TEM, in which the insets indicate the electron diffraction patterns [17].

2.4.3 Dynamic light scattering

The size of the nanoparticle can also be determined by using dynamic light scattering (DLS). The size determination concerns with the diffusion coefficient property of synthesized particles in solution. This can provide the approach to hydrodynamic radius and to the polydispersity of the colloid. If the system appears to be monodisperse, the average diameter of the particles can be easily determined. This technique varies with many factors, including particle concentration, the size of core and surface structure, and the sorts of ions in solution. Its software typically shows the population at different diameters of particles. If the system appears to be monodisperse, it probably shows one population. In contrast, a polydisperse system will show multiple populations of particles.

DLS can be used to notice the process of particle aggregation. DLS measurements can also demonstrate the aggregation with the change of time and with the increasing hydrodynamic radius. If particles tent to aggregate, a larger population of particles with a larger radius will be shown. Thus, the recent studies have applied to reveal magnetic nanoparticle stability over time. Other applications of DLS include the size characterization of various particles, such as proteins, polymers, micelles, carbohydrates and other nanoparticles. The disadvantage of this DLS method is that it is not reliable in the case of the fluorescent nanoparticles.

2.4.4 Vibrating sample magnetometry

Vibrating sample magnetometry (VSM) is the most mutual method applied to evaluate the magnetization value of magnetic particles. Generally, the graph that plot the magnetization curve (magnetization, M versus magnetic field strength, H) shows the saturation magnetization M_s, the residual magnetization at H = 0. Figure 2.16 shows the example of VSM results of Fe_3O_4 and other ferrite particles.
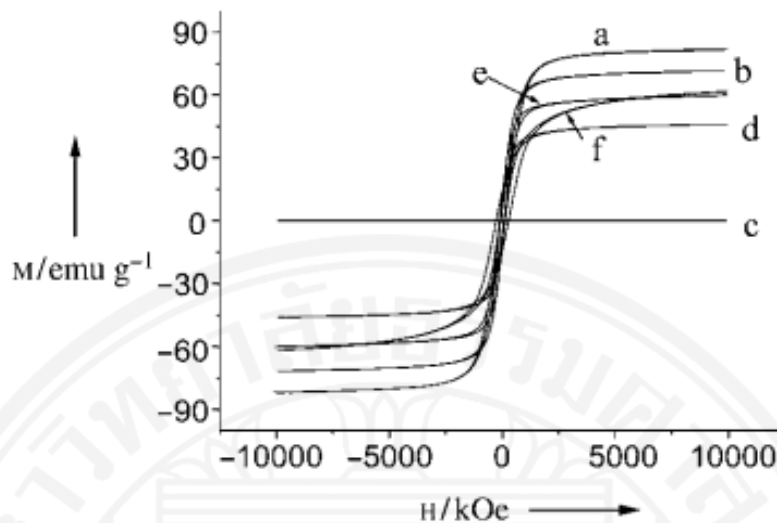
Figure 2.16 Ferrite microspheres were tested to find the saturation magnetization with the diameter of about 200 nm, including (a) Fe_3O_4, (b) γ-Fe_2O_3, (c) α-Fe_2O_3, (d) $MnFe_2O_4$, (e) $ZnFe_2O_4$ and (f) $CoFe_2O_4$. This experiment was tested at room temperature [17].

2.4.5 Zeta potential

Zeta potential is a physical property for any particle in suspended form, which plays an essential role. The formulations of suspensions and emulsions can be optimized by zeta potential value. The information from the zeta potential can diminish the time consumed in order to analyze formulations. Zeta potential has been widely applied to forecast the stability of particle over time in suspension. The liquid layers, which surround the particle, have two regions, firstly an inner region known as Stern layer where the ions are powerfully bonded and secondly an outer known as diffuse region where the ions are less powerfully bonded. At the outer region, there is a border where stable ions and particles are formed. If the particle moves, according to gravitation force, ions inside the boundary will move too. Outside the boundary, ions will remain with the bulk. The potential will be measured at this boundary and will be called zeta potential. Moreover, this boundary is the surface of hydrodynamic shear (Figure 2.17).
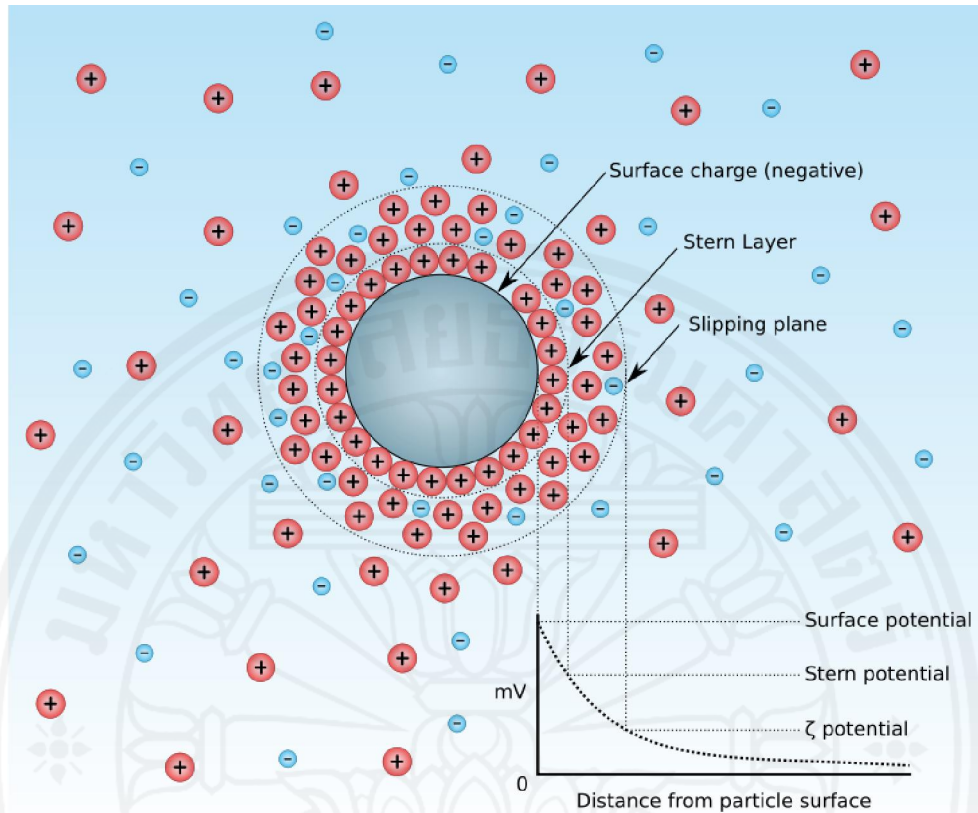
Figure 2.17 Schematic configuration of zeta potential.

The stability of the colloidal suspension can be interpreted from zeta potential magnitude. In case of a large magnitude, both negative and positive zeta potential will tend to repulse each other. It means that there is no chance for the particles to stick together and aggregate. On the contrary, low zeta potential particles have no force to avoid the particles that are coming to stick together and start to gravitate because of aggregation with less stability. The well-known guideline to compare the particle with high or low stability is normally considered at +30 or -30 mV. Stable particles will have more positive than +30 mV or more negative than -30 mV of zeta potential. However, the difference of density between particle and dispersant will cause the gravitation and form a close-packed bed at the bottom. In addition, the degree of electrostatic repulsion between adjacent can also be obtained from the magnitude of zeta potential. In case of small molecules, a high zeta potential will provide stability and the solution will defy aggregation of the particles. If zeta potential is small,

33

attractive force is higher than the repulsive force and the dispersion may consequently break and particle will eventually flocculate as it is outlined in the Table 2.7.

Table 2.7 Zeta potential ranges predict the stability behavior of the colloid.

Zeta potential (mV)	Stability of the colloid
from 0 to ±5	Coagulate or flocculate very fast
from ±10 to ±30	Incipiently unstable
from ±30 to ±40	Mild stable
from ±40 to ±60	Good stable
higher than ±61	Excellently stable

The pH of the colloidal suspension is one of the most important factors that impact the value of zeta potential and the stability. A zeta potential value is a genuinely meaningless number without solution conditions. If the alkali substances are added into negative zeta potential suspension, the particles will receive more negative charge. Next, the suspension with more added acidic solution will become neutral. This acidic addition will result more positive charge, then the plot between zeta potential versus pH curve at low pH will be positive. The isoelectric point a point is where the plot travels through naught zeta potential. The isoelectric point is so important that it can tell the colloidal system with the least stability. The plot between zeta potential and varied pH indicate the place of the isoelectric point with specific pH where the stability of dispersion can be obviously seen. In Figure 2.18, pH 5.5 represents the isoelectric point of the sample. This means that at pH values less than 4 the particles in suspension stay stable. At this pH, adequate positive charge is seen and at pH higher than 7.5 where adequate negative charge is seen. Therefore, pH

values between 4 and 7.5 can cause some problems with dispersion stability due to the zeta potential magnitudes which are in between +30 and -30 mV.
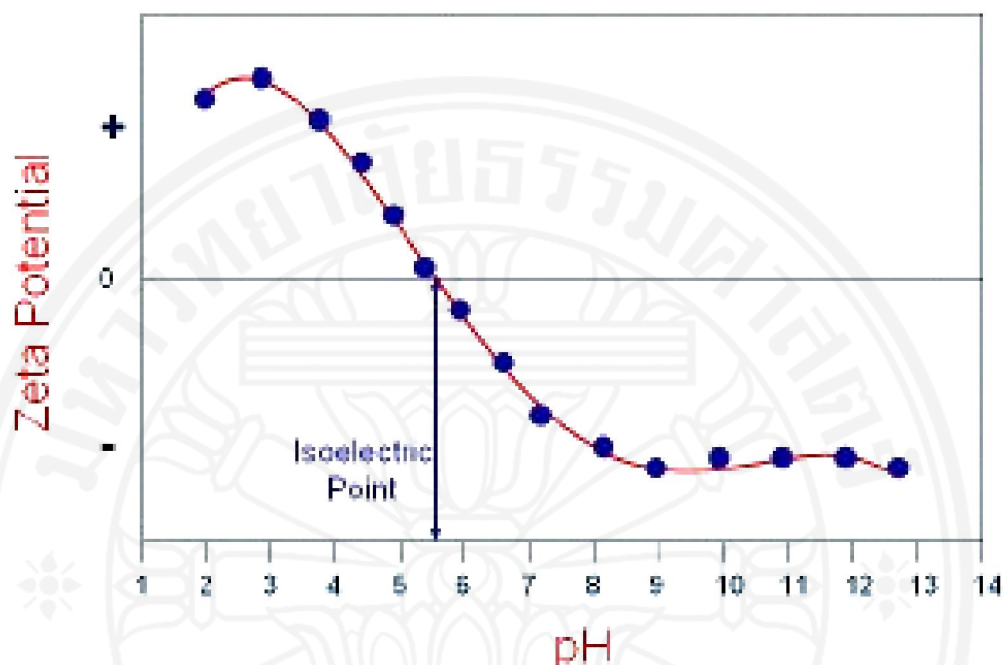
Figure 2.18 The plot between zeta potential and varied pH showing the position of isoelectric point with the pH values where the stability of dispersion can be expected.

2.4.6 Thermogravimetric analysis

Thermogravimetric analysis (TGA) is a thermal analysis method in which materials can be changed in both physical and chemical characteristics. It is normally applied to determine either mass loss or mass gain during the oxidation, decomposition and loss of volatile matters, like moisture.

Wang *et al.* studied the simple method for synthesizing oleic acid coated on magnetite. In order to confirm the performance of the coating of oleic acid on those particles, TGA was used to determine the weight loss of prepared particles by increasing decomposition temperature. The result indicated that there is a significant loss of particle weight in the temperature range of about 150 to 400 ˚C. This decomposition can be related to the capping agent loss (oleic acid) with the percent

loss of about 38.9 and 17.8 for sample S1 and S2, respectively. Additionally, both magnetite samples were prepared by thermal decomposition method at quite low temperature of 140 ˚C in which S1 was synthesized with 10 mL of $N(CH_3)_4OH$ and S2 was prepared with 7 mL of $N(CH_3)_4OH$. Figure 2.19 shows the TGA spectra of both S1 and S2 samples with requisite weight loss at 150 – 400 ˚C and there is a moisture loss at the beginning at around 100 ˚C [23].
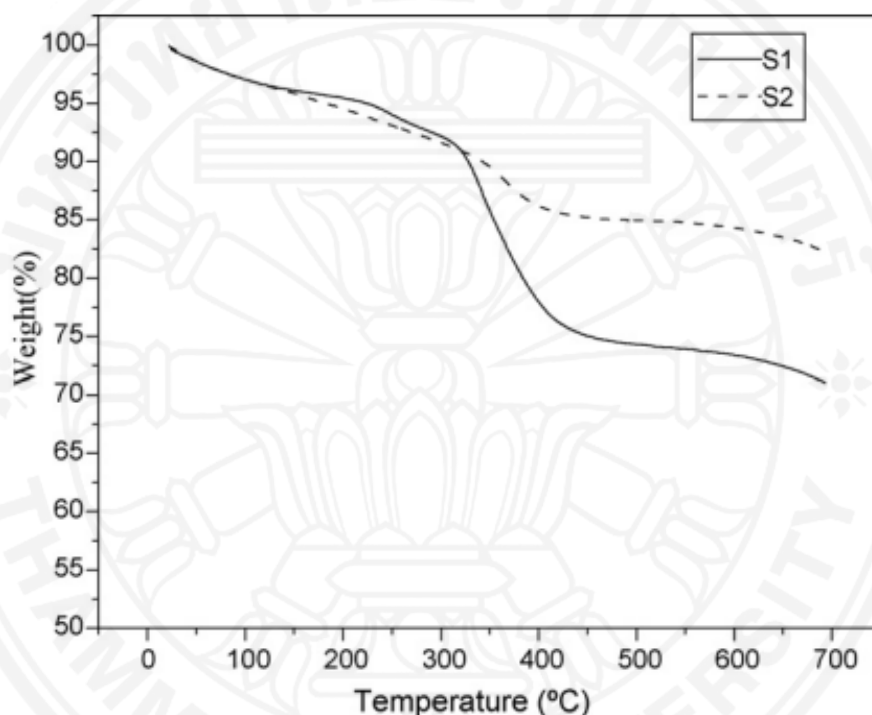
Figure 2.19 TGA spectra of sample S1 (prepared with 10 mL of $N(CH_3)_4OH$) and sample S2 (prepared with 7 mL of $N(CH_3)_4OH$) [23].

Zhang *et al.* synthesized monodisperse magnetite with oleic acid coating by using seed-mediated high temperature thermal decomposition of iron(III) acetylacetonate. TGA results were used to indicate the appearance of coating surfactant (oleic acid) on iron particles. The second weight loss is very crucial because this range represents the loss of capping agent at around 400 ˚C with percent loss of about 17.6% for sample with the size of 7 nm and 4.6% for sample with the size of 19 nm. Figure 2.20 can be concluded that the amount of oleic adsorption inverses with the size of magnetite. Thus, the density of cover layer of oleic acid molecules on iron surface varies with the size of synthesized particles [6].
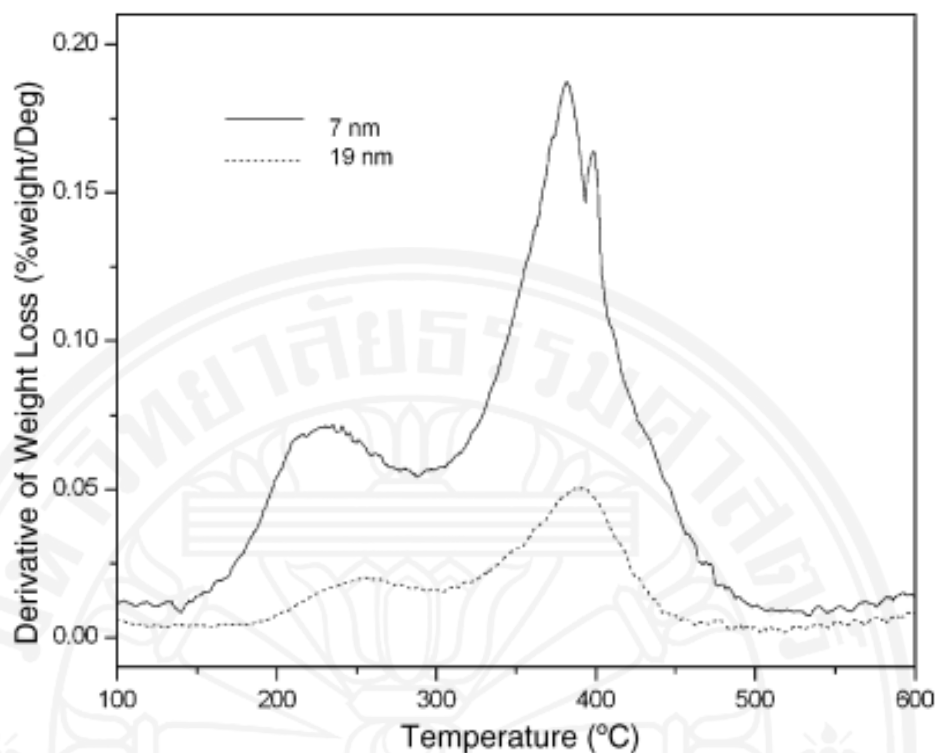
Figure 2.20 TGA of weight loss derivative as the function of temperature of monodisperse magnetite synthesized by thermal decomposition [6].

2.4.7 Inductively coupled plasma

Inductively couples plasma (ICP) is another characterization technique which can be used to detect metals and several non - metals at very low concentration. In oil-related application, ICP can be used to evaluate the metal trace in oil. For example, some metals are limited in biodiesel specification and this instrument should be used to determine the content of those metals.

Bakircioglu *et al.* studied about food application to determine the content of elements. Recently, finding trace metal in edible oil has become interesting for consumers because it defines the quality of oil. In this work, several metals, including Cd, Cr, Cu, Fe, Mn, Ni, Pb and Zn in various kinds of edible oils were studied and inductively coupled plasma optical emission spectrometry (ICP-OES) was used to find trace of those metals in edible oil. Additionally, the oil samples were prepared with acidic wet digestion. The results indicated that in sunflower oil, Fe content is around 0.636 ppm

and 1.090 ppm in olive oil. For heavy metals, like Cd and Cr, there are 0.050 and 0.078 ppm for sunflower and olive oils, respectively. In case of Cr, there are 0.228 and 0.012 ppm for sunflower and olive oils, respectively [29]. This information is very important for consumer to consider buying edible oil with less heavy metal content. Since this work uses iron oxide as adsorbent to adsorb free fatty acid in oil, it is very significant to find the iron trace after adsorption procedure and ICP is very suitable to use for determining the iron trace in oil [24].

2.5 Interaction between iron oxide magnetic nanoparticles and free fatty acids

In preparation of MNP, it is a usual procedure to modify MNP surface by using various functional groups. One of the most common groups is the carboxylic acid group, like free fatty acids, because it has been characterized that the carboxylic acid group can easily bind onto the MNP surface due to the polar nature of the carboxylic group and also that of the MNP. Carboxylic compounds, such as oleic acid, has been widely used as surfactant coating in the preparation of magnetic nanoparticles in order to avoid the agglomeration of MNP particle and provide monodisperse magnetic nanoparticles which will have drawn attention in many applications especially in biomedical applications such as the separation of bio-molecule, target-drug delivery, hyperthermia treatment for cancer and DNA detection. Thus, the interaction of complex formed between iron oxide magnetic nanoparticles and free fatty acids, like oleic acid, should have been studied to confirm the existence of free fatty acids on metal surface.

Lyudmila *et al.* directly studied about the impacts of iron oleate complex on iron oxide nanoparticles formation and reported about the possible structure of iron oleate complex which simply synthesized by interacting between Fe(III) chloride and sodium oleate. This research also studied the effects of post-synthesis treatment on the iron oleate complex. This can offer the insight key of the nanoparticle synthesis through the Fe oleate methods. FTIR can be used to study the formation of Fe-oleate complex. FTIR spectra were recorded on a Nicolet spectrometer. The samples were evaporated using chloroform on the KBr disk. There are four different categories of

coordination modes (Figure 2.21) which can be expected for metal carboxylates, including ionic, unidentate, bridging bidentate and chelating bidentate [25].
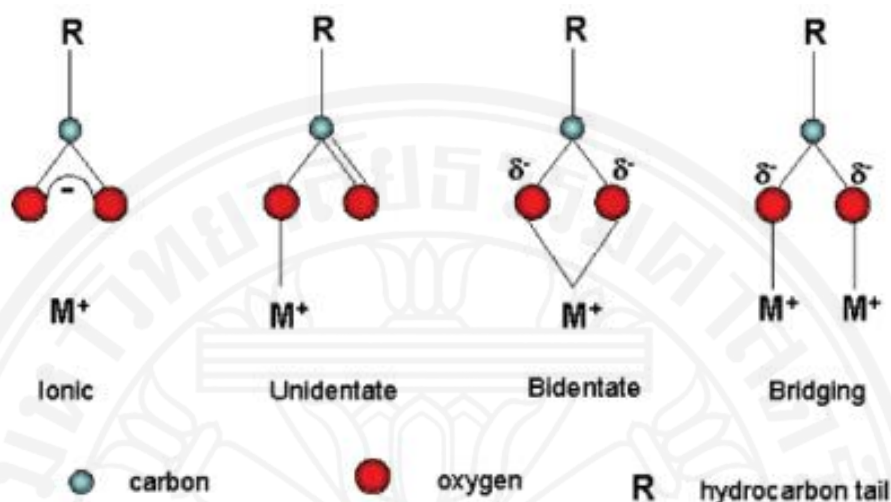
Figure 2.21 Four coordination modes of metal carboxylate. For simple illustration, the monovalent metal is shown instead of trivalent [25].

Both asymmetrical vibrations in the ranges of 1650 - 1510 cm^{-1} and symmetrical vibrations in the range of 1400 - 1280 cm^{-1} are the characteristic peaks for metal carboxylate. Figure 2.22 indicates oleic acid spectrum and two Fe oleates as metal carboxylates, which were synthesized and dried at the two different temperatures in vacuum. 30°C (FeOl-1) and 70°C (FeOl-2). Both Fe oleate spectra have many obvious peaks in the $v(COO^-)$ range such as 1711, 1607, 1519 and 1444 cm^{-1}. The 1711 cm^{-1} band is referred to either the carbonyl group of oleic acid or the asymmetric vibrations of unidentate carboxylate although the second of the two is less common. C=C group can be seen at 1608 cm^{-1}. But, this interpretation of this band may be incorrect because of the absence of this band in oleic acid and in sodium oleate. For non-conjugated compounds, 1660 - 1640 cm^{-1} of C=C stretching vibration shows quite weak band. This range is not often seen due to the overlapping with strong carbonyl vibrations or the trans-symmetry of the double bond. Therefore, 1608, 1519, and 1444 cm^{-1} of vibration frequencies should be concluded as carboxylate groups.

The differences at $v(COO^-)$ bands or wave number separation, Δ, in the range of 1300 - 1700 cm^{-1} region can be applied to predict coordination modes of metal carboxylate. Briefly, a unidentate has $\Delta > 200$ cm^{-1} whereas chelating bidentate has $\Delta < 110$ cm^{-1}. Wave number separation between 140 and 200 cm^{-1} is bridging bidentate. The wave number separation of Fe oleate in this research between two characteristic bands at 1519 and 1444 cm^{-1} is 75 cm^{-1}, interpreted as bidentate. Because the 1444 cm^{-1} band may result from overlap of the $v(COO^-)$ stretching and $\delta(CH_2)$ scissoring bands, its position can be unreliable. The 1443 cm^{-1} shoulder peak is around 1415 cm^{-1}, resulting 104 of Δ and this result is shown as the bidentate coordination as well. The 1608 cm^{-1} peak is a result of band splitting (a doublet at 1608 and 1519 cm^{-1}) due to the presence of two coordination modes which are bidentate and bridging (or unidentate) coordination modes (Δ is either 193 or 165 cm^{-1}, respectively). The dimer of oleic acid is at a very broad shoulder around 3300 cm^{-1} in the FTIR spectra of oleic acid and FeOl-1. The dimer band is absent in the FeOl-2 spectrum because of the dimer dissociation of the oleic acid while it was heated at 70°C.
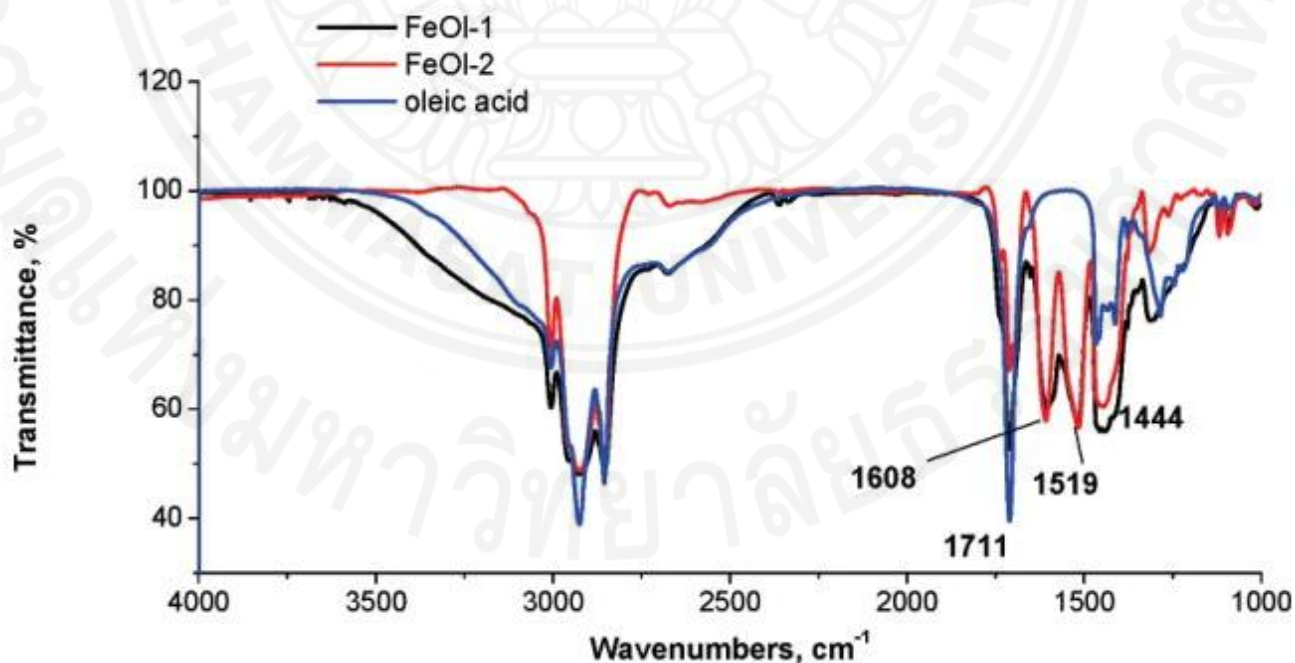
Figure 2.22 Oleic acid spectra and Fe oleate spectra, which are dried at different temperatures, including 30°C (FeOl-1) and 70°C (FeOl-2) [25].

40

FeOl-3 is the iron oleate which was washed twice with ethanol and acetone and dried at 30°C. The FTIR spectrum changes drastically in Figure 2.23. There is no band at 1711 and 1608 cm^{-1} and it shows two vibrational frequencies at 1527 and 1436 cm^{-1}. The strong band at 1711 cm^{-1} can be seen in sample with ethanol wash because oleic acid can be formed by hydrolyzing sodium oleate during the reaction. In this sample, bidentate coordination ($\Delta = 91$ cm^{-1}) of the oleate is observed. The removal of free oleic acid impurity with ethanol gives the higher degree of freedom in Fe oleate. Moreover, the acetone wash sample is not different from the ethanol-washed sample. After being cleaned by acetone, a waxy solid of Fe oleate is shown. It means that some impurities are washed out due to the acetone extraction. The 3589 cm^{-1} sharp band of FeOl-3 is from the free OH group of ethanol, whereas the broad band at about 3270 cm^{-1} is the characteristic of the OH group association. The incorporation of ethanol in the Fe oleate complex can be confirmed by the presence of these bands. The insertion of alcohol into the metal carboxylate structure had been reported earlier. At 70°C, this drying of FeOl-3 shows the removal of non-ethanol molecule, while ethanol molecules still appear in the iron oleate.
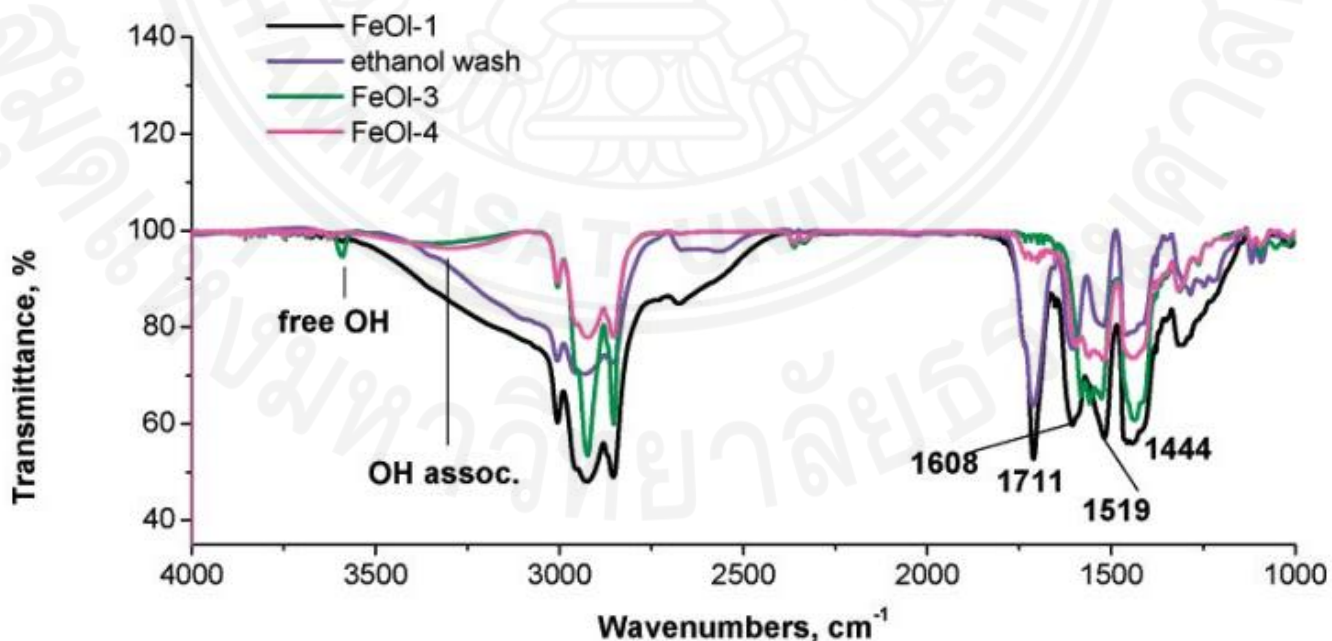
Figure 2.23 FeOl-1 represents the spectra of Fe oleate after being extracted with ethanol and acetone and dried at different temperatures, including 30°C as FeOl-3 and 70°C as FeOL-4, and ethanol-wash, respectively [25].

Zhang *et al.* reported the simple procedure to prepared monodisperse oleic acid-capped magnetite nanoparticles with the size of 4 and 7 nm by thermal decomposition and adjusting the degree of alkalinity of the reaction system. Actually, there are several methods used to produce these particles, including co-precipitation, thermal decomposition and hydrothermal. Thermal decomposition is one of the facile methods which an organic metal precursor is used. The disadvantages of thermal decomposition of organometallic precursors are toxicity, expensive cost of precursor and high reaction temperature, usually ranging from 250 to 320°C. For this mentioned research, an oleic acid coated on magnetite nanoparticles using $(NH_4)_2Fe(SO_4)_2 \cdot 6H_2O$ or $FeSO_4 \cdot 7H_2O$ as the raw material at a quite low temperature of 140°C for 1 hr and using the dimethyl sulfoxide (DMSO) to oxidize Fe^{2+} precursor is simply synthesized. In addition, 25% (w/w) $N(CH_3)_4OH$ was used as alkalinity source and was varied to 10 mL for S1 and 7 mL for S1 [6].

In order to study the presence and function of oleate in the particles, Fourier transform infrared spectrometer (FTIR) was carried out to observe the synthesized magnetite nanoparticles. The FTIR spectra of bare magnetite nanoparticles are also shown as a comparison. In Figure 2.24, the wide band of O-H vibrations at 3130–3630 cm^{-1} is indicated. At 580 cm^{-1}, the characteristic peak of Fe-O is observed for all samples. It can be clearly seen that synthesized magnetite nanoparticles show more characteristic peaks at the range of 1000 - 3000 cm^{-1}. The sharp bands at 2924 and 2851 cm^{-1} are corresponding to the asymmetric and symmetric C-H vibrations of the methylene groups and 1560 and 1443 cm^{-1} are corresponding to the asymmetric and symmetric COO^{-} stretching, respectively. According to the FTIR spectra, the coating of oleic acid on the surface of magnetite particles can be confirmed. Moreover, the wave number separation (Δ) between asymmetric and symmetric COO^{-} stretches, which can be forecast the coordination mode of carboxylate (Fe-oleate), is 117 cm^{-1}. This value can be represented to chelating bidentate.
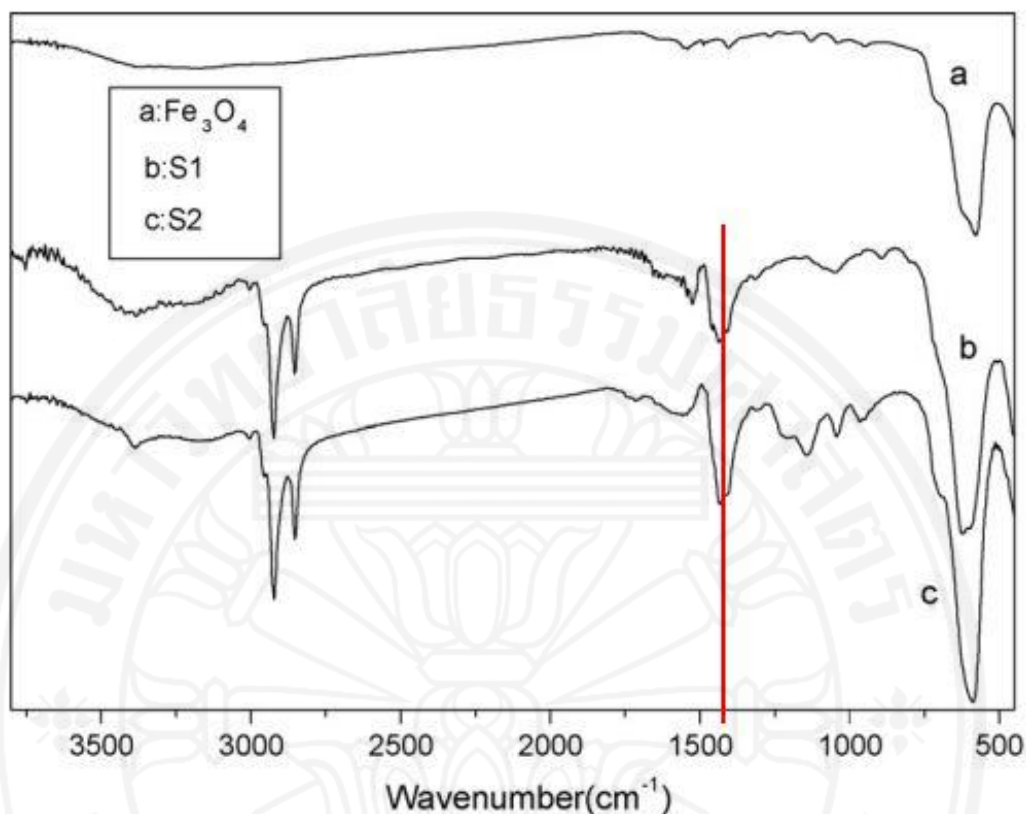
Figure 2.24 (a) is bare magnetite spectrum, (b) is sample S1 with 10 mL of N(CH₃)₄OH) and (c) is sample S2 with 7 mL of N(CH₃)₄OH [6].

Manuel *et al.* reported the deacidification of fatty acids using iron oxide nanoparticles and its application. The separation of fatty acids from ethanol-hexane and vegetable oils using iron oxide magnetic nanoparticles (MNP) was studied. The experiment was studied at room temperature using equilibrium batch and the influence of reaction time and concentration on the adsorption of OA from ethanol-hexane as organic solution was observed. FTIR characterization of the OA-MNP gives the covalent bonding of the carboxylic group onto the MNP surface in the coordination mode of chelating bidentate and/ or bridging bidentate. Figure 2.25 shows FTIR spectra of the MNP before and after the OA adsorption. They assure that the adsorption of OA is through chemical interactions (Figure 2.26) between the carboxylic groups and the iron oxide particles. The vibrational band of the Fe-O bond of the iron oxide core is at 590 cm⁻¹ and the bands of the OH groups are assigned at 3420 and 1637 cm⁻¹. The appearance of the C-H stretching bands at 2926 and 2850 cm⁻¹ together with the two

asymmetrical and symmetrical carboxylate vibrations at 1524 and 1402 cm^{-1} confirm the adsorption of OA on iron for Fe_3O_4@OA sample. The wave number separation (Δ) is 122 cm^{-1}. This value suggests that oleic acid is on the surface of Fe_3O_4 particles by covalent bonding between a carboxylate (COO^-) and Fe atom as it can be seen in Scheme 1. The separation of the carboxylate stretching bands can be interpreted as a chelating bidentate and/or bridging coordination [26].
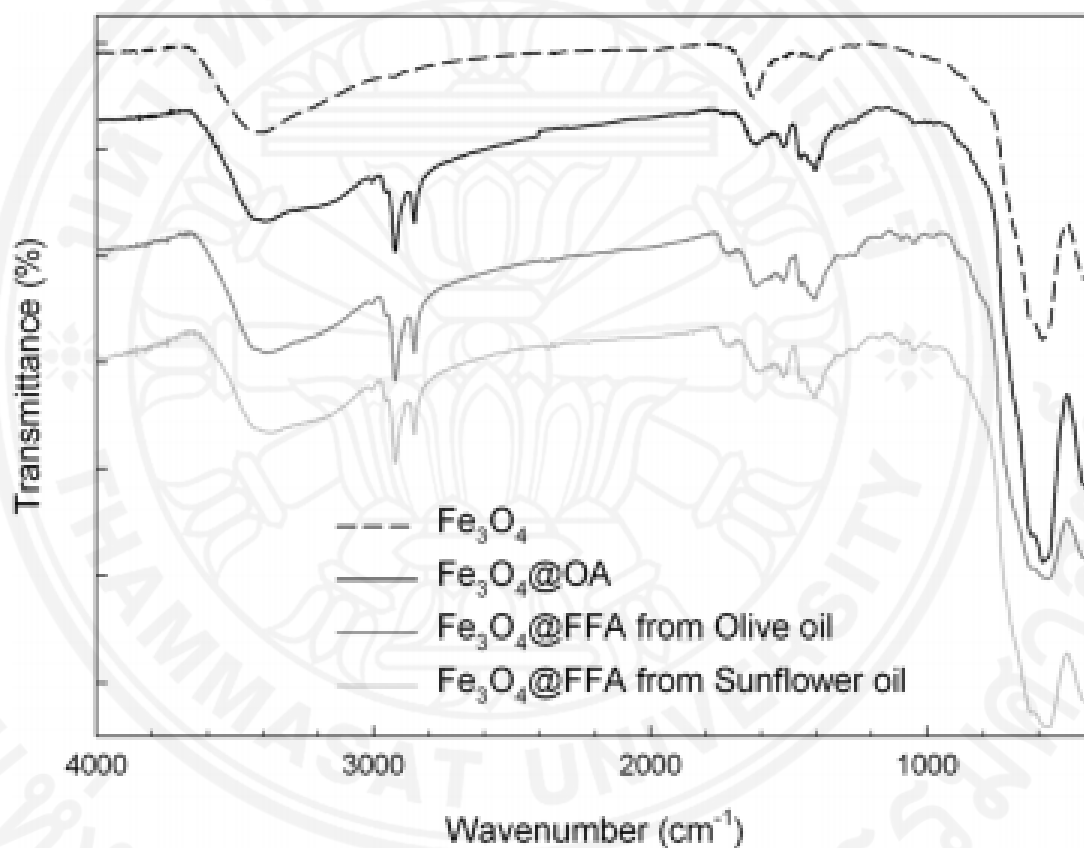
Figure 2.25 FTIR spectra of fresh Fe_3O_4 and Fe_3O_4 coated with OA which was separated from ethanol - hexane solution (Fe_3O_4@OA), and separated from olive and sunflower oils (Fe_3O_4@FFA) [26].
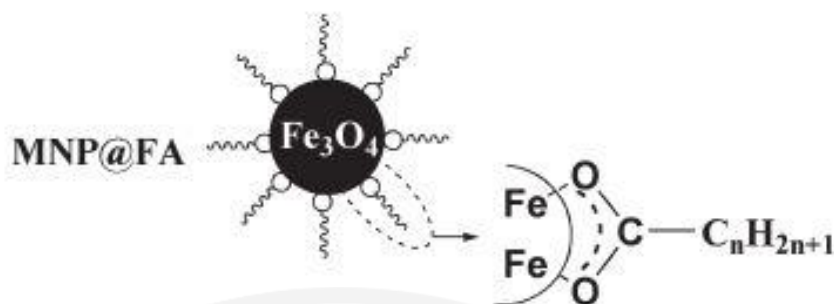
Figure 2.26 The illustration of the interaction between MNP and fatty acid [26].

Ling *et al.* revealed the synthesis of oleic acid coating on the monodisperse magnetite (Fe_3O_4) nanoparticles in order to reveal the interactions on surface between the oleic acid, known as surfactant, and magnetic magnetite. Magnetite was obtained with the size of 7 and 19 nm and the particles were coated with specific surfactant which is oleic acid (OA). The experiment was carried out by thermal decomposition of metal precursor which is iron(III) acetylacetonate or $Fe(acac)_3$. The density of oleic acid on metal oxide particle's surface significantly determines the size of synthesized Fe_3O_4. This is because surface coating can lower the interactions among the nanoparticles and this result can be observed from magnetic characterization of nanoparticles, like VSM. After the reaction was carried out, magnetite nanoparticles were washed many times with ethanol to remove free oleic acid and particles were then heated and obtained as dry powder. The temperature used to heat is 150 °C at a rate of 10°C/min in order to assure the dryness for 2 hr [6].

Fourier transform infrared measurement was carried out to study the interaction of synthesized particles in which all spectra of the nanoparticles were recorded with a Bruker spectrometer. The synthesized powders were mixed and grounded with KBr and they were compressed as a pellet to be recorded their spectra. A few drops of pure oleic acid were mixed with KBr and compressed at 20000 psi where collected spectra were used as a reference. To reveal the mechanism of this adsorption, the neat oleic acid and OA-Fe_3O_4 nanoparticles which were coated with oleic acid were studied. Figure 2.27 shows the general FTIR spectrum of the neat oleic acid (a) and Fe_3O_4 nanoparticles which were coated with oleic acid (b). In curve (a), two strong bands at 2924 and 2854 cm^{-1} were assigned to the asymmetric CH_2 stretch and the symmetric CH_2 stretch, respectively. The significant peak at 1710 cm^{-1} was attributed from the

presence of the C=O stretch while the band at 1285 cm^{-1} represented the C-O stretch. The O-H in-plane and out-of-plane bands showed at 1462 and 937cm^{-1}, respectively [6].
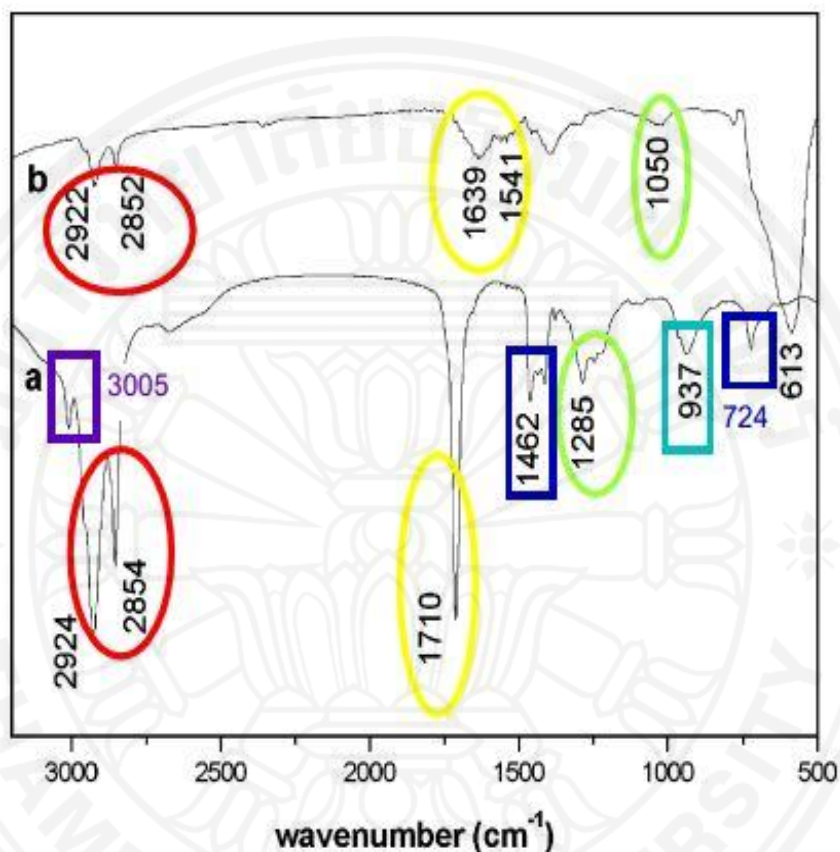
Figure 2.27 FTIR spectra of (a) pure oleic acid, (b) Fe$_3$O$_4$ nanoparticles which was coated with oleic acid (OA) [6]

In the curve (b), the asymmetric CH$_2$ stretch and the symmetric CH$_2$ have been moved to 2922 and 2852 cm^{-1}, respectively. The reason behind this shift is that the absorbed OA surfactant molecules were attached to the metal surface. As a result, these two bands moved to lower frequency. It revealed that the chains of hydrocarbon are in the monolayer surrounding the nanoparticles with a close packed crystalline state. It is worth observing that the C=O stretch band of the carboxyl group showed at 1710 cm^{-1} in the curve (a) and was absent in the curve (b) which is the coated nanoparticle spectrum. According to the presence of two new bands at 1541 and 1639 cm^{-1}, these two bands were assigned to the characteristic of the asymmetric v_{as}(COO$^-$) and the

symmetric v_s(COO-) stretch [25]. These bands can explain the bonding pattern of the coating surfactant on the metal surface which was a combination of molecules bonded symmetrically and molecules bonded at an angle to the surface. C-O single bond stretching was strongly adsorbed at 1050 cm^{-1}. These results indicated that OA were in chemisorptions on the Fe_3O_4 as a carboxylate.

Theoretically, the carboxylate head and the metal atom can interact with four different bonding patterns, including ionic interaction, monodentate, bridging bidentate and chelating bidentate. Wavenumber separation, abbreviated as Δ, between the v_{as}(COO$^-$) and v_{as}(COO$^-$) bands can be applied to differentiate the class of the mentioned interaction between the carboxylate head and the metal atom. The biggest difference in wave number, Δ, in the range of 200-320 cm^{-1} was referred to the monodentate. In contrast, the smallest difference in wave number, Δ, in the range of <110 cm^{-1} was related to the chelating bidentate. Wave number in the medium range around 140-190 cm^{-1} represents the bridging bidentate. The wave number separation in this previous research, (1639-1541 = 98 cm^{-1}) can be described as chelating bidentate, where the interaction between the carboxylate and Fe atom was covalent bonding [6].

Alexandr *et al.* studied the temperature-based synthesis of PbTe nanoparticles and their interaction with surfactant (oleic acid) which was produced by a high temperature solution phase (HTSP). Both diphenyl ether and squalane were used as high-boiling heat-transfer agents. Interaction between OA and PbTe nanoparticles was studied by using Fourier transform infrared spectroscopy (FTIR). The results from this previous work revealed that oleic acid was bonded to the particles symmetrically through carboxyl groups. Moreover, the boding patterns interpreted by wave number separation were both bridging bidentate and chelating bidentate. The strong coordination made the particles stable against oxidation due to monolayer of oleic acid coating [27].

The significant differentiation between the FTIR spectra of free oleic acid and oleic acid coated on nanoparticles is the absence of 1710 cm^{-1} strong peak which is referred to the C=O stretching mode. This disappearance cause the two new band splitting,

including the asymmetric $v_{as}(COO^-)$ stretch at 1525–1560 cm^{-1} and the symmetric $v_s(COO^-)$ stretch at 1400 cm^{-1} due to C=O bond dissociation. The confirmation of the disappearance of the free oleic acid and persuade the result to be forecast that the particles are enclosed by a pretty dense oleic acid monolayer. The wave number difference between the asymmetric $v_{as}(COO^-)$ and symmetric $v_s(COO^-)$ bands can be used to anticipate the carboxylate coordination modes on the nanoparticle surfaces. In this case, symmetric $v_s(COO^-)$ stretches are assigned at 1400 cm^{-1} and both at 1525 and 1559 cm^{-1} refer to asymmetric $v_{as}(COO^-)$ stretches. These asymmetric stretching peaks have split and revealed that carboxylic group interacts with PbTe surface atoms with two different coordination modes, and the predominant interaction is classified by a more strong peak at 1525 cm^{-1}of asymmetric COO$^-$ stretching (as shown in Figure 2.28 b) [27].
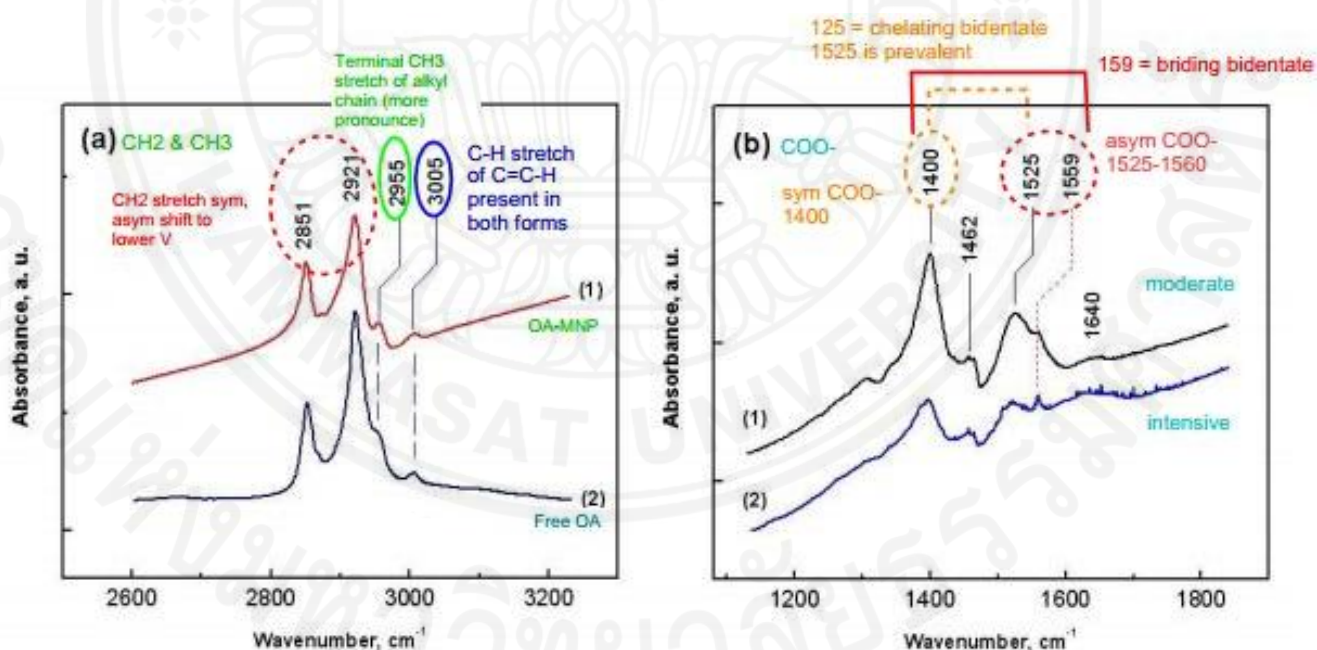
Figure 2.28 FTIR absorption bands of (a) CH$_2$ and CH$_3$ groups including curve (1) represents FTIR absorption spectra of PbTe nanoparticles coated with OA, curve (2) is the spectrum of free OA, and (b) COO$^-$ group including curves (1) and (2) represent FTIR spectra of PbTe NPs with moderate and intensive coating [27].

48

Therefore, the wavenumber difference of $\Delta_1 = 125$ cm^{-1} is referred to chelating with bidentate coordination mode, and $\Delta_2 = 159$ cm^{-1} represents the bridging bidentate coordination mode, associating that chelating interaction is prevalent. Bidentate means two oxygen atoms of the carboxylic group bind with one or two atoms of the nanoparticle (as shown in Figure 2.29). Since Δ values are between chelating ($\Delta \leq$ 110–115 cm^{-1}) and bidentate ($\Delta > 140$ cm^{-1}) interactions, it is not easy to summarize a concrete bonding pattern. Thus, it is important to conclude that mixed coordination with bridging bidentate and chelating interaction are present.
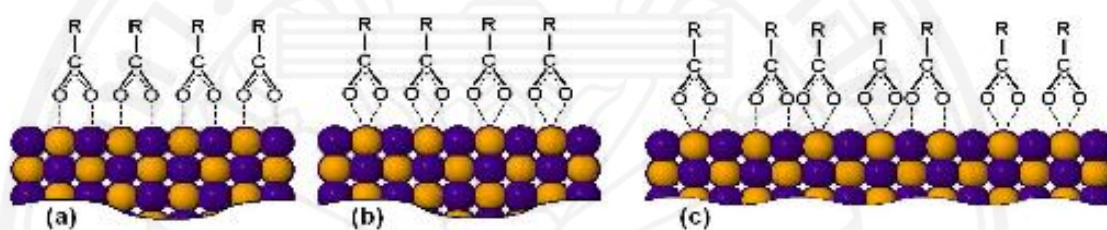
Figure 2.29 Simplified models of: (a) bridging bidentate interaction between the carboxylic group and PbTe nanoparticle, (b) chelating interaction, (c) both bridging bidentate and chelating interaction between the capping layer and nanoparticle [27].

Chapter 3
Methodology

3.1 Introduction

Since the aim of this research is to develop a new technique in removal of FFA from both biodiesel feedstock and biodiesel using MNP for FFA adsorption, a fast and inexpensive means compared to conventional acid treatment should be obtained. Figure 3.1 shows the overview of methodology, which includes the synthesis of MNP by co-precipitation followed by the characterization of the bare MNP, the adsorption of FFA on MNP in both the FFA-spiked oil model and the biodiesel, the regeneration of MNP, and the characterization of used MNP and treated oil in order to analyze the interactions between FFA and MNP, respectively.
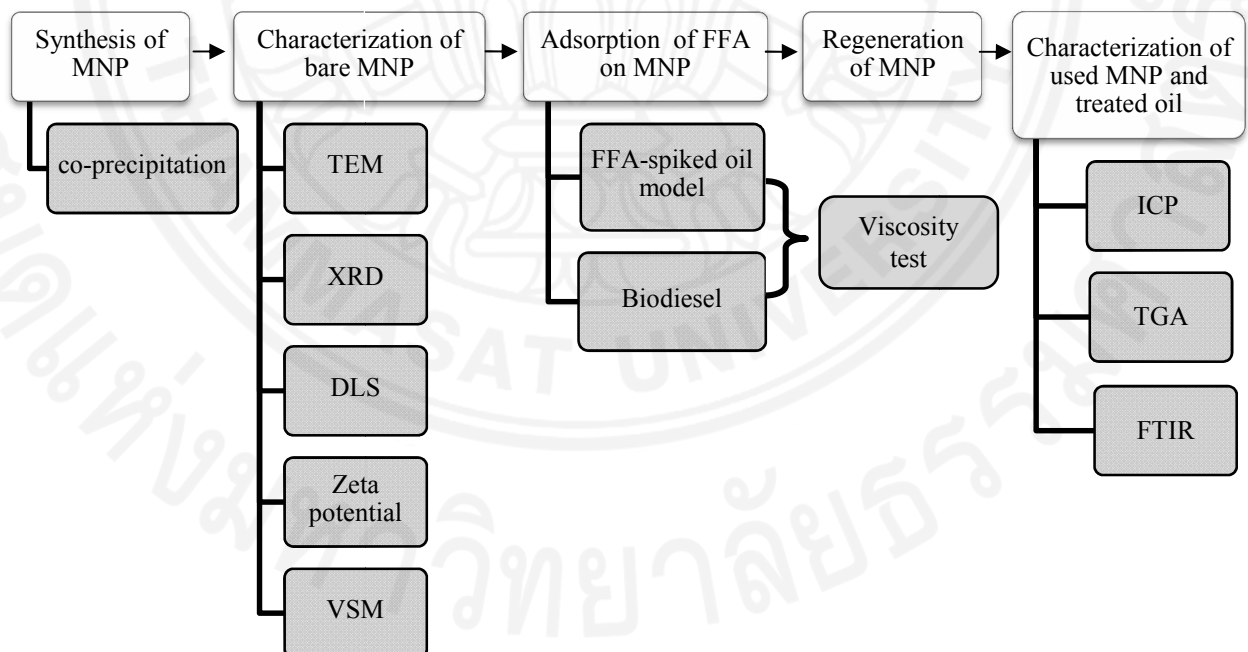
Figure 3.1 The overview of methodology.

3.2 Experimental

3.2.1 Materials

Ferric chloride anhydrous sublimed, ferrous chloride tetrahydrate, 30% ammonium hydroxide, toluene, iso-propanol, potassium hydroxide, sodium hydroxide pellet, phenolphthalein (as an indicator), and oleic acid (as free fatty acid) were purchased from Carlo Erba in analytical grade. Soybean oil used as biodiesel feedstock was purchased from fresh market in Thailand. Concentrated nitric acid and hydrogen peroxide were also purchased from Carlo Erba and were used in acidic digestion prior to analyzing with ICP.

3.2.2 Experimental procedures

3.2.2.1 Synthesis of iron oxide magnetic nanoparticles by co-precipitation method

Nanoparticles of magnetite (Fe_3O_4) were firstly prepared by co-precipitation of an aqueous solution which contains both ferrous and ferric iron salts, and base at room temperature in ambient atmosphere. Both ferrous chloride tetrahydrate ($FeCl_2·4H_2O$) and ferric chloride anhydrous ($FeCl_3$) were used as iron salts, and ammonium hydroxide (30% NH_4OH) was used as base. According to 1:2 mole ratio of Fe^{2+}/Fe^{3+} [20], $FeCl_2·4H_2O$ (2.48 g, 1 mol) was dissolved in reverse osmosis water (50 mL) and $FeCl_3$ (4.08 g, 2 mol) was also dissolved in reverse osmosis water (50 mL), followed by mixing both iron salt solutions under vigorous stirring (300 rpm) for 10 min to form clear aqueous solution. 30% NH_4OH (50 mL) was then slowly added to the mixture under elevated stirring (350 rpm). Black precipitation of Fe_3O_4 could be formed and observed after the first drop of NH_4OH. To complete the reaction, the mixture was continuously stirred for 30 min after the last drop of NH_4OH.

Additionally, to improve the properties of Fe_3O_4 nanoparticle, hydrothermal method was applied by pouring the mixture into a 250 mL Teflon-lined stainless-steel autoclave, sealing tightly and heat at various temperatures (120, 150, 200 and 250 °C) for 4 hr in furnace [21, 22]. The autoclave was cooled down to room temperature. The decantation of black Fe_3O_4 would be carried out by using magnet to remove excess solvents and NH_4OH. The black Fe_3O_4 precipitate was subsequently washed by reverse osmosis water and ethanol alternatively until obtaining pH 7. Fe_3O_4 precipitate products were dried at 60 °C in vacuum oven and crushed by mortar to obtain black powder. The synthesis procedures of Fe_3O_4 are shown in Figure 3.2.

Figure 3.2 Synthesis procedures of Fe_3O_4 using co-precipitation, followed by hydrothermal treatment.

3.2.2.2 Physical characterization of bare iron oxide magnetic nanoparticles

The physical properties of bare Fe_3O_4, including morphology, elemental composition, crystalline structure, particle size and magnetic behavior, would be tested by the following characterization techniques in order to understand the nature of Fe_3O_4 and to forecast the performances of Fe_3O_4 used as adsorbent in FFA adsorption processes. Firstly, transmission electron microscope (TEM) is used to evaluate the shape of Fe_3O_4, the size of Fe_3O_4, and the size uniformity. TEM images were obtained using JEOL, JEM-2010 at an accelerating voltage of 200 keV. The particles were suspended in isopropanol, sonicated for 10 min, and deposited onto a carbon-coated copper grid.

Secondly, X-ray diffraction (XRD) is one of the most common techniques used to characterize the phase purity and crystalline structure of synthesized particles. XRD patterns of dried nanoparticles were obtained using a JEOL JDX-3530 with CuK_α x-ray radiation (λ=1.5406 nm) for $10° \leq 2\theta \leq 80°$ with the step range of $0.02°$. Furthermore, d value of Fe_3O_4 lattice space could be precisely calculated by using reflection peak obtained from XRD pattern with Bragg equation. Owing to the application of Scherrer equation, the crystalline size of Fe_3O_4 could also be determined using the same lattice space and reflection peak from XRD pattern. Additionally, the cluster size and the size distribution of synthesized particles in the actual oil media may be revealed more clearly using the dynamic light scattering (DLS) technique (HORIBA SZ-100) at 25 ºC with the oil viscosity set to 58.5 mPa•s determined using a glass capillary viscometer. Another physical characterization of bare iron oxide magnetic nanoparticles is zeta potential; these particles were analyzed by zeta potential analyzer (Zetasizer ZR, Malvern) in order to determine the stability of particles in dispersion medium (water).

One of the significant features of using iron oxide magnetic nanoparticles is the ease of separation process, using an external magnet for removal of FFA from biodiesel feedstock or biodiesel without involving a high-temperature process, or the need for corrosive resistance equipment. Thus, vibrating sample magnetometer (VSM) would

be used to characterize the magnetic properties of synthesized particles, including the magnetic behaviors, the saturation magnetization, and the remanent magnetization.

3.2.2.3 Adsorption of FFA on MNP in FFA-spiked oil and in biodiesel

In order to determine the optimal condition of FFA adsorption on MNP and analyze some mechanistic understandings on the adsorption process, simulated biodiesel feedstock model was first used. Oleic acid, which is a typical FFA found in biodiesel feedstock such as waste cooking oil and palm oil, was used as a representative FFA for making the simulated biodiesel feedstock. To represent typical biodiesel feedstock, refined soybean oil was chosen and later spiked with various percentages of oleic acid.

The amount of FFA content adsorbed on MNP was quantified by measuring the remaining acid concentration in the solution after magnetic separation of the particles. The FFA content in each oil sample was determined according to the ASTM standard D 684 [15]. In brief, the FFA in oil is titrated with KOH solution using phenolphthalein as an indicator. The procedure for calculation of the acid value and corresponding FFA percentage is shown in Figure 2.7. Optimized loading condition of MNP was initially determined in a batch mode by varying the amount of the MNP loading from 1, 3, 5 and 7 g in 20 g oil with approximately 1% initial FFA concentration. The oil-MNP mixture was ultrasonicated for 30 min followed by continuous stirring for a contact time of 2 hr. The percent FFA reduction from the initial value was then determined for each loading. The kinetic of FFA adsorption was then studied using 25% w/w, MNP/oil with varying contact time (1, 2, 4, 8, 12, 16 hr). The equilibrium contact time determined from the kinetic study was then used in sorption isotherm measurement where FFA concentration was varied from 0.5%, 1%, 2%, 3%, 5% and 7% w/w, FFA/oil. The procedures used are shown pictorially in Figure 3.3.
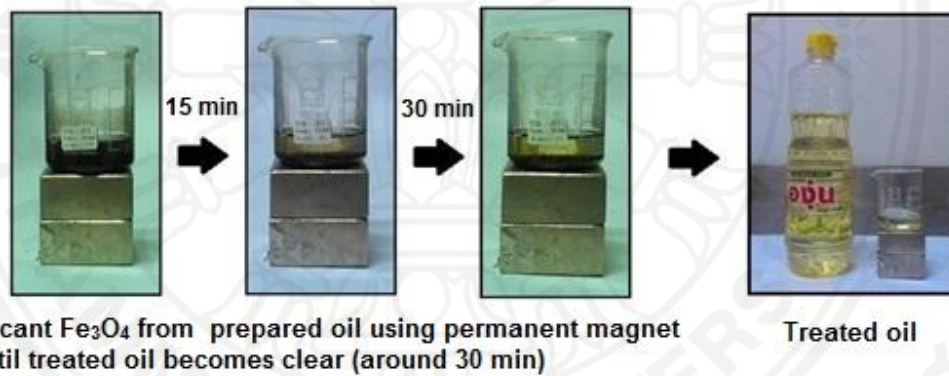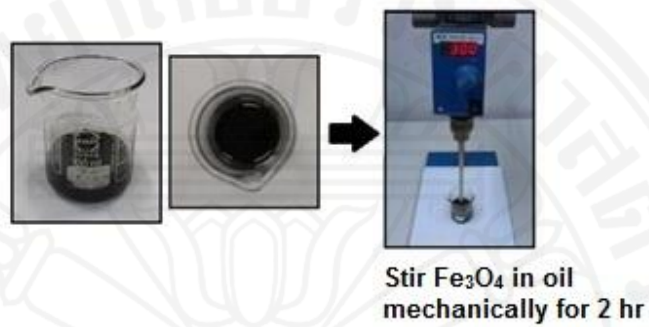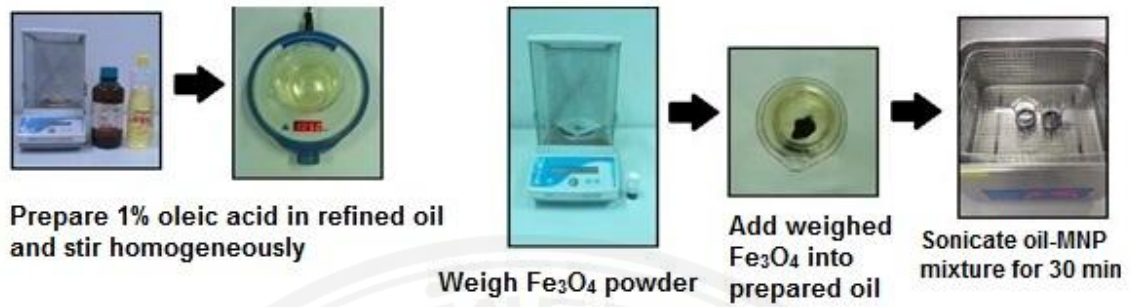
Figure 3.3 Procedures for determination of FFA adsorption.
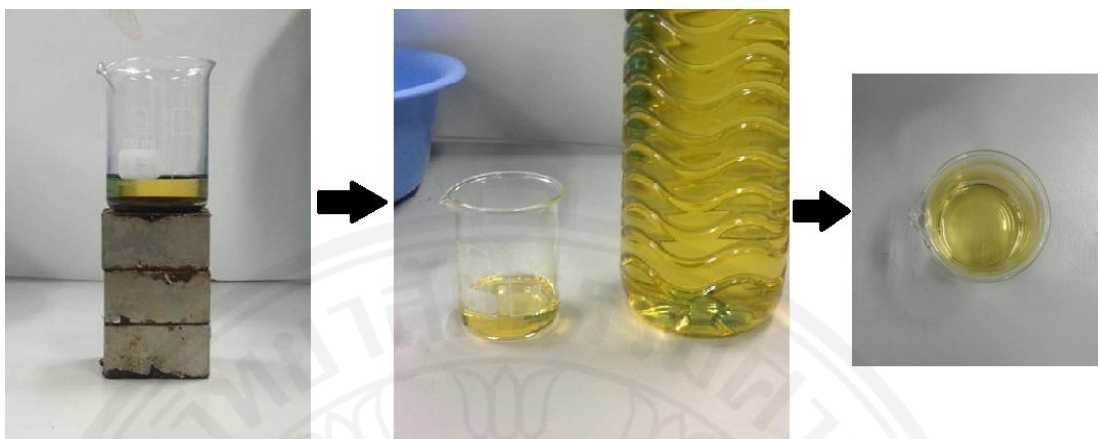
Figure 3.4 Decantation of biodiesel which shows the same appearance as the original.

The adsorption experiment procedures were also performed with real biodiesel as post-treatment process in order that the FFA percentage could be lower and met the ASTM D 6751 criteria [5]. Biodiesel used in this experiment was obtained from the Vehicle Building and Physical Plant Division, Kasetsart University, Thailand with the in existing acid value of 0.82 mg_{KOH}/g_{oil} (or 0.41%FFA). The MNP loading in biodiesel was then determined by directly adding MNP into biodiesel with different loadings which range from 1.5, 4.5, 7.5 and 10.5 g in 30 g oil. The mixture was ultrasonicated for 30 min followed by continuous stirring for a contact time of 2 hr using mechanical stirrer. The equilibrium contact time was also found by using the optimized loading determined from above (25% w/w, MNP/oil) and varying contact times from 10 min, 30 min, 1 hr, 2 hr, 4 hr, 8 hr, and 12 hr. The equilibrium contact time determined from the kinetic study was then used in sorption isotherm measurement where FFA concentration spiked in biodiesel was varied from 0.37% (initial existing value in biodiesel), 1%, 3%, 5%, 7% and 9% w/w, FFA/oil. After performing both the oleic acid-spiked soybean oil, which represents biodiesel feedstock, and real biodiesel, the results from both experiments could be compared in order to study the performance of MNP toward the FFA adsorption in different oil media. Additionally, the treated oil after magnetic decantation shows similar appearance and color as the original oil as shown in Figure 3.5. The time taken for the magnetic decantation is 30 minutes.

3.2.2.4 Regeneration of MNP adsorbent for repeated use

Because of the easy and fast separation of MNP from oil media using external magnet, the used MNP should not be used only one batch and disposed, but it should be regenerated to enhance the reusability of MNP itself. Consequently, the MNP could be used efficiently and the number of MNP regeneration cycles would also be tested. This experiment starts with 1% oleic acid spiked in biodiesel (60 g), 25% MNP loading and 6 hr of contact time. After the first cycle had performed, the oil solution would be carried out to identify the remaining FFA percentage with the same testing method (ASTM D 684) [5]. For desorption and repeated use, oleic acid loaded on MNP would be immersed in 30 mL of 0.1 N NaOH in 50 : 50 v/v ethanol-water and the solution was sonicated for 30 min and mechanically stirred for 90 min [26]. The MNP was then removed by an external magnet and washed with water until pH is neutral. Then, MNP was finally washed with ethanol before drying under vacuum at 50 ºC. The oleic acid adsorption experiments (both adsorption and desorption cycles) were then repeated for the same batch of MNP to identify the number of cycles that MNP can be regenerated and reused.

3.2.2.5 Characterization of the used MNP and the treated oils

Oil medium after being treated with MNP in adsorption experiment will be characterized with ICP in order that iron trace from MNP in both oil mediums (FFA-spiked oil and biodiesel) can be determined. MNP after being used in adsorption experiment will be characterized to confirm the interaction and the attachment between FFA and the iron surface with TGA and FTIR.

First, inductively couple plasma (ICP) is used to determine the iron concentration in both soybean oil and biodiesel after performing the adsorption of FFA on MNP. These oil samples were tested before and after the separation of FFA with MNP to observe the differences in the amount of iron content before and after the use of MNP treatment. To analyze with ICP, the samples prepared by acidic wet extraction of iron. In Figure 3.5, sample prepared by acidic wet digestion for ICP analysis are shown

in which 0.5 g of oil sample were place in 100 mL conical flask, followed by adding 10 mL of the mixed HNO_3-H_2O_2 solution (2:1 v/v) and then leaving the sample for 10 min at room temperature. The sample was then heated at 80 ºC until the sample became clear. After the sample had been evaporated into semidried form, take this form of sample to dissolve in 5 mL of 0.2 M HNO_3, followed by filtering sample through filter paper no. 42. Make up the sample volume to 10 mL in volumetric flask with de-ionized water before taking the sample to be measured with ICP. Figure 3.6 shows products from acidic wet digestion including the semidried sample before filtering and the oil residue after filtering [24].

Weigh 0.5 g of oil in 100 mL conical flask

↓

Add 10 mL of HNO_3-H_2O_2 solution (2:1 v/v) into sample and leave it for 10 min at room temp

↓

heat sample at 80 ºC until sample becoming clear

↓

Take semidried sample to dissolve in 5 mL of 0.2 M HNO_3

↓

Filter sample through filter paper no. 42

↓

Make up sample volume to 10 mL in volumetric flask with de-ionized water

↓

Measure filtrate with ICP
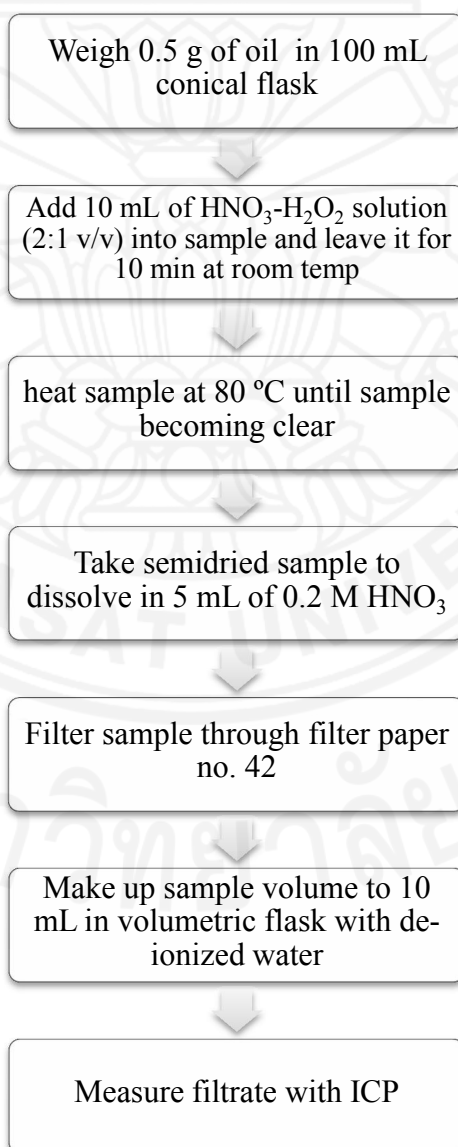
Figure 3.5 Sample preparations by acidic wet digestion for ICP analysis.
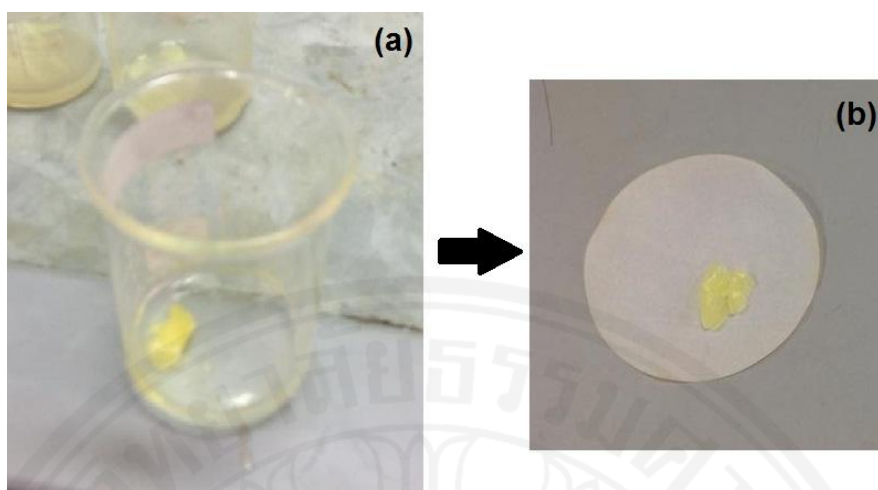
Figure 3.6 The wet acid digestion in which (a) is a semidried sample dissolved in 0.2 M HNO_3 before filtering with filter paper and (b) is a oil residual after filtering.

Secondly, thermogravimetric analysis (TGA) is also normally used to analyze both qualitative and quantitative molecules adsorbed on metal surface by detecting the percent weight loss of each molecule with respect to the change of decomposition temperature. Mettler Toledo Thermogravimetric analyzer with large furnace was carried out by decomposing approximate 5 – 7 mg of sample with 10 °C/min of heating rate up to 600 °C. The samples, including bare MNP, MNP that has been in oil, and also neat oleic acid, were used in this experiment. The results obtained from TGA would be further analyzed which molecules absorb on MNP surface and also the amount of those molecules. Moreover, the amount of absorbed molecules from TGA would be compared to the results from the adsorption isotherm calculation.

Thirdly, Fourier transform infrared (FTIR) spectra were used to characterize the functional groups of samples using a Nicolet iS5 spectrometer in the ATR mode (attenuated reflectance mode). This technique can confirm the interaction of FFA and MNP surface. Additionally, the coordination modes between the carboxylic group and iron oxide particle can be predicted from observing the differences of wave number at symmetric and asymmetric carboxylate vibrations.

3.2.2.6 Determination of kinematic viscosity of oil mediums using the glass capillary viscometer

Viscosity can be normally referred to the resistance of fluid to flow and it was generally categorized into dynamic viscosity and kinematic viscosity. In brief, dynamic viscosity is usually presented in Centipoise (cP) and Brookfield rotational viscometer in Figure 3.7 is useful for this viscosity measurement. Moreover, the dynamic viscosity is more appropriate if the interaction between molecules that can be interpreted in terms of mechanical stress is interested. On the other hand, kinematic viscosity is alternatively employed by recording the time for a fluid sample used to travel through a glass capillary viscometer under gravity force which is shown in Figure 3.8. The kinematic viscosity is generally recommended when the experiment focuses on the fluid motion and the velocity field. Additionally, it can be used to inform about the propagation of the movement by friction. In this experiment, kinematic viscosity was chosen to determine both soybean oil and biodiesel viscosities using Cannon-Fenske Routine glass capillary viscometer where the time taken is recorded and converted into kinematic viscosity, reported in Centistoke units (cSt). In addition, dynamic viscosity (cP) is equal to kinematic Viscosity (cSt) multiplied by fluid density (kg/m^3).

Figure 3.7 Brookfield Rotational Viscometers.
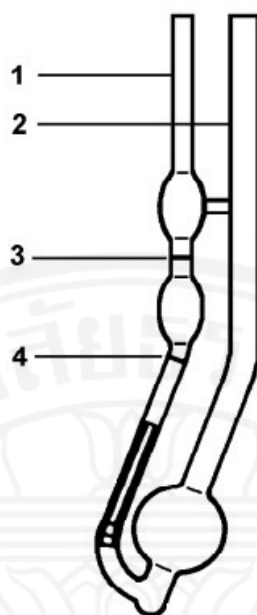
Figure 3.8 Glass capillary Viscometers.

Here are the directions for using Cannon-Fenske Routine glass capillary viscometer and Table 3.1 shows the viscosity range recommendation for the Cannon-Fenske Routine glass capillary viscometer.

1. Suitable solvents were used to clean the viscometer and the viscometer was dried to remove some solvent traces. Generally, organic traces deposited in viscometer should be cleaned with chromic acid or non-chromium cleaning solution.

2. The sample was filtered through a filter or fine mesh screen in case of the presence of dust or other solid materials in the liquid sample.

3. To charge the sample into the viscometer, the viscometer was inverted and suction was applied to tube arm 2, tube 1 was immersed in the liquid sample, and then liquid was drawn to mark 4. The viscometer was turned to its normal vertical position.

4. The viscometer was placed into the holder and it was put into the constant temperature bath. The viscometer was aligned vertically in the bath.

5. The temperature was heated to 40 °C and waited for 15 minutes, or the temperature was heated to 100 °C and waited for 15 minutes, depending on the temperature used to heat the sample.

6. Apply suction to tube 1 and draw the liquid over mark 3.

7. To record the efflux time, the liquid sample was allowed to flow freely through mark 4 and the time for the meniscus to pass from mark 3 to mark 4 was measured.

8. To confirm the recording, a check run may be made by repeating steps 6 and 7.

9. The kinematic viscosity in mm^2/s of the sample was calculated by multiplying the efflux time in seconds with the viscometer constant.

Table 3.1 Viscosity range recommendation for the Cannon-Fenske Routine glass capillary viscometer.

Size	mm^2/s^2, (cSt/s)	Kinematic Viscosity Range mm^2/s, (cSt)		
25	0.002	0.5	to	2
50	0.004	0.8	to	4
75	0.008	1.6	to	8
100	0.015	3	to	15
150	0.035	7	to	35
200	0.1	20	to	100
300	0.25	50	to	250
350	0.5	100	to	500
400	1.2	240	to	1200
450	2.5	500	to	2500
500	8	1600	to	8000
600	20	4000	to	20000
650	45	9000	to	45000
700	100	20000	to	100000

Kinematic viscosity of both soybean oil and biodiesel was measured by using Cannon-Fenske Routine glass capillary viscometer and the efflux times of both samples were recorded in second as indicated in Table 3.2. The efflux times of both oil samples were evaluated by multiplying efflux time with the viscometer constant (mm^2/s^2) of glass capillary viscometer (size 300) in Table 3.1. The result indicated that biodiesel possesses lower kinematic viscosity compared to soybean oil around 7 times and this viscosity property of oil will further affect the performance of MNP adsorption, in which the lower kinematic viscosity could cause higher chance for FFA in oil medium to adsorb on MNP.

Furthermore, the lower kinematic viscosity could possibly cause higher iron solubility so that biodiesel should dissolve iron more easily to become iron ion and result in a high percentage of FFA adsorption. However, in the real experiment, the kinematic viscosity will increase due to the loading of MNP adsorbent, so the kinematic viscosity of oil medium together with MNP will be also determined and discussed. The Figure 3.9 shows the setting up of Cannon-Fenske Routine glass capillary viscometer, size 300 in which the soybean oil was used as oil medium while Figure 3.10 shows glass capillary viscometer in which soybean oil and 25% MNP was loaded and causes the oil medium become black solution.

Table 3.2 The kinematic viscosity obtained from noting the efflux time (s) and multiplying with the viscometer constant (mm^2/s^2).

Types of oil medium	Efflux time (s)	Kinematic Viscosity (mm^2/s)
Soybean oil	181.33±0.57	45.33±0.14
Biodiesel	27.10±0.03	6.78±0.01
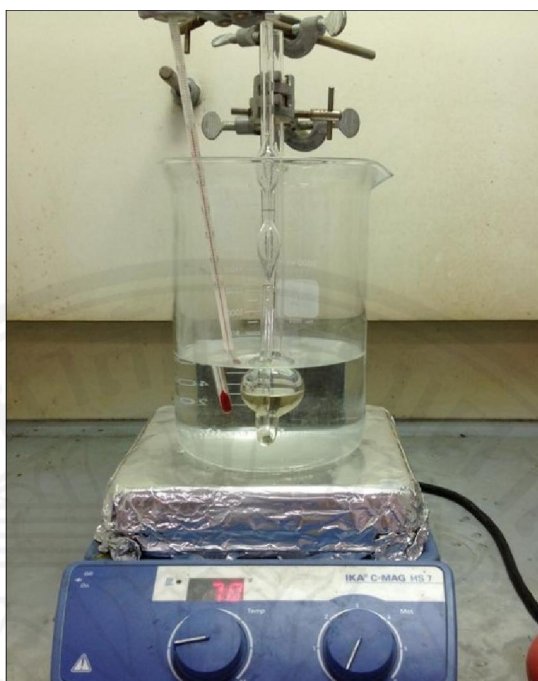
Figure 3.9 The setting up of Cannon-Fenske Routine glass capillary viscometer; size 300 in which the soybean oil was used as oil medium.
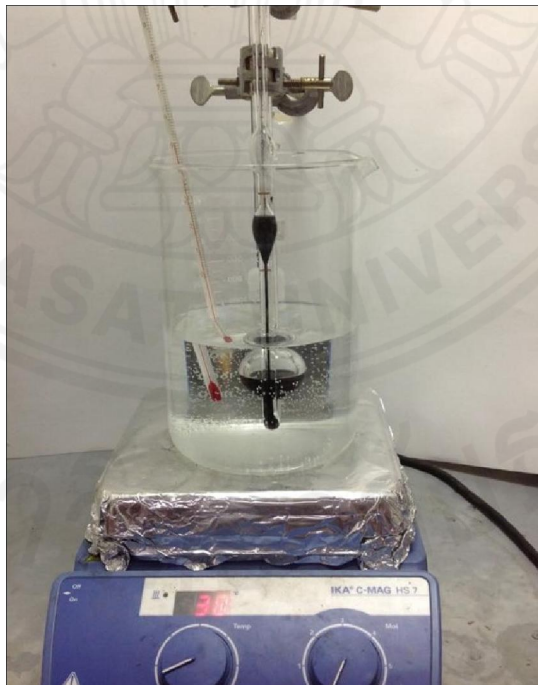
Figure 3.10 The setting up of Cannon-Fenske Routine glass capillary viscometer; size 300 in which the soybean oil with 25% MNP loading was used as oil medium.

Chapter 4
Result and Discussion

This chapter explains and discusses the reasons behind each result from the experimental sections. The results include the physical characterization of iron oxide magnetic nanoparticles, the adsorption of FFA on MNP in FFA-spiked oil as pre-treatment, the adsorption of FFA on MNP in biodiesel as post-treatment, the determination of regeneration cycles, and the characterization of the used MNP and treated oils.

4.1 Physical characterization of synthesized MNP

Before applying the synthesized MNP in FFA adsorption experiment, the MNP synthesized by co-precipitation was characterized to study the physical properties which would further affect to the FFA adsorption performance on MNP, including particle size, its morphology and magnetization behavior.

Firstly, size and morphology of the synthesized nanoparticles were identified using transmission electron microscope (TEM). The TEM image in Figure 4.1 (a) shows that the synthesized MNP are in the nanometer size range with the average particle size of about 10 - 14 nm. Moreover, broad ring ED patterns were obtained from the samples with some spotty ED patterns, shown in the inset, are attributed to the diffraction from crystal planes of Fe_3O_4 and also reflect the differences in the particle sizes of the sample which significantly consist of fine particles. The use of both ferrous and ferric chloride salts in the MNP synthesizing procedures is the reason behind these fine particles. On the other hand, if ferrous salts were only used in MNP synthesizing, the particles would become larger. In Figure 4.1 (b), it is obvious that MNP tends to aggregate and form a larger cluster in various sizes on the order of 200 – 300 nm. Even though TEM image shows that the synthesized particles have size uniformity with quite spherical shape, the cluster particles formed in Figure 4.1 (b) may reduce the capability of nanosize, which can provide more surface area for

adsorption. Normally, it is important to finalize the growth of particle and provide the stability of the surface in order to provide stable particles and retain their high activity and this becomes crucial for many applications except this work. Because the use of other organic compounds, like polymer, to control both steric and electrostatic effects will increase the particle preparing cost and may not provide the surface [16], which can attract and bond with FFA presenting in oil media. Consequently, bare Fe_3O_4 surface is used though the cluster is formed.
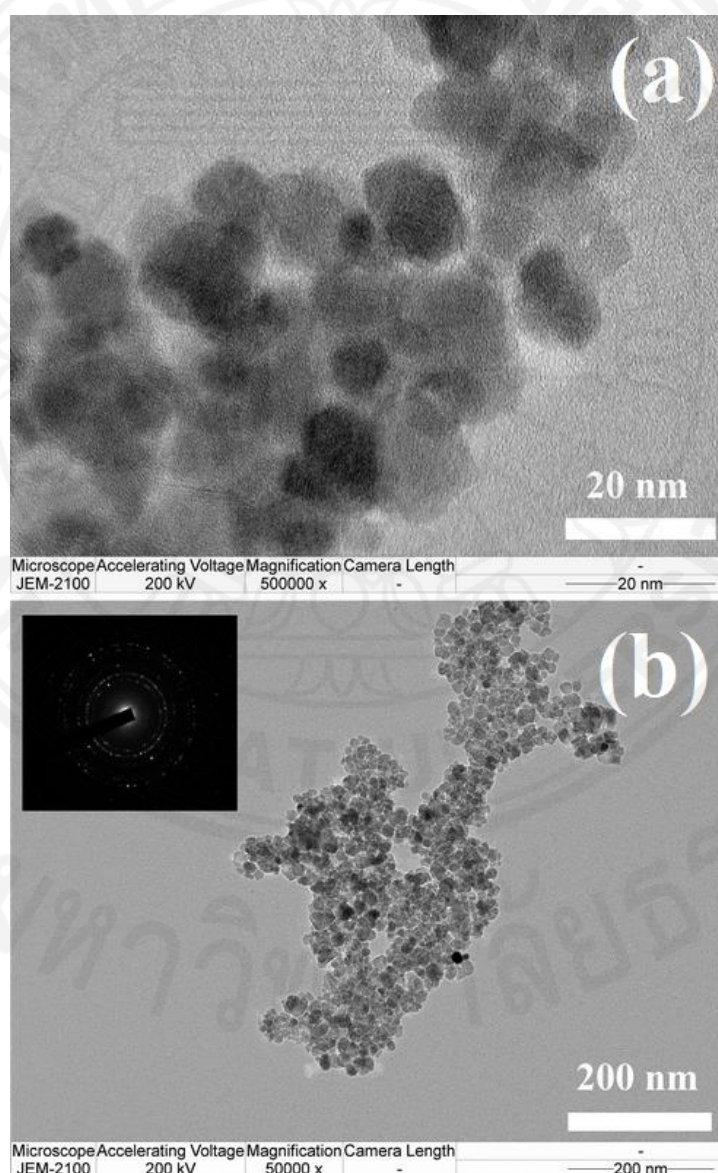
Figure 4.1 TEM images and ED pattern of the synthesized MNP at two different magnifications. The scale bars are 20 and 200 nm in (a) and (b), respectively. Clustered particles can be seen in both images.

Additionally, the cluster size of the synthesized particles in the actual oil media could be revealed more clearly using the dynamic light scattering (DLS) measurement which reveals the hydrodynamic diameter of these clusters in oil media to be about 442 ± 99 nm with 1.425 of polydispersity index. This hydrodynamic diameter is on the similar order of magnitude with the cluster size observed in the TEM images. In addition, while suspended particles in oil were chosen to be measured by DLS, there is the presence of some gravitating particles. Thus, before FFA adsorption experiment, sonication would be applied to the experiment to de-agglomerate the cluster particles.

To confirm this conclusion, X-ray diffraction (XRD) was employed to evaluate and confirm the crystalline structure of iron oxide particles by comparing the experimental and reference diffractograms. In Figure 4.2, the formation of magnetite (Fe_3O_4) was indicated based on the comparison of XRD patterns with the standard pattern of Fe_3O_4. Each peak agrees in positions and intensities with the published Fe_3O_4 pattern (Powder diffraction file, PDF 01-074-1909). The d value of lattice spacing of (311) was evaluated to be 2.524 Å by applying with Bragg equation for the reflection peak observed at $2\theta \sim 35.539°$ (n=1 and λ=1.5406 nm). This evaluated value agrees with the corresponding standard value of 2.532 Å (JCPDS# 19-629) [20]. Generally, it is quite difficult to differentiate Fe_3O_4 from γ-Fe_2O_3 with no precise measurement of d value because γ-Fe_2O_3 and Fe_3O_4 have the similar crystal structure and lattice spacing. In this case, it was concluded that the product composed of a small quantity of γ-Fe_2O_3, based on the appearance of synthesized particles which show brownish color. This is correspondent to the synthesizing procedure without stabilizing the iron oxide surface which causes the oxidation on iron oxide surface. As a result, Fe_3O_4 changes the color to be more brownish and transforms some parts of surface to become γ-Fe_2O_3 with probably reveals lower magnetization compared to pure Fe_3O_4.

Moreover, by applying lattice spacing of (311) with reflection peak at $2\theta \sim 35.539°$ to Scherer equation, crystallite size of magnetic nanoparticles can also be calculated. Using CuK_α x-ray radiation of 1.5406 nm, shape factor (k) of 0.9 and line broadening at half the maximum intensity (FWHM) of 0.614 radians, the mean size of the

crystalline domain can be deduced to be about 13.60 nm, which is corresponded to the particle size observed in the TEM images.
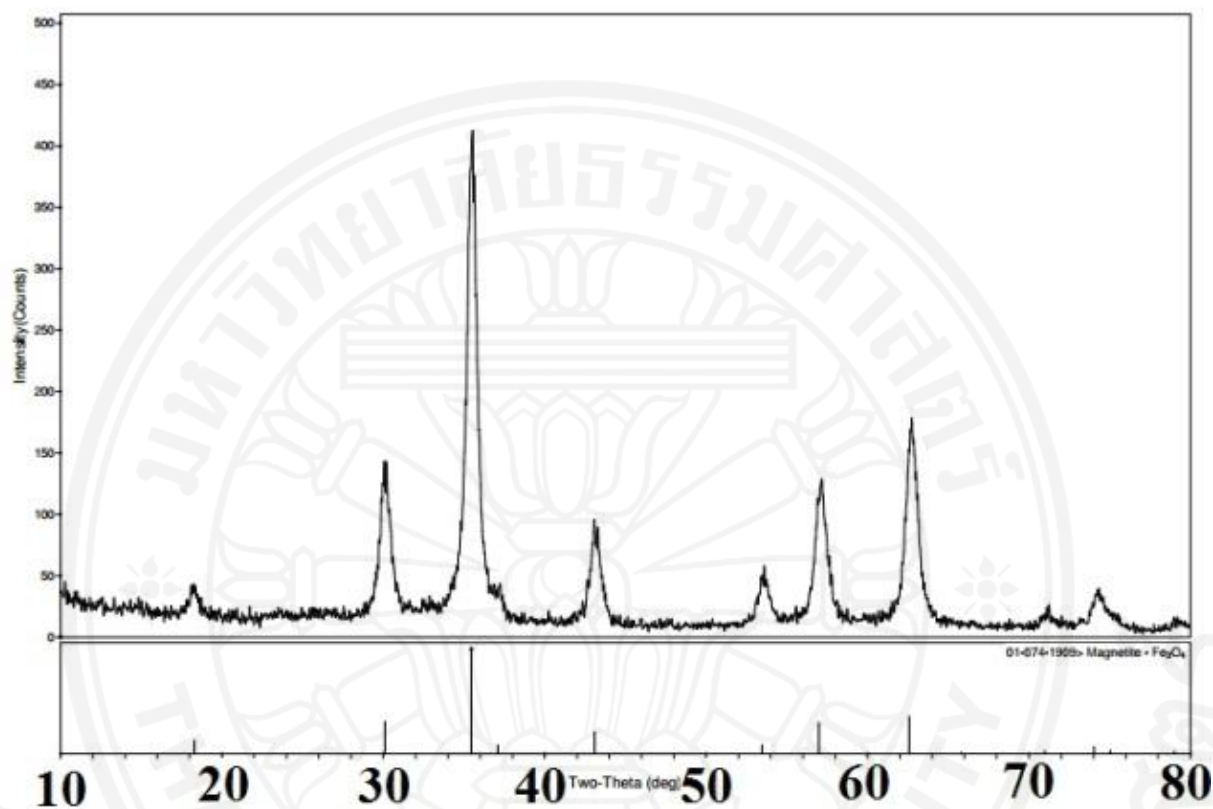
Figure 4.2 XRD patterns of the prepared MNP. Standard diffraction peaks of Fe_3O_4 are presented at the bottom.

One of the important features of MNP particles is the stability of particles in the colloidal system which can be determined using zeta potential value as an indicator. Particles on suspension with a huge negative or positive zeta potential will lead to the electrostatic repulsion with other particles and there is no trend for the particles to stick together. Conversely, particles with snall zeta potential values will have no force to protect the particles not to come together and they will eventually agglomerate. The useful dividing line between stable suspension and unstable suspension is generally considered at either +30 or -30 mV. Particles with zeta potentials more positive than +30 mV or more negative than -30 mV are normally considered stable. Mean zeta potential can be categorized using Laser scattering particle size distribution analyzer. Synthesized iron oxide nanoparticles were measured under room temperature using

water as dispersion medium with 0.895 mPa.s of viscosity, 0.075 mS/cm of conductivity and 3.9V of electrode voltage.
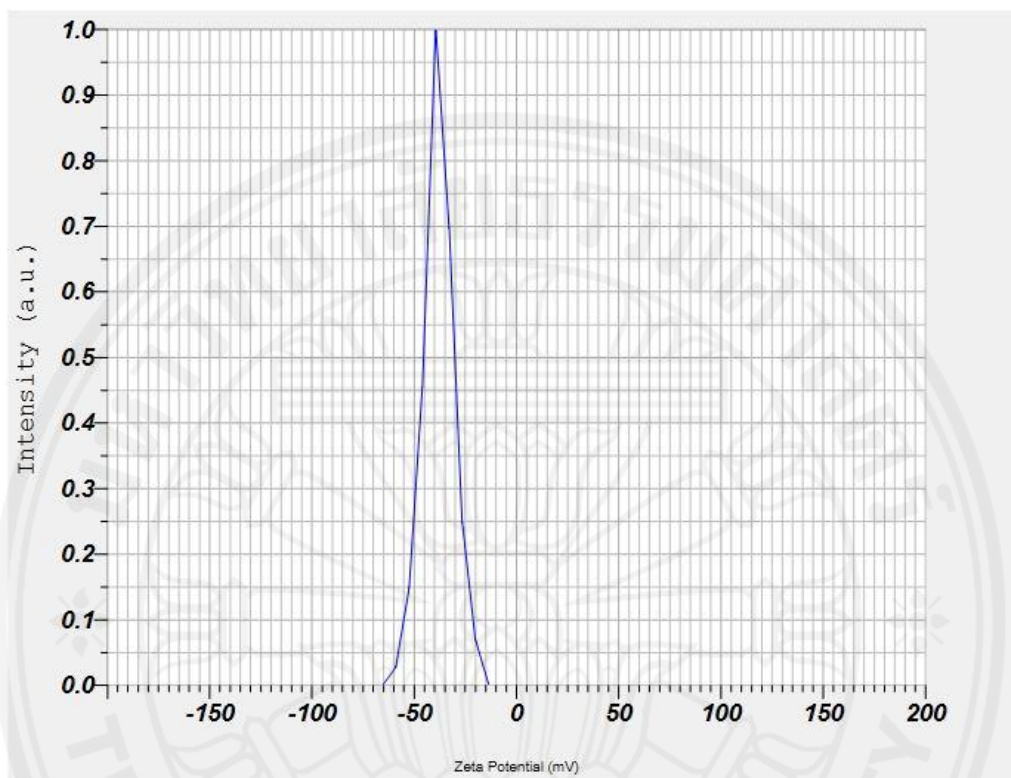
Figure 4.3 Zeta potential of the synthesized MNP in water as dispersion medium at room temperature.

As can be seen from the Figure 4.3, the result indicated that MNP possesses -38.1 mV of mean zeta potential with 0.000295 cm^2/Vs of mean electrophoretic mobility. According to the stability outline in Table 2.7, this zeta potential shows quite large negative magnitude in the range of ±30 to ±40 mV which can be interpreted as moderate stability. It is understandable that the synthesized MNP is not in good or excellent stability range because their synthesized procedure has not involved with the stabilization processes. Thus, bare Fe$_3$O$_4$ surface is used though the particle stability might not be high. In this experiment, it can be observed that after MNP were added to dispersion medium (water), MNP show the suspending on top of the dispersion medium with less agglomeration while the others tend to flocculate and sediment to the bottom of the flask. Moreover, in real adsorption experiment the stability behavior of particles in oil medium can be worse compared to in water medium because of the

higher viscosity from oil medium and it can be also easily noticed after adding MNP particles in oil, they will assemble in the center of oil medium and agglomerate to become a cluster.

Figure 4.4 shows the magnetic properties of synthesized MNP and indicates the superparamagnetic behavior with saturation magnetization (M_S) of 83 emu/g at 300 K. This high value of M_S of the synthesized MNP allows for a strong attraction between particles and easy separation of the magnetic particles after treatment using simple permanent or electromagnet bar. The particles also show very small remanent magnetization of 4.1 emu/g, which is small enough for particles to be easily released from applied magnetic field. Small remanent magnetization are suitable for use in adsorption as they can be easily dispersed for regeneration once the applied magnetic field used for separation is turned off.
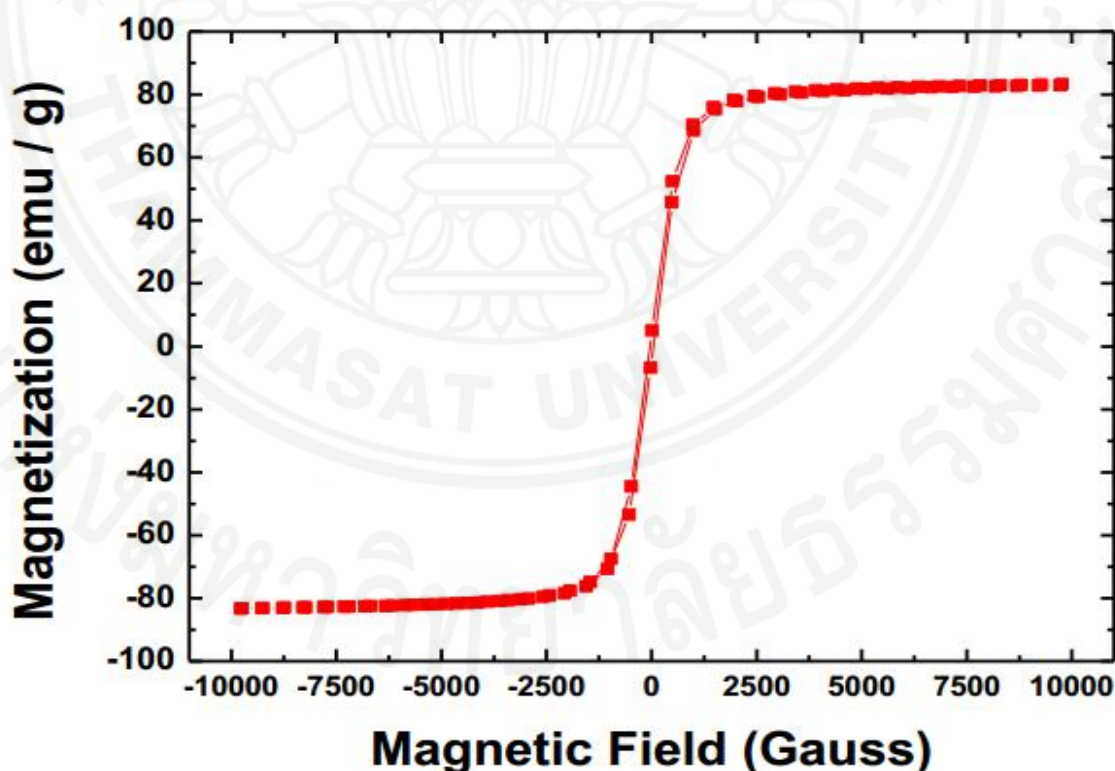
Figure 4.4 Magnetization of the synthesized MNP with saturation magnetization (M_S) of 83 emu/g.

4.2 Adsorption of FFA on synthesized MNP in FFA-spiked oil model as pre-treatment process

In order to evaluate the optimal condition for Fe_3O_4 separation of FFA and to obtain some insight mechanisms on adsorption, 1% oleic acid spiked in commercial soybean oil is used to simulate biodiesel feedstock system. The amount of FFA content adsorbed on MNP was quantified by calculating acid concentration, remaining in the oil, after magnetic removal of the particles. Additionally, this FFA adsorption performance was evaluated in batch mode. Investigations on the effects of %MNP loading and contact times were carried out, and kinetic modeling of FFA adsorption on MNP would also be studied. The optimized loading was firstly determined by mixing different amount of MNP with 1% oleic acid spiked in commercial soybean oil. Before applying oleic acid in commercial edible soybean oil obtained from Thailand's convenient store, %FFA of soybean oil is shown around 0.1128% (0.2246 mg_{KOH}/g_{oil}) which is quite low. The value has become 1.3544% (2.6953 mg_{KOH}/g_{oil}) after applying 1% of oleic acid. This experiment was conducted at room temperature for 2 hr with 250 rpm (using mechanical stirrer) and 30 min sonication in order to de-agglomerate the MNP clusters.

Figure 4.5 shows the percent of FFA reduction as a function of MNP loading in which 5%, 15% 25% and 35% of MNP in 20 g of oil solution were tested. 5% of MNP loading (or 1g MNP in 20 g oil) can reduce FFA presenting in oil solution to only 13.6%. On the other hand, it can be obviously seen that as the amount of MNP loading is increased, the percent FFA reduction increases until the loading of about 25% MNP loading (or 5g MNP in 20 g oil) where the percent reduction seems not to change any further or even slightly reduced. At 25% MNP loading, %FFA presenting in prepared oil solution can be reduced up to 48.9% by continuous stirring within 2 hr. The drop in performance may be due to the increased viscosity of the oil which has made the oil–MNP composite becomes more viscous at large loading amount and cause the difficulty for MNP to contact with FFA due to less diffusion capacity of adsorbents. The increasing of viscosity can be reported in term of kinematic viscosity which can be determined using glass capillary viscometer and the efflux times were

71

recorded in second before multiplying with viscometer constant (0.25 mm^2/s^2 for size 300). The differences in kinematic viscosity of 1% oleic acid spiked in soybean oil (both before and after additions of MNP) are shown in Table 4.1. It is obvious that adding MNP adsorbent can cause higher kinematic viscosity from 45.33±0.14 mm^2/s to 63.17±0.14 mm^2/s and result in the drop of FFA adsorption performance. Consequently, there is no use wasting too much amount of MNP to cause more viscosity with slightly different adsorption efficiency. In addition, 35% of MNP loading can reduce FFA presenting in oil solution to 42.4%. The MNP loading amount of about 25% by weight is therefore chosen for later experiment to investigate other factors contributing to FFA adsorption efficiency on MNP.
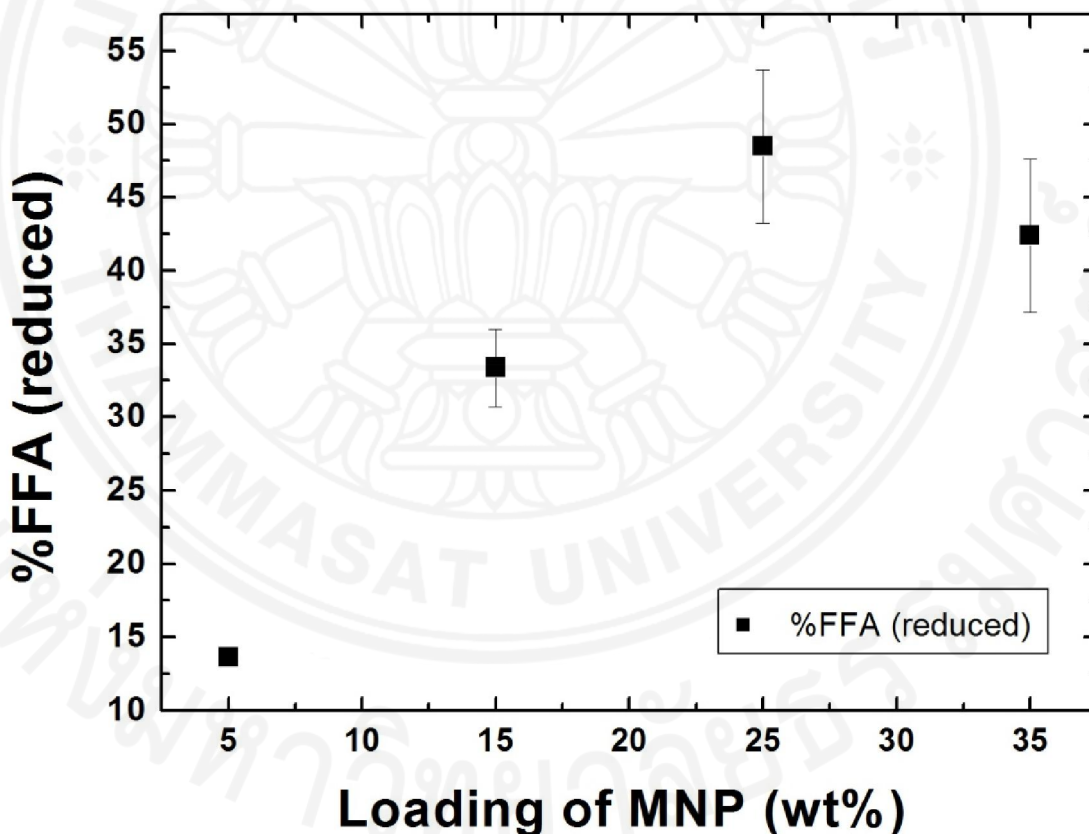
Figure 4.5 The percent FFA reduction as a function of MNP loading (g of MNP in 20 g oil sample at 1% FFA concentration).

Table 4.1 The kinematic viscosity obtained from noting the efflux time (s) and multiplying with the viscometer constant (mm^2/s^2) from soybean oil and soybean oil with 25% MNP loading.

Types of oil medium	Efflux time (s)	Kinematic Viscosity (mm^2/s)
Soybean oil	181.33±0.57	45.33±0.14
Soybean oil with 25%MNP	253.66±0.57	63.17±0.14

In addition, the kinematic viscosity of oil-MNP composite can be actually reduced by increasing temperature from room temperature to higher temperature while the oil-MNP composite is being stirred in the process. The alteration of kinematic viscosity due to the increasing of temperature is shown in Figure 4.6 where the kinematic viscosity of soybean oil and soybean oil with 25% MNP is compared at various temperatures including 25, 30, 40, 50, 60, 70 and 80 $^{\circ}$C. It can be seen from the Figure 4.6 that soybean oil with 25% MNP has higher kinematic viscosity at all temperatures compared to soybean oil without MNP and interestingly, soybean oil with 25% MNP needs to be heated up to around 40 $^{\circ}$C to achieve the same kinematic viscosity as pure soybean at 25 $^{\circ}$C. However, the objective of this research is to minimize the FFA content in the oil medium so that moisture and heat need to be carefully concerned, otherwise the process itself might be the factor that increases the FFA content such as by increasing too high temperature. In summary, to reduce processing cost and time this work will use at room temperature only and for the suggestion, the process can be actually heated to around 40 - 60 $^{\circ}$C to lower the kinematic viscosity and yield better FFA adsorption performance.
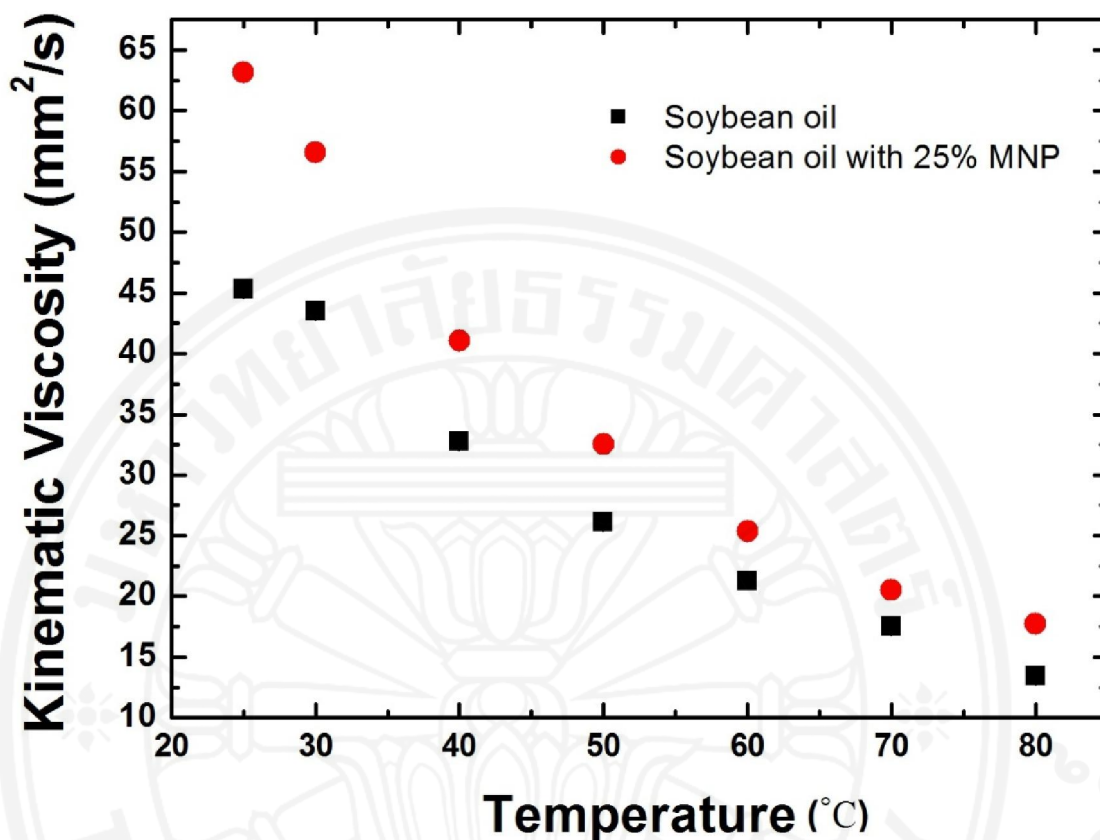
Figure 4.6 Kinematic viscosity (mm^2/s) of soybean oil (black color) and soybean oil with 25% MNP (red color) was compared at various temperatures including 25, 30, 40, 50, 60, 70 and 80 $^\circ$C.

Contact time between MNP adsorbent and FFA in oil solution has great influence on adsorption process. This adsorption experiment was carried out with 1% oleic acid spiked in commercial soybean oil at various time intervals (60 – 960 min) with 25% MNP loading in 20 g oil solution, 250 rpm (using mechanical stirrer) and 30 min sonication in order to de-agglomerate the MNP clusters. To further evaluate FFA adsorption performance, the kinetics of adsorption was studied in order to determine suitable amount of contact time for the MNP adsorbent to fully adsorb the FFA. Figure 4.7 shows the kinetics of FFA adsorption by using 25% MNP loading.

As contact time increases, the concentration of FFA remained in oil is reduced. It can also be seen that after the contact time of about 720 min (12 hours), the amount of

FFA remained does not change any further. This time was therefore taken as sufficient long enough for the equilibrium between the FFA adsorbed onto the MNP and the FFA remained in solution to be established and used as equilibrium contact time for determination of adsorption isotherm. However, it was difficult to determine the order of reaction from this plot.
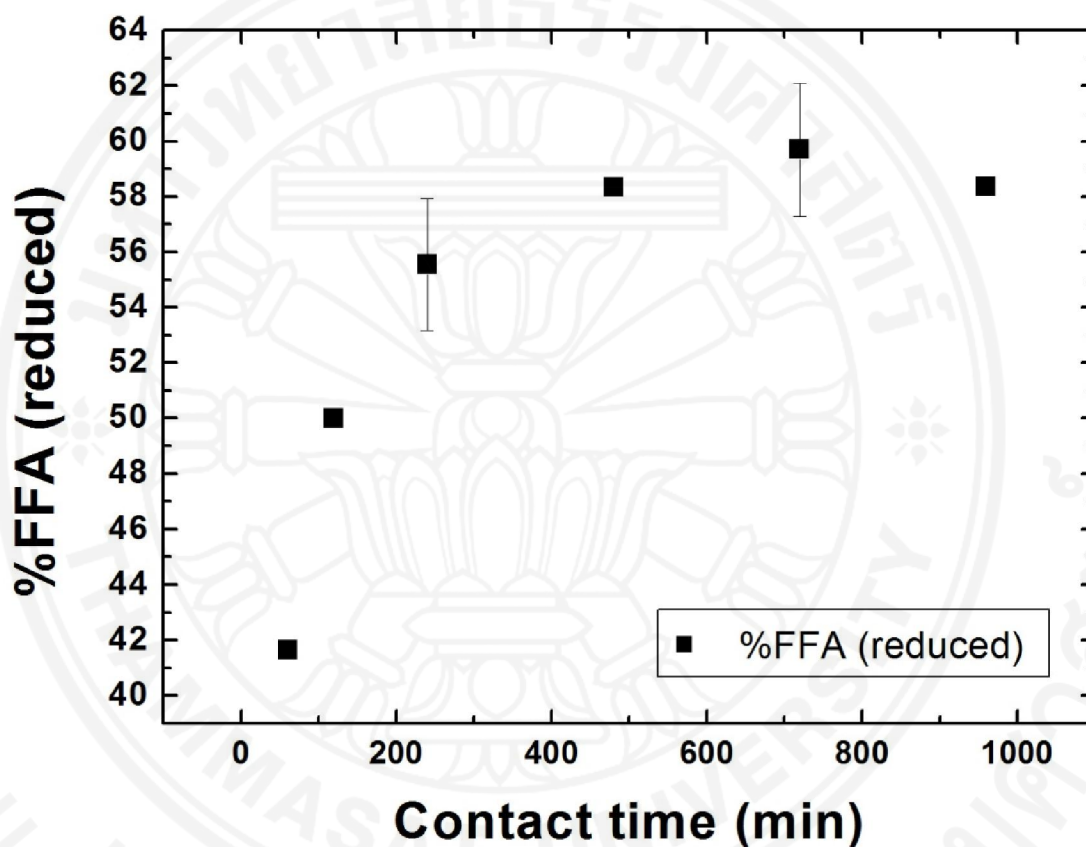
Figure 4.7 Plot between the percent FFA reductions versus contact time using 25% MNP loading.

Figure 4.8 shows a good linear behavior observed here indicating that the kinetic of FFA adsorption onto MNP can be better described by the pseudo-second order reaction kinetics rather than that of the first-order type. This implies that doubling the FFA amount will quadruple the sorption rate [28]. This indicates that the MNP sorbent should have a good kinetic sorption performance at high FFA content, and becomes slower as the FFA content is reduced. In case of pseudo-second order reaction, the kinetic of reaction is rapid at initial time and becomes slower at longer

time as compared to those of the first-order type. The pseudo-second order kinetic equation shows the linear form of Equation 4.1 [26], where Q_e is the equilibrium sorption capacity of the MNP sorbent, and k_2 is the reaction rate constant. From the fit shown in Figure 4.8, Q_e was obtained to be 32.7547 mg FFA/ g MNP sorbent at 1% FFA content. This value is in good agreement with the value seen in the adsorption isotherm discussed below.

$$\frac{t}{Q_t} = \frac{1}{k_2 Q_e^2} + \frac{t}{Q_e} \tag{4.1}$$
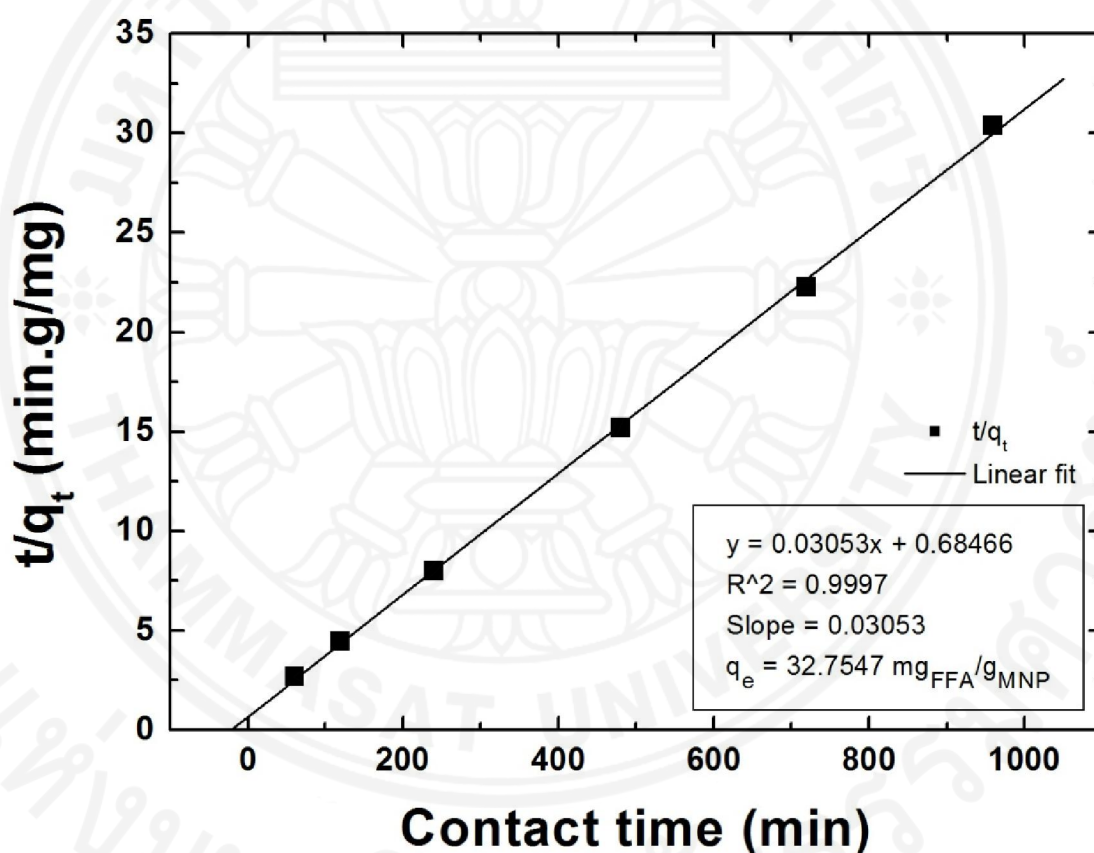
Figure 4.8 The plot between t/q_t against contact time according to the linearized form of the pseudo-second order kinetic reaction model.

From knowledge of equilibrium contact time obtained from the kinetic experiment, we then proceed to determine the maximum capacity of FFA adsorption on the synthesized MNP. Figure 4.9 shows the adsorption isotherm, plotted between the equilibrium FFA adsorbed onto MNP (Q_e) against the equilibrium amount of FFA

in the oil solution (C_e). The isotherm can be well explained using the Langmuir model which gives relationship between C_e and Q_e as follows in Equation 4.2 [26]. Here Q_{max} is the maximum adsorption capacity of the sorbent and b is the affinity constant for FFA of the MNP sorbent. The non-linear fitting of the Langmuir relationship to the experimental results yields the Q_{max} value in this system to be about 64.15 mg FFA/ g MNP sorbent.

$$Q_e = \frac{Q_{max}bC_e}{1 + bC_e} \qquad (4.2)$$
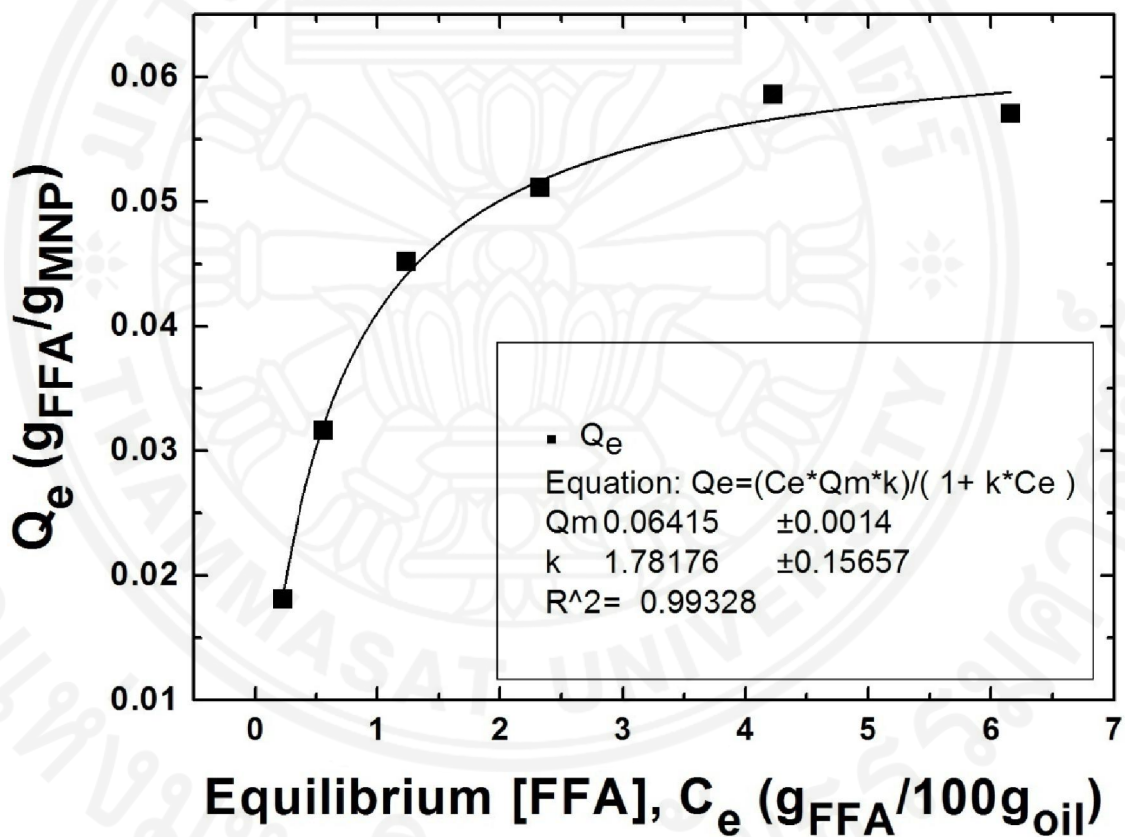
Figure 4.9 Plot between the equilibrium concentration of FFA on MNP (Q_e) and the equilibrium concentration of FFA in solution (C_e).

According to Figure 4.10, it is obvious that using MNP to adsorb oleic acid spiked in soybean oil is suitable and performs well at lower FFA concentration. At 0.5%FFA, MNP can reduce %FFA up to 66.69% and this performance is gradually decreased because of the increase of %FFA spiked in soybean oil. At about 7%, the %FFA

reduction can be achieved at 18.67% only. These results imply that MNP adsorption should be used to treat biodiesel feedstock with low content of FFA. Compared to the use of alkali catalyst, using MNP will not cause a significant loss of oil and saponification waste is not generated too. In addition, MNP can be reusable and easy to separate. Interestingly, MNP can not only be used to treat biodiesel feedstock with low FFA content as pretreatment process but also be applied to treat biodiesel product as post-treatment process which FFA content may exceed biodiesel criteria to further promote the use of high quality biodiesel and contribute towards a greener environment and a lower carbon society.
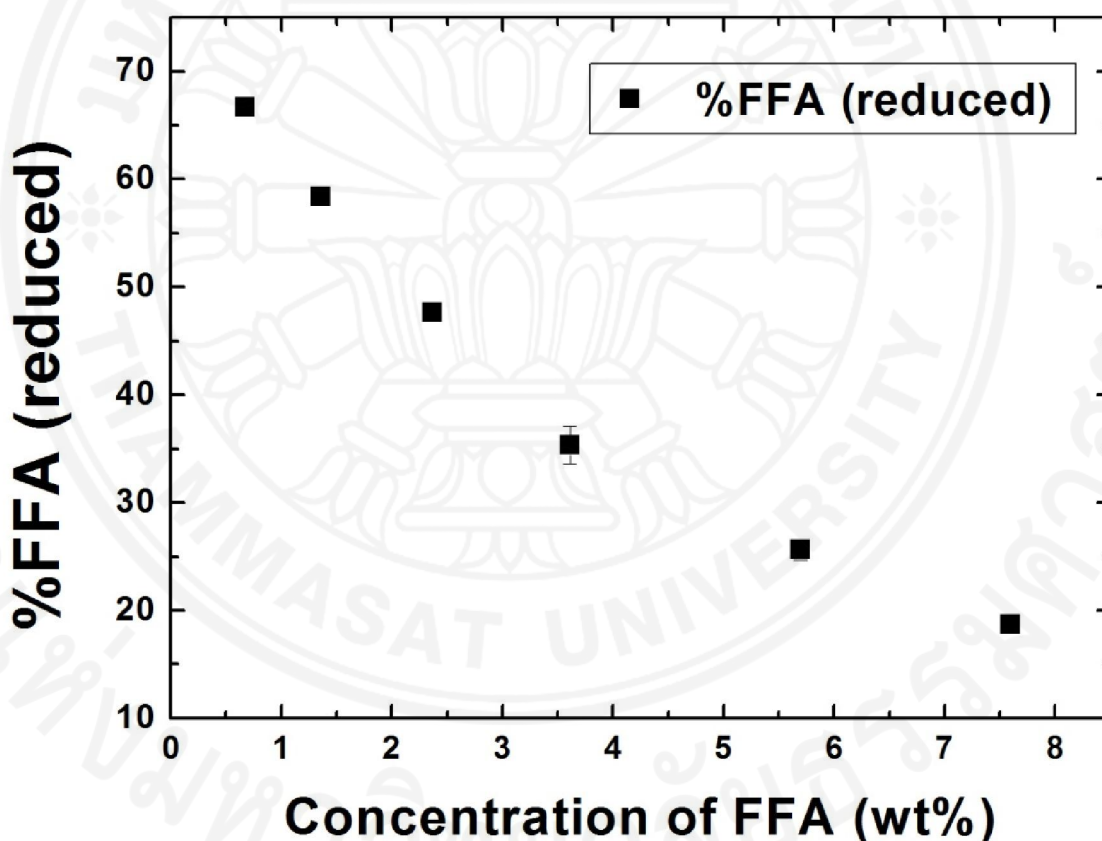
Figure 4.10 The plot between %FFA reductions versus various spiked-FFA concentrations from (0.5 - 7% FFA) in soybean oil.

4.3 Adsorption of FFA on synthesized MNP in biodiesel as post-treatment process

Originally, biodiesel used in this experiment is obtained from Vehicle Building and Physical Plant Division, Kasetsart University, Thailand. This biodiesel is used instead of diesel engine for agricultural purposes within university. Figure 4.11 shows the comparison between MNP loading used in 1% oleic acid-spiked soybean oil and in biodiesel, and the percent FFA reduction. Both systems indicated the same trend. By using 25% MNP loading in biodiesel, MNP can reduce %FFA up to 83.33% which is almost double compared to soybean oil system. The reason behind this better result is the differences of medium viscosity. The kinematic viscosity of commercial soybean oil is 45.33 mm^2/s while 6.78 mm^2/s is the kinematic viscosity of biodiesel which is less than soybean oil about seven times. However, 25% by weight MNP loading is therefore chosen for later experiment.
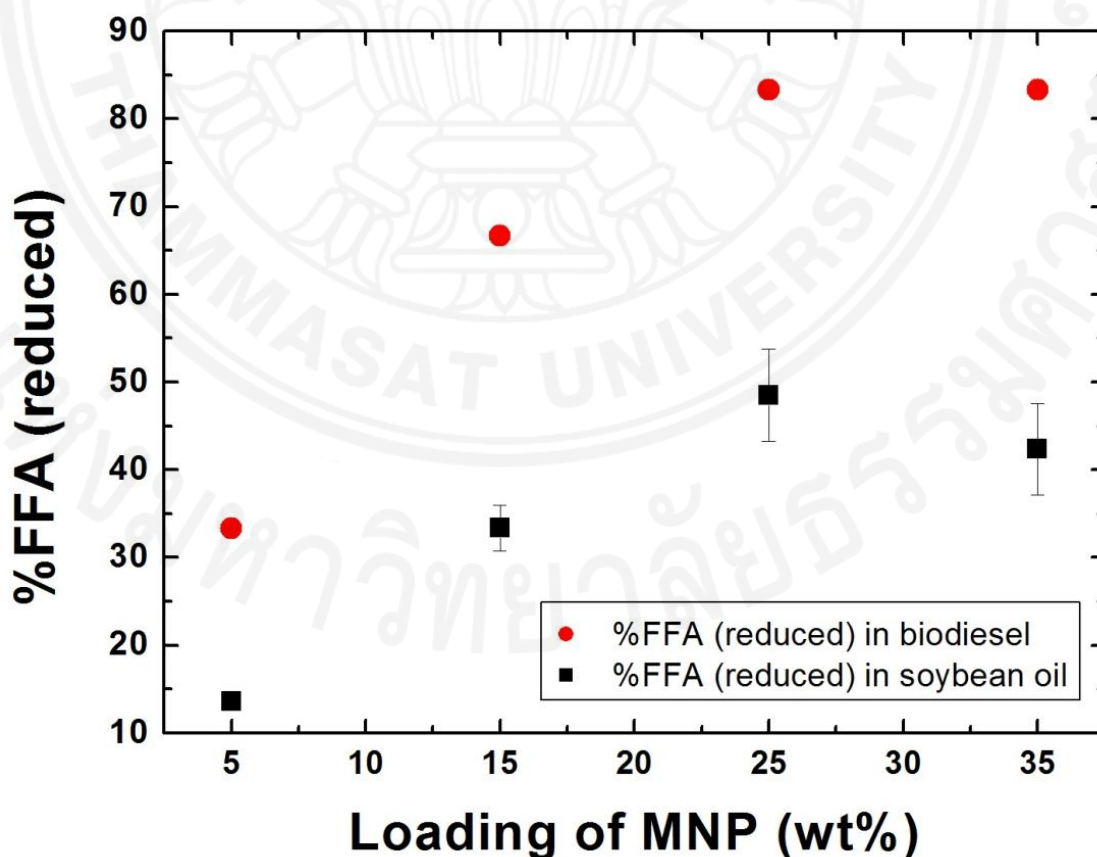
Figure 4.11 The comparison between FFA reduction as a function of MNP loading used in 1% oleic acid-spiked soybean oil (black color) and in biodiesel (red color).

Table 4.2 The kinematic viscosity obtained from noting the efflux time (s) and multiplying with the viscometer constant (mm^2/s^2) from biodiesel and biodiesel with 25% MNP loading.

Types of oil medium	Efflux time (s)	Kinematic Viscosity (mm^2/s)
Biodiesel	27.10±0.03	6.78±0.01
Biodiesel with 25%MNP	38.52±0.33	9.63±0.08

The increased viscosity of the oil has made the oil–MNP composite becomes more viscous at large loading amount and cause the difficulty for MNP to be in contact with FFA due to less diffusion capacity of adsorbents. The increasing of viscosity can be reported in term of kinematic viscosity which can be determined using glass capillary viscometer and the efflux times were recorded in second before multiplying with viscometer constant (0.25 mm^2/s for size 300). The differences in kinematic viscosity of biodiesel (both before and after additions of MNP) are shown in Table 4.2. In biodiesel, it is obvious that adding MNP adsorbent can cause slightly higher kinematic viscosity from 6.78±0.01 mm^2/s to 9.63±0.08 mm^2/s that makes the 25% and 35% MNP loading show almost the same FFA reduction around 83%. Therefore, there is no need using too much amount of MNP to cause more viscosity with slight gain in adsorption efficiency. The MNP loading amount of about 25% by weight is therefore chosen for later experiment to investigate other factors contributing to FFA adsorption efficiency on MNP.

Initially, biodiesel used in this experiment possesses the acid value of 0.82 mg_{KOH}/g_{oil} (or 0.41%FFA) which is higher than the ASTM D 6751 value (limit to 0.5 mg_{KOH}/g_{oil}) [5]. Figure 4.12 shows the kinetics of FFA adsorption by using MNP in biodiesel. As contact time increases, the concentration of FFA remained in oil is decreased. The amount of FFA remained does not change after the contact time of about 480 min (8 hours) which can reduce up to 80.12% to 0.1472 mg_{KOH}/g_{oil} (or 0.0739%FFA). This time is therefore taken as sufficient long for the equilibrium between the FFA adsorbed onto the MNP and the FFA remained in solution.
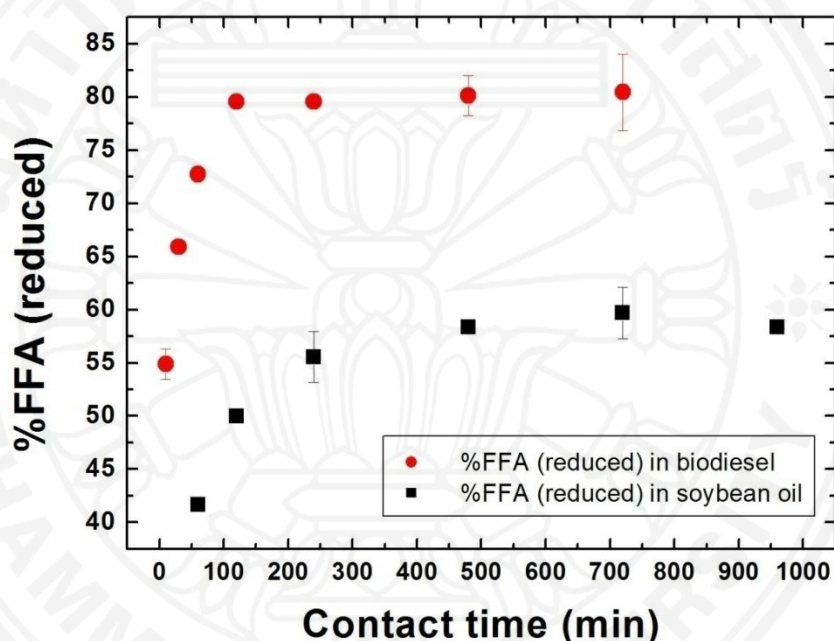
Figure 4.12 The comparison between the percent FFA reduction versus contact time using 25%MNP loading in 1% oleic acid-spiked soybean oil (black color) and in biodiesel (red color).

The kinetic of FFA adsorption onto MNP can also be described by the pseudo-second order reaction kinetics in Equation 4.1 [26]. Figure 4.13 shows a good linear behavior indicating that doubling the FFA amount will quadruple the sorption rate. This indicates that the MNP sorbent should have a good kinetic sorption performance at high FFA content, and becomes slower as the FFA content is reduced. For pseudo-second order reaction, the kinetic of reaction is rapid at initial time and becoming slower at longer time [28]. From the fit shown in Figure 4.13, Q_e was obtained to be 32.42 mg_{FFA}/g_{MNP} at 0.41% FFA content.

81
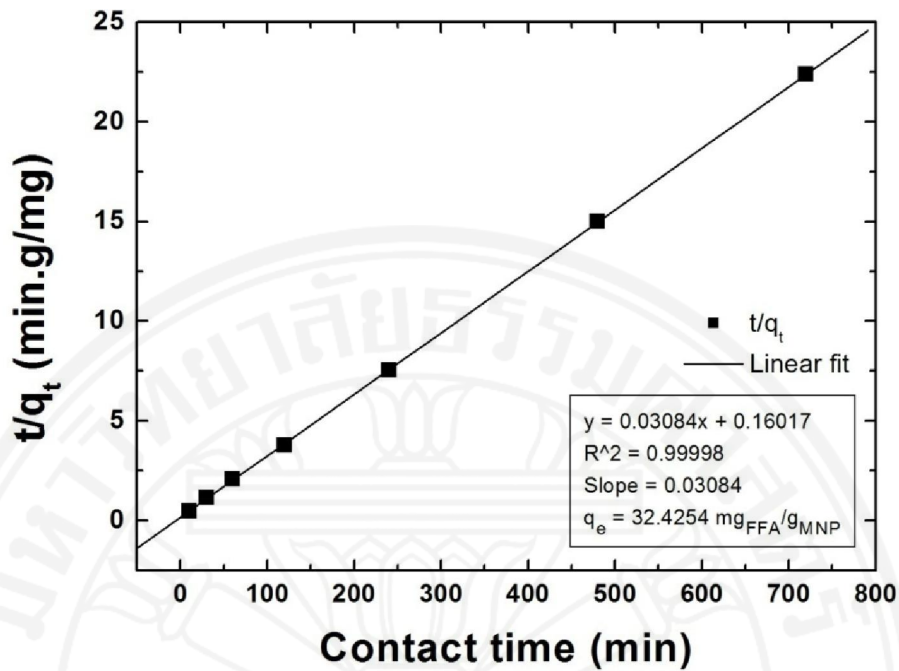
Figure 4.13 The plot between t/q_t against contact time according to the linearized form of the pseudo-second order in biodiesel.
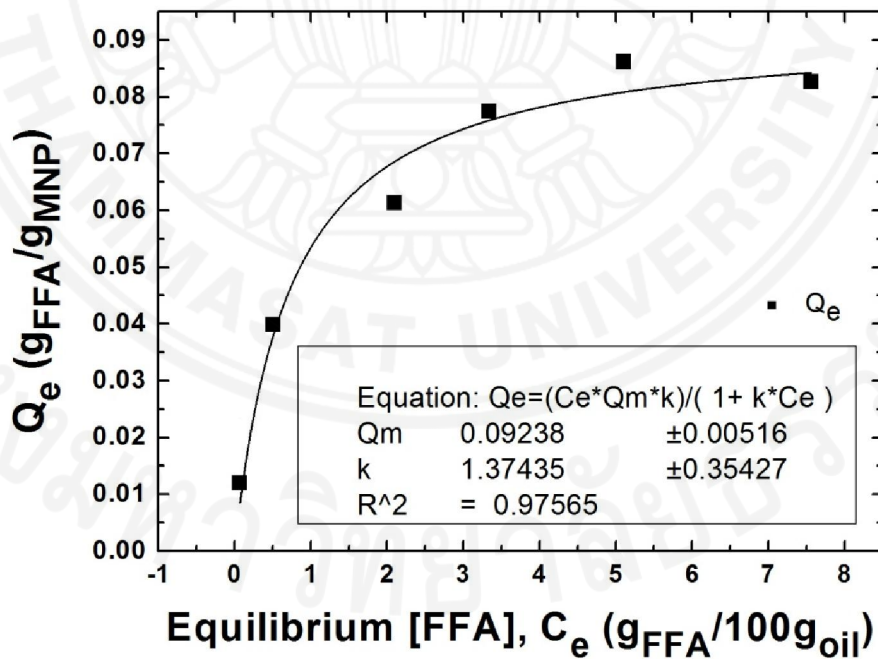
Figure 4.14 Plot of adsorption isotherm by Langmuir equation between the equilibrium concentration of FFA in solution (C_e) and the equilibrium concentration of FFA on MNP (Q_e) in biodiesel.

Figure 4.14 shows the adsorption isotherm, plotted between the equilibrium FFA adsorbed onto MNP (Q_e) against the equilibrium amount of FFA in the oil solution (C_e). The isotherm can be well explained employing the Langmuir model which gives relationship between C_e and Q_e as follows in Equation 4.2 [26]. Q_{max} value in this system is obtained to be about 92.38 mg$_{FFA}$/ g$_{MNP}$ sorbent.

4.4 Determination of regeneration cycles for repeated use

Another advantage of using magnetic nanoparticles over other novel adsorbents is the possibility to regenerate and recycle the adsorbents for repeated use. Because of the lower viscosity in biodiesel causing the easy separation of MNP from oil media compared to the FFA-spiked oil model (soybean oil), 1% oleic acid spiked-biodiesel together with its optimal conditions, including 25% of MNP loading and 6 hr of contact time, was chosen in this regeneration experiment. In order to repeatedly perform the same batch of MNP, desorption FFA from MNP is readily achieved by treatment with basic solution in which FFA loaded on MNP was immersed in 0.1 N solution of NaOH in EtOH-H$_2$O (1:1) at room temperature [26]. The methodology for FFA desorption is fully described in 3.2.2.4.

Interestingly, in Figure 4.15, after desorption had been performed, the same batch of MNP could be reused for subsequent adsorption for many cycles. As a result, MNP can be reused for at least 3 adsorption cycles with conservative adsorption capacities, especially the first three batches which seemed that the efficiency remains quite high and yielded around 71% FFA reduction. However, the decrease in FFA percent reduction is limited to about 10% in the fourth cycle (61% FFA reduced) and FFA percent reduction is decreased to about 30% in the fifth cycle (41% FFA reduced) compared to the first cycle.

When %FFA reductions on MNP in biodiesel was compared, the %FFA reduction was slightly reduced from the previous result in section 3.2.2.4, this may be due to the large amount of oil media which was used to provide the experiment for many cycles and may directly affect on the chance of interaction between MNP adsorbent and

FFA. It can be seen from the Figure 4.15 that the first three cycles in regeneration experiment possess 71% FFA reduction which remains high enough to apply for repeated uses. For the fourth and fifth cycles, which seem to yield the lower %FFA reduction, the reason behind these lower adsorption efficiency is from the desorption procedures in which 0.1 N solution of NaOH may cause the slow oxidizing reaction and directly affect the form of iron oxide that results in the deterioration of FFA-MNP interaction and magnetization value, which will further affect on the separation process as well.
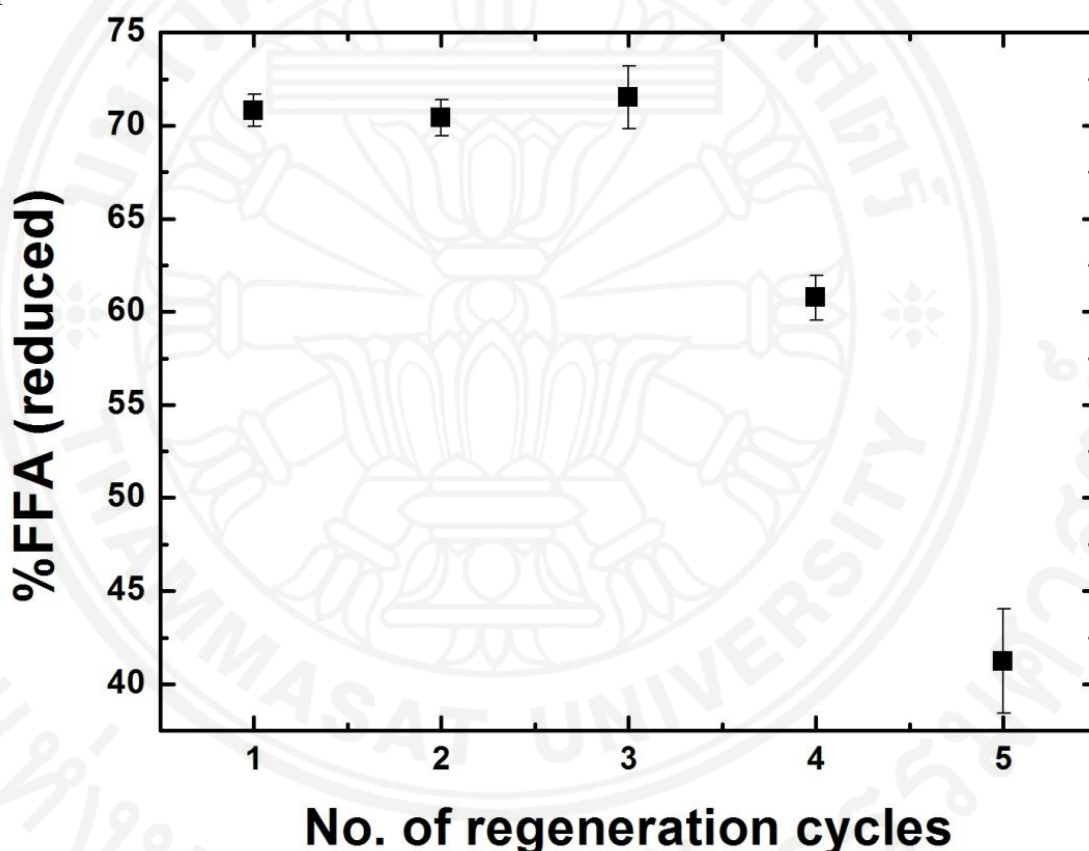
Figure 4.15 Plot of FFA reduction with MNP after being regenerated for 5 cycles.

This result is correspondent to the previous work, in which the adsorption mechanism of C18 fatty acids on iron based surfaces has been successfully studied and it was concluded that the more iron surface is oxidized, the less it is reactive with the fatty acid. For instance, Fe_2O_3 can have both physisorption and chemisorptions whereas FeOOH can only have physisorption or no adsorption [29]. In addition, desorption procedure by using 0.1 N solution of NaOH is concentrated enough to wash the MNP surface and provide FFA-free MNP surface. After washing

with 0.1 N NaOH, the concentrated basic solution may cause the oxidation of the MNP surface, which will further affect on the adsorption efficiency and separation process. So, the number of cycles and the concentration of basic solution should be carefully optimized. Above all, this is a benefit of using MNP compared to other previously reported adsorbents for FFA removal because it cannot be recycled or very difficult to recycle [13].

4.5 Characterization of used MNP and treated oils

After MNP adsorbent had been used in adsorption experiment, treated oil was characterized by using ICP technique in order to determine the iron trace or the leakage of iron from the adsorbent. Additionally, used MNP adsorbent would also be characterized to identify the interaction between FFA and iron surface with TGA and FTIR techniques.

4.5.1 Determination of iron concentration in oil mediums after being used with MNP

Inductively coupled plasma (ICP) is used to determine the trace of iron concentration in both soybean oil and biodiesel before and after treatment with MNP. These samples were tested to observe the differences in remaining iron content. Acidic wet extraction of iron method was used to prepared sample to be analyzed with ICP and the steps were described in the section 3.2.2.5. Normally, edible oils manufactured without refining contain relatively high quantities of iron while the usual concentrations of iron in good quality oils range from 2 to 5 ppm [24]. According to the Table 4.3, there are several samples tested with ICP to determine iron trace; for example, in commercial soybean oil used as biodiesel feedstock model and soybean oil after treating with MNP, the difference in concentration of iron content is 2.06 ppm, which is considered as good quality oil. Moreover, the difference in concentration of biodiesel before and after treatment is 5.04 ppm, which is in a good range. The reason behind the higher value of iron content in biodiesel compared to in soybean oil is that the lower viscosity of biodiesel may cause higher iron solubility in biodiesel

compared to in soybean oil so, it is easy for iron to be dissolved in biodiesel. In summary, there are no potential variations of the iron contents in both soybean oil and biodiesel after FFA was removed with MNP. It can be concluded that the amount of iron leached into both soybean oil and biodiesel are not significant while treating with MNP. Therefore, Using MNP as an adsorbent to remove FFA should be considered as a good adsorbent for treating both biodiesel and feedstock. Even though there is no specific value in ASTM D 6751 for iron content limited in biodiesel, it is very important to observe whether the MNP absorbent used in the process contributes other impurities in the system or not. In addition, Na and K content in biodiesel are limited at 5.0 $mgkg^{-1}$ by EN 14108 testing method, and P content is limited at 0.001% (w/w) by EN 14107 testing method [5].

Table 4.3 The iron concentration in oil mediums (ppm) after treating with MNP.

Samples tested with ICP	Concentration (ppm)
Soybean oil	0.16
Soybean oil after treatment with MNP	2.22
Biodiesel	48.76
Biodiesel after treatment with MNP	53.8

4.5.2 The interaction between FFA and MNP using TGA and FTIR

Thermogravimetric analysis (TGA) was carried out to identify both qualitative and quantitative evidence of molecule adsorbed on nanoparticles. The samples, including bare MNP, MNP in SO and in BD, and also MNP in pure commercial oil, were used in this experiment. Figure 4.16 shows the TGA curve of bare MNP and MNP in SO,

and in BD with their weight losses at different decomposition temperatures. In the case of pure MNP which was washed with chloroform before TGA measurement, there is a slight weight loss at the beginning around 30 - 150 °C. This is ascribed to the moisture. Throughout the decomposition temperature ranges (30 - 600 °C), MNP has lost their weight only 3%. For the MNP+SO and MNP+BD, at low temperature, there is also slight weight loss of about 0.6 and 1.13%. This can also be interpreted as the moisture and possibly small molecules adsorbed on the MNP surface. When the temperature is increased to about 200 °C, the samples start to decompose and show the second weight loss which continues until about 450 °C. These decomposition temperature ranges are very crucial because the second weight loss can be assigned to the removal of fatty acids adsorbed onto the MNP surface [6, 23, 26]. MNP+SO graph has an amount of weight loss about 6.47% which is slightly lower than MNP+BD that has lost of about 6.62% of its weight. This second weight loss is very significant because it can be used to confirm the adsorption of fatty acids on iron oxide magnetic nanoparticles.
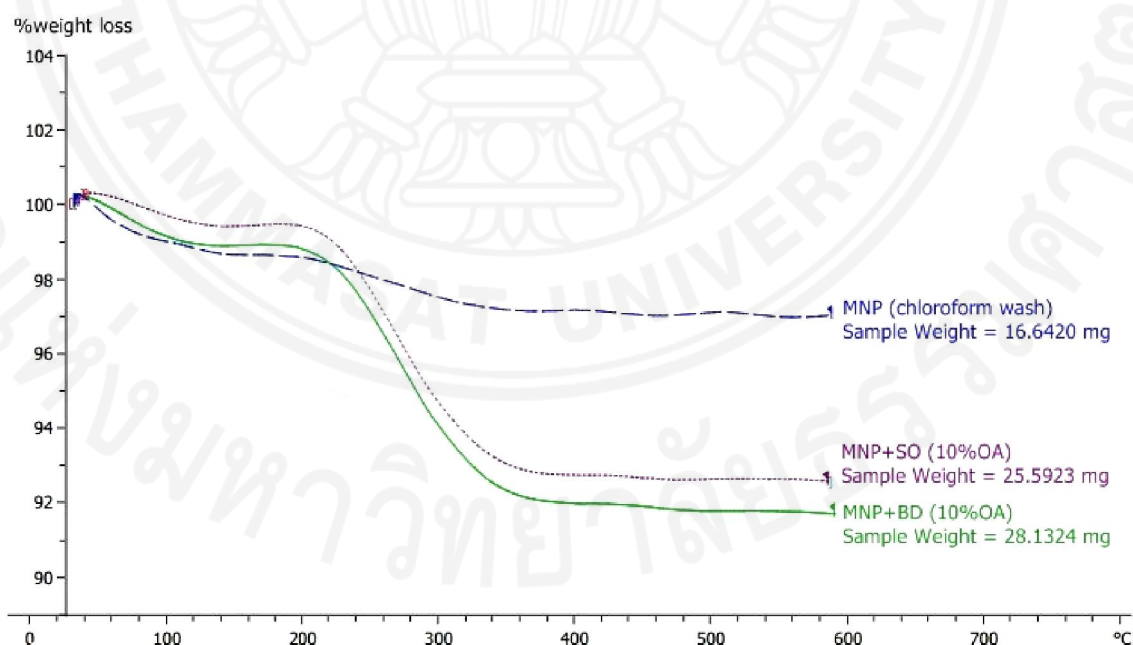
Figure 4.16 TGA curves the bare MNP after chloroform wash (blue), MNP+SO (10%OA) (purple) and MNP+BD (10%OA) (green).

Interestingly, the percent weight loss of oleic acid in both soybean oil and biodiesel is equivalent to about 64.7 and 66.2 mg_{FFA}/g_{MNP}, respectively, which is below what we have obtained from the adsorption isotherm calculation (64 and 92 mg_{FFA}/g_{MNP} in soybean oil and biodiesel, respectively. This result is likely an indication that fatty acids are both physisorbed and chemisorbed onto the iron oxide surface. The chloroform washing of the MNP is strong enough to remove the physisorbed fatty acids, leaving behind the chemisorbed fatty acids, and consequently lower the amount of adsorbed fatty acids observed in the TGA measurement. Thus, there is some partial desorption of oleic acid in the washing step prior to the TGA measurement. This result is in good agreement with Ekemini B. *et al.* who reported that in stearic acid adsorption from oil medium, some of the stearic molecules were seen to be physically adsorbed onto the steel surface [31].
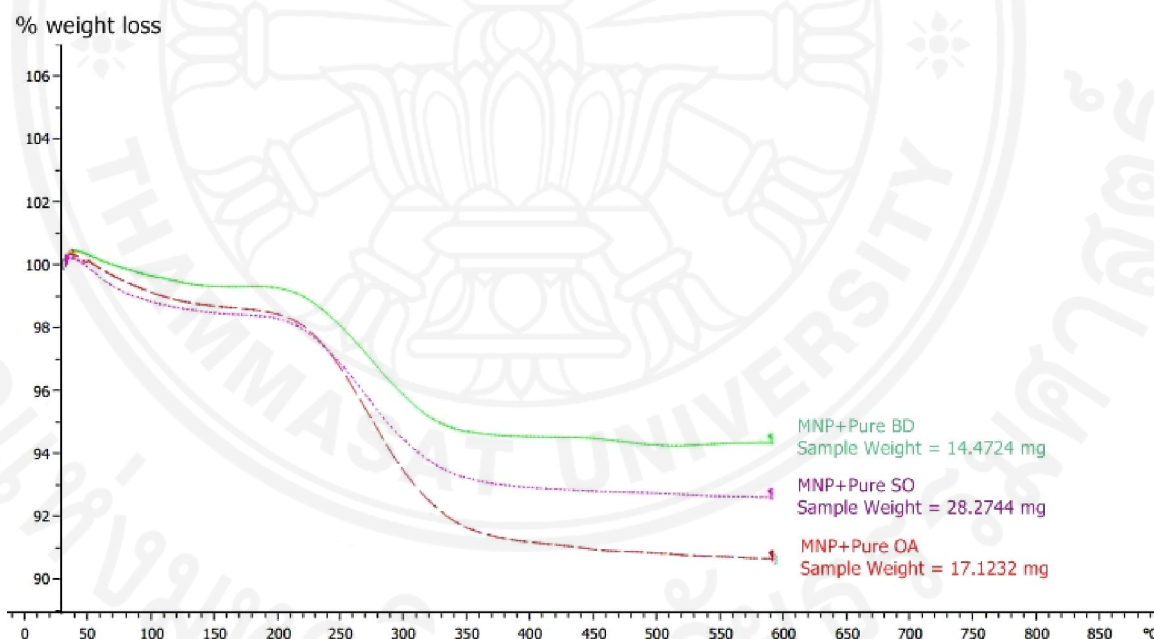
Figure 4.17 TGA curves of MNP in pristine media, including MNP+Pure BD (green), MNP+Pure SO (purple) and MNP+Pure OA (red).

In addition, Figure 4.17 shows that there is a small amount of FFA present in pure SO and BD at the second weight loss of about 5.19% and 4.61%, respectively. In pure OA, the percent weight loss at the second weight loss is quite high (7.77%). This result implies that FFA present in those media can absorb on metal oxide surface.

However, the reason behind this quite high FFA content in those pristine media is probably from the hydrolysis of the alkyl ester. Although the ester hydrolysis is quite a slow process in the absence of strong base, the hydroxyl group on the MNP surface may cause the cleavage of the ester bond, though at slow rate. This result can be clearly confirmed with the FTIR analysis.

In order to understand the adsorption mechanism between carboxylic groups from free fatty acid and iron oxide particles, the FTIR spectra of MNP both before and after the oleic acid adsorption were determined and analyzed. Not only can FTIR technique reveal the role of oleic acid absorbed on MNP surface but also provide the details about the coordination modes. Figure 4.18 shows the FTIR spectra of fatty acids that have been chemically adsorbed onto the MNP surface. For the neat oleic acid, it is well-documented that there is a strong peak at 1710 cm^{-1}, which is assigned to C=O carbonyl stretching and this peak is absent in OA coated on MNP surface spectra. This indicated that all the physisorbed oleic acid molecules are likely to be removed from the used MNP surface [6]. The disappearance of 1710 cm^{-1} causes the peak dissociation into symmetric and asymmetric carboxylate stretching at around 1280 - 1400 cm^{-1} for symmetrical vibration and 1510 - 1650 cm^{-1} for asymmetric vibration. Additionally, the wave number difference of these two peaks can be used to anticipate the types of metal carboxylate coordination modes [25].

From Figure 4.18, spectra of oleic acid adsorbed on MNP in various oil mediums have almost similar characteristic peaks. Obviously, MNP in neat oleic acid (red) shows several strong peaks at 1575, 1505, 1460, 1430 and 1290 cm^{-1}. There are two peaks that can be assigned to be asymmetric carboxylate stretching (COO$^-$), which are 1575 and 1505 cm^{-1}. The peak at 1430 cm^{-1} has been referred to be symmetric carboxylate stretching (COO$^-$). This result revealed the difference of wave number separation of about 145 and 75 cm^{-1}, respectively. This result shows the presence of two coordination modes, which can be interpreted as the bridging bidentate and chelating bidentate coordination, respectively, although the bridging bidentate is more eminent. Additionally, it also contains other peaks, including the stronger background peak at 1630 cm^{-1} of the magnetite, which is assigned to the OH vibration of moisture

adsorbed on the iron oxide surface. The peak at 1460 cm^{-1} is assigned to be a methylene group vibration (-CH$_2$) on the main chain [27]. The peak at 1290 cm^{-1} represents the C-O stretching [6].
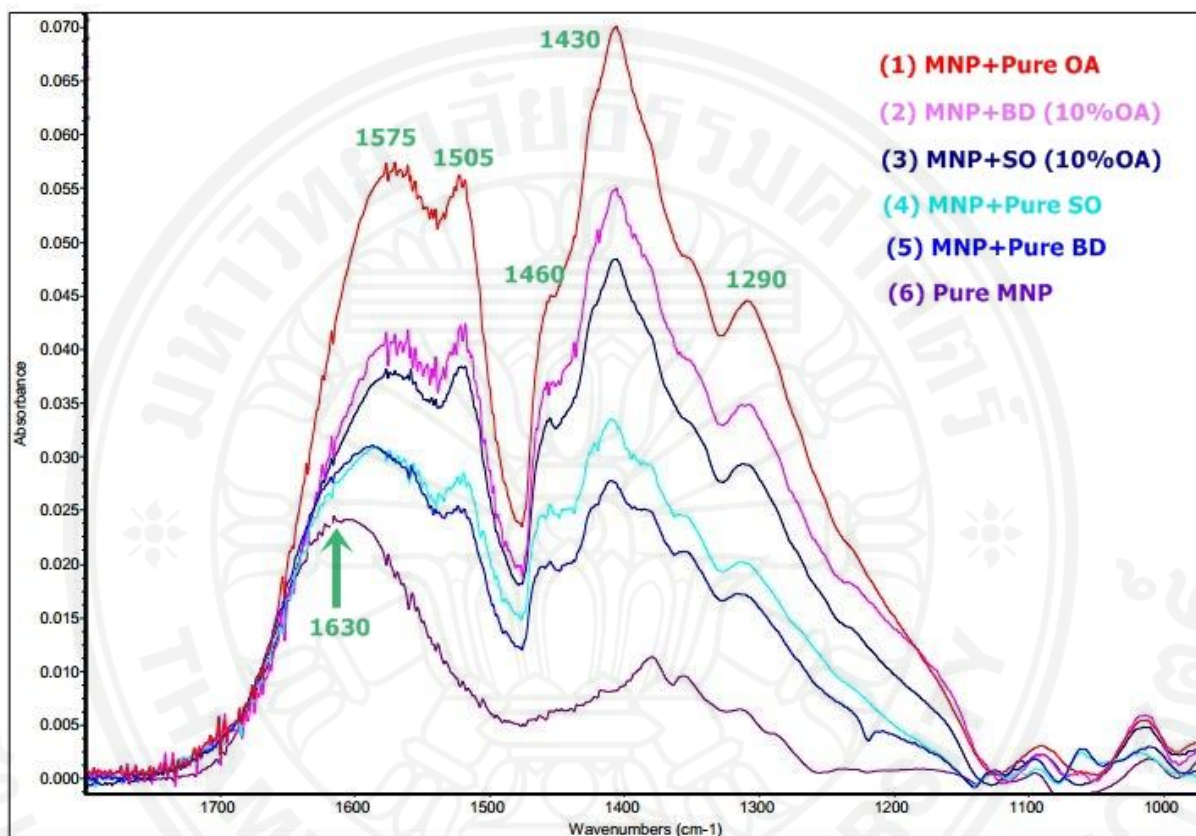
Figure 4.18 FTIR spectra of oleic acid adsorbed on MNP in various oil mediums.

It is also interesting to note that in pristine oils, both the neat BD and the neat vegetable oil (SO), that have very small amount of fatty acids (0.06% and 0.03% FFA for neat BD and neat SO, respectively), the carboxylate peaks are still clearly visible in the FTIR spectra. This is an indication that the alkyl esters in both the BD and the SO probably can undergo hydrolysis. Although the kinetics of this decomposition into free fatty acids is probably slow in the absence of strong base, but given that this is an equilibrium process, and with the presence of large amount of esters, the hydroxyl group on the MNP surface together with the nearby Fe may act together to cause the cleavage of the ester bond. However, once the fatty acid is adsorbed onto MNP surface, it seems to protect the MNP surface. Free fatty acid is known and has been

used for lubrication and protection of steel from corrosion and in tribology. It protects the steel surface from corrosion by complexion with the iron or iron oxide on the surface and prevents water and oxygen from reaching the Fe [31].

Chapter 5
Conclusions and Recommendations

5.1 Conclusions

The presence of free fatty acid is an obstacle for biodiesel production. For biodiesel feedstock, FFA content needs to be low enough; otherwise, it can affect the alkali-transesterification. In other words, FFA removal in feedstock becomes undeniable in biodiesel production and iron oxide magnetic nanoparticles have been introduced in this research as a new and effective means to lower FFA content in feedstock. This process can be considered as pre-treatment process. In this experiment, soybean oil was spiked with oleic acid and was used as biodiesel feedstock. On the other hands, biodiesel final product is also necessary to satisfy the ASTM D 6751 standard for the FFA content (acid value) in order to avoid many problems, such as rancidity and corrosion. So, MNP could be used in this process too and this stage was considered as post-treatment process. Noted that biodiesel final product was obtained from the Vehicle Building and Physical Plant Division, Kasetsart University, Thailand. This biodiesel is used instead of diesel engine for agricultural purposes with 0.8220 mg_{KOH}/g_{oil}.

A number of characterization techniques were employed with different purposes; for example, TEM reveals the average particle size of MNP about 10 - 14 nm. These particles aggregate and form a larger cluster in various sizes on the order of $200 - 300$ nm. (DLS) measurement also exhibits the hydrodynamic radius of these clusters in oil media to be about 442 ± 99 nm. So, sonication was applied to the experiment to de-agglomerate the cluster particles before adsorption process. This result also co-ordinates -38.1 mV of zeta potential which is in the medium moderate range. XRD can be used to confirm the structure of synthesized particles and each peak agrees in positions and intensities with the published Fe_3O_4 pattern (Powder diffraction file, PDF 01-074-1909). With lattice spacing of (311) at $2\theta \sim 35.539°$ and at half the maximum intensity (FWHM) of 0.614 radians, the mean size of the crystalline domain can be deduced to be about 13.60 nm, which is corresponded to the particle

size observed in the TEM images. For magnetic properties, VSM indicates the superparamagnetic behavior with saturation magnetization (M_S) of 83 emu/g at 300 K. This magnetism is very beneficial because MNP can be applied to other experiments, like regeneration, with the easy and fast separation from oil.

For FFA-spiked oil, the suitable MNP loading was found to be 25% with 12 hours of contact time. Increasing MNP loading may cause higher viscosity of oil and affect the MNP-FFA interaction. Langmuir isotherm can be used to describe the adsorption process with the maximum FFA adsorption capacity of 64 mg_{FFA}/g_{MNP}. For biodiesel final product, 25% MNP loading is used instead of 35% MNP loading. The kinetic was found to be 6 hours. This shorter contact time may result from its viscosity, where biodiesel has only 6.78 mm^2/s compared to soybean oil with 45.33 mm^2/s. Langmuir isotherm can also be used to describe the adsorption process with the maximum FFA adsorption capacity of 92 mg_{FFA}/g_{MNP}. The used MNP adsorbent was washed with 0.1 N solution of NaOH in EtOH-H_2O (1:1) at room temperature for desorbing FFA on iron surface. The same batch of MNP could be reused for subsequent adsorption for many cycles at least 3 adsorption cycles with conservative adsorption capacities around 71%.

ICP was used to determine the iron trace in treated oil mediums. In soybean oil, the difference in concentration of iron content is 2.06 ppm, which is considered as good quality oil and the difference in concentration of biodiesel before and after treatment is 5.04 ppm, which is also in a good range. In summary, there are no potential variations of the iron contents in both soybean oil and biodiesel. Although there is no specific value in ASTM D 6751 for iron content limited in biodiesel, it is very important to observe that the MNP absorbent used in the process does not contribute other impurities into the system. In TGA, MNP sample starts to decompose and show the second weight loss at 200 - 450 $^{\circ}$C. These decomposition temperature ranges are very crucial because the second weight loss can be assigned to the removal of fatty acids adsorbed onto the MNP surface. FTIR showed the difference of wave number separation of carboxylate vibrations of about 145 and 75 cm^{-1} which revealed the

presence of two coordination modes, including the bridging bidentate and chelating bidentate coordinations.

5.2 Recommendations

Firstly, in this work, iron oxide magnetic nanoparticles were simply synthesized by co-precipitation method. It is interesting that besides the size benefit, further research should focus on particle morphology. For example, hollow nanoparticles possibly yield better adsorption result, which is challenging. Secondly, from TEM images, synthesized particles easily form a cluster due to the absence of stabilization process. So, it is critical to de-agglomerate the MNP adsorbent during adsorption experiment with either sonication or stirring, but this needs to be carefully performed. Otherwise, heat and moisture will cause more undesired FFA. Thirdly, oil medium should be reduced its viscosity to cause more interacting chance between FFA and MNP, and heating is optional. The recommendation temperature range is maximized at around 60 $^\circ$C. However, both temperature and contact time need to be optimized. Finally, due to low capacity of this adsorbent, MNP may be more suitable for treatment of low amount of FFA in biodiesel as post-treatment process.

References

1.   Gerpen, Jon Van. (2005). Biodiesel processing and production. *Fuel Processing Technology, 86*(10), 1097-1107. doi: 10.1016/j.fuproc.2004.11.005

2.   Suksri, Piyawan, Moriizumi, Yue, Hiroki, Hondo, & Yoko, Wake. (2008). An introduction of biodiesel to Thai economy – Community biodiesel and oil palm biodiesel complex. *Digital Asia Discussion Paper Series, DP 08-003*

3.   Zhang, Y. (2003). Biodiesel production from waste cooking oil: 1. Process design and technological assessment. *Bioresource Technology, 89*(1), 1-16. doi: 10.1016/s0960-8524(03)00040-3

4.   Suseno, S.H, Tajul, A.Y & Wan, Nadiah, W.A. (2011). The use of passive filtration for optimization of Magnesol XL Function for improving the quality of Sardinella lemuru Oil. *International Research Journal of Biochemistry and Bioinformatics,* 1(5), 103-113

5.   Hayyan, Adeeb, Alam, Md Zahangir, Mirghani, Mohamed E. S., Kabbashi, Nassereldeen A., Hakimi, Noor Irma Nazashida Mohd, Siran, Yosri Mohd, & Tahiruddin, Shawaluddin. (2011). Reduction of high content of free fatty acid in sludge palm oil via acid catalyst for biodiesel production. *Fuel Processing Technology, 92*(5), 920-924. doi: 10.1016/j.fuproc.2010.12.011

6.   Zhang, Ling, He, Rong, & Gu, Hong-Chen. (2006). Oleic acid coating on the monodisperse magnetite nanoparticles. *Applied Surface Science, 253*(5), 2611-2617. doi: 10.1016/j.apsusc.2006.05.023

7.   Edward, Crabbe, Cirilo, Nolasco-Hipolito, Genta, Kobayashi, Kenji Sonomoto, &

Ayaaki, Ishizaki. (2001). Biodiesel production from crude palm oil and evaluation of butanol extraction and fuel properties. *Process Biochemistry, 37*, 65 – 71

8.   Mekhilef, S., Siga, S., & Saidur, R. (2011). A review on palm oil biodiesel as a source of renewable fuel. *Renewable and Sustainable Energy Reviews, 15*(4), 1937-1949. doi: 10.1016/j.rser.2010.12.012

9.   Pleanjai, Somporn, & Gheewala, Shabbir H. (2009). Full chain energy analysis of biodiesel production from palm oil in Thailand. *Applied Energy, 86*, S209-S214. doi: 10.1016/j.apenergy.2009.05.013

10.   Song, Eun-Seok, Lim, Jung-won, Lee, Hong-Shik, & Lee, Youn-Woo. (2008). Transesterification of RBD palm oil using supercritical methanol. *The Journal of Supercritical Fluids, 44*(3), 356-363. doi: 10.1016/j.supflu.2007.09.0105

11.   Siriwardhana, Manjula, Opathella, G. K. C., & Jha, M. K. (2009). Bio-diesel: Initiatives, potential and prospects in Thailand: A review. *Energy Policy, 37*(2), 554-559. doi: 10.1016/j.enpol.2008.09.081

12.   Meng, Xiangmei, Chen, Guanyi, & Wang, Yonghong. (2008). Biodiesel production from waste cooking oil via alkali catalyst and its engine test. *Fuel Processing Technology, 89*(9), 851-857. doi: 10.1016/j.fuproc.2008.02.006

13.   Leung, Dennis Y. C., Wu, Xuan, & Leung, M. K. H. (2010). A review on biodiesel production using catalyzed transesterification. *Applied Energy, 87*(4), 1083-1095. doi: 10.1016/j.apenergy.2009.10.006

14.   Huali, Wang, Haiying, Tang, John, Wilson, Steven, O. Salley, & K. Y. Simon Ng (2008). Total Acid Number Determination of Biodiesel. *J Am Oil Chem Soc (2008) 85.* 1083–1086. doi: 10.1007/s11746-008-1289-8 and Biodiesel Blends

15.   Standard Test Method for Acid Number of Petroleum Products by Potentiometric Titration. *An American National Standard British Standard.* 4457

16.   Lu, A. H., Salabas, E. L., & Schuth, F. (2007). Magnetic nanoparticles: synthesis, protection, functionalization, and application. *Angew Chem Int Ed Engl, 46*(8), 1222-1244. doi: 10.1002/anie.200602866

17.   Deng, H., Li, X., Peng, Q., Wang, X., Chen, J., & Li, Y. (2005). Monodisperse magnetic single-crystal ferrite microspheres. *Angew Chem Int Ed Engl, 44*(18), 2782-2785. doi: 10.1002/anie.200462551

18.   Shylesh, S., Schunemann, V., & Thiel, W. R. (2010). Magnetically separable nanocatalysts: bridges between homogeneous and heterogeneous catalysis. *Angew Chem Int Ed Engl, 49*(20), 3428-3459. doi: 10.1002/anie.200905684

19.   G.A., van, Ewijk, (1999). Convenient preparation methods for magnetic colloids. *J Magnetism and Magnetic Materials, 201.* 31-33

20.   Iida, H., Takayanagi, K., Nakanishi, T., & Osaka, T. (2007). Synthesis of Fe3O4 nanoparticles with various sizes and magnetic properties by controlled hydrolysis. *J Colloid Interface Sci, 314*(1), 274-280. doi: 10.1016/j.jcis.2007.05.047

21.   Ge, S., Shi, X., Sun, K., Li, C., Baker, J. R., Banaszak Holl, M. M., & Orr, B. G. (2009). A Facile Hydrothermal Synthesis of Iron Oxide Nanoparticles with Tunable Magnetic Properties. *J Phys Chem C Nanomater Interfaces, 113*(31), 13593-13599. doi: 10.1021/jp902953t

22.   Liang, Ming-Tsai, Wang, Shih-Han, Chang, Yu-Lun, Hsiang, Hsing- I., Huang, Huang-Jhe, Tsai, Meng-Huan, . . . Lu, Shih-Fu. (2010). Iron oxide synthesis using a continuous hydrothermal and solvothermal system. *Ceramics International, 36*(3), 1131-1135. doi: 10.1016/j.ceramint.2009.09.044

23.   Wang, Chun Yu, Hong, Jian Ming, Chen, Gong, Zhang, Yu, & Gu, Ning. (2010). Facile method to synthesize oleic acid-capped magnetite nanoparticles. *Chinese Chemical Letters, 21*(2), 179-182. doi: 10.1016/j.cclet.2009.10.024

24.   Dilek, Bakircioglu, Yasemin, Bakircioglu, Kurtulus & Selcuk, Yurtsever. (2013). Comparison of extraction induced by emulsion breaking, ultrasonic extraction and wet digestion procedures for determination of metals in edible oil samples in Turkey using ICP-OES. *Food Chemistry, 138,* 770–775

25.   Lyudmila M., Bronstein, Xinlei, Huang, John, Retrum, Abrin, Schmucker, Maren, Pink, Barry D., Stein, & Bogdan, Dragnea. (2007). Influence of iron oleate complex structure on iron oxide nanoparticle formation. *Chem. Mater,19*, 3624-3632

26.   Cano, Manuel, Sbargoud, Kamal, Allard, Emmanuel, & Larpent, Chantal. (2012). Magnetic separation of fatty acids with iron oxide nanoparticles and application to extractive deacidification of vegetable oils. *Green Chemistry, 14*(6), 1786. doi: 10.1039/c2gc35270b

27.   Alexandr, Todosiciuc, Andrey, Nicorici, Tatyana, Gutsul, Fabian, Gramm, Leonid, Braginsky, & Valery Shklover. (2010). Study of Temperature-Based Synthesis of PbTe Nanoparticles and Their Interaction with Surfactant. *J Information science and technology, 13 (1),* 84–97

28.   Y.S, Ho, & G. McKay. (1999). Pseudo-second order model for sorption processes. *Process Biochemistry, 34.* 451 – 465

29.   Sophie Loehle, Clotilde, Minfray, Christine, Matta, Thierry, Le Mogne, Jean-Michel, Martin, Raphaele, Iovine,Yukiko, Obara, Ryuji, Miura, & Akira, Miyamoto. (2013). Effects of iron oxide layers on adsorption mechanism of C18 fatty acid: A

computational study. *40th Leeds-Lyon Symposium on Tribology Tribochemistry Forum*

30.   Xiangyang, Xu, Zhiming, Yu, Yongwei, Zhu, & Baichun, Wang. (2005). Effect of sodium oleate adsorption on the colloidal stability and zeta potential of detonation synthesized diamond particles in aqueous solutions. *Diamond & Related Materials 14*. 206 – 212

31.   Ekemini B., Ituen, Edidiong A., Essien, Uwemedimo E., Udo, & Ogede R., Oluwaseyi. (2014). Experimental and theoretical study of corrosion inhibition effect of Cucumeropsis manniiN. seed oil metallic soap of zinc on mild steel surface in sulphuric acid. *Advances in Applied Science Research, 5(3),* 26-53